TECHNISCHE UNIVERSITÄT DRESDEN

13th German Ferrofluid Workshop

Benediktbeuern
September 25th – 27th.
2013

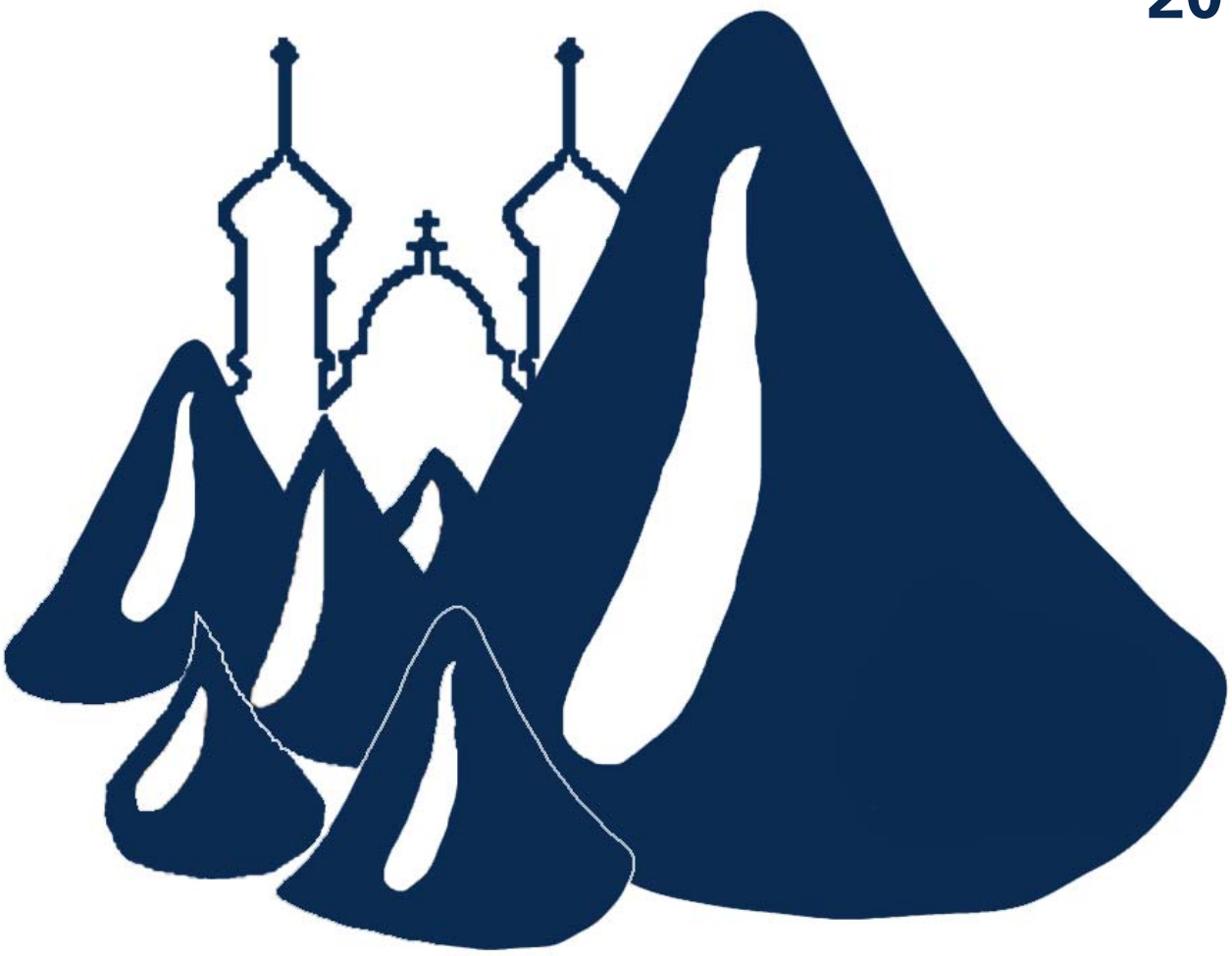

Book of Abstracts

Elongational flow effects on the vortex growth out of Couette flow in ferrofluids

S. Altmeyer[1,2,⋆], A. Leschhorn[3], Ch. Hoffmann[4] and M. Lücke[4]

[1] *Institute of Science and Technology Austria (IST Austria), 3400 Klosterneuburg, Austria*
[2] *Max Planck Institute for Dynamics and Self-Organization, 37073 Göttingen, Germany*
[3] *Institut für Grundlagen und Materialien der Elektrotechnik, Universität des Saarlandes, 66123 Saarbrücken, Germany*
[4] *Institut für Theoretische Physik, Universität des Saarlandes, D-66123 Saarbrücken, Germany*

The growth behavior of stationary axisymmetric vortices ($m = 0$) and of oscillatory, non-axisymmetric helical spiral vortices ($m = 1$) in Taylor Couette flow of a ferrofluid in between differentially rotating cylinders is analyzed using a numerical linear stability analysis [1]. The investigation is done as function of the inner and outer cylinder's rotation rates $Re_{1,2}$, of the axial wave number k of the vortex flows, and of the magnitude of an applied homogeneous axial magnetic field. In particular, the consequences of incorporating *elongational flow* effects in the magnetization balance equation on the marginal control parameters that separate growth from decay behavior are determined. That is done for several values of the so-called *transport coefficient* λ_2 which measures the strength of these elongational flow effects [2, 3]. In the presence of a magnetic field, the growth rates for vortex flow can either be reduced or enhanced, respectively, relative to the $\lambda_2 = 0$ reference situation. However, in any case, i.e., for all parameter configurations that we have explored, the elongational effect was *never* big enough to overcompensate the general, field induced stabilization; only the magnitude of the latter was modified by taking into account a finite λ_2. These modifications are typically larger for non-axisymmetric spiral vortices than for axisymmetric Taylor vortices but offer a strong dependence on other control parameters (see Figure). Their variations with Re_2 and k are qualitatively similar. Furthermore, for $m = 0$ as well as for $m = 1$ vortices, the λ_2 terms cause a significant relative growth enhancement of vortex flow with small k but a growth reduction when k is larger.

⋆ **sebastian_altmeyer@t-online.de**

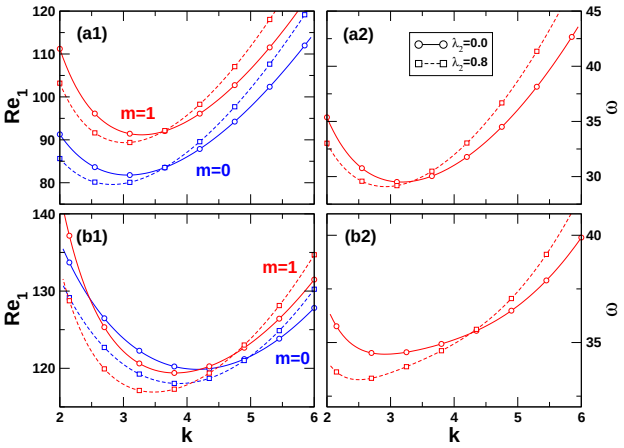

The left column shows the stability boundaries of the basic state, i.e. the circular Couette flow, against the growth of m=0 and m=1 vortex flow in the $k - Re_1$ plane for λ_2=0 and λ_2=0.8. The right column shows the marginal spiral frequencies at the $m = 1$ thresholds that are displayed in the left column. The top row refers to $Re_2 = 0$ and the bottom one to $Re_2 = -100$. The magnetic field is H=80 kA/m.

References

[1] S. Altmeyer, A. Leschhorn, Ch. Hoffmann, and M. Lücke, *Elongational flow effects on the vortex growth*

out of Couette flow in ferrofluids, *Phys. Rev. E*, **87**, 053010 (2013).

[2] H. W. Müller and M. Liu, *Structure of ferrofluid dynamics*, *Phys. Rev. E*, **64**, 061405 (2001).

[3] S. Odenbach and H. W. M üller, *Stationary Off-Equilibrium Magnetization in Ferrofluids under Rotational and Elongational Flow*, *Phys. Rev. Lett.*, **89**, 037202 (2002).

Effect of elongational flow on ferrofuids under a magnetic field

S. Altmeyer[1,2,⋆], Y. Do[2], J. M. Lopez[3]

[1] *Institute of Science and Technology Austria (IST Austria), 3400 Klosterneuburg, Austria*
[2] *Department of Mathematics, Kyungpook National University, Daegu 702-701, Korea*
[3] *School of Mathematical and Statistical Sciences, Arizona State University, Tempe, Arizona 85202, USA*

To set up a mathematical model for the flow of complex magnetic fluids, noninteracting magnetic particles with a small volume or an even point size are typically assumed. Real ferrofluids, however, consist of a suspension of particles with a finite size in an almost ellipsoid shape as well as with particle-particle interactions that tend to form chains of various lengths.

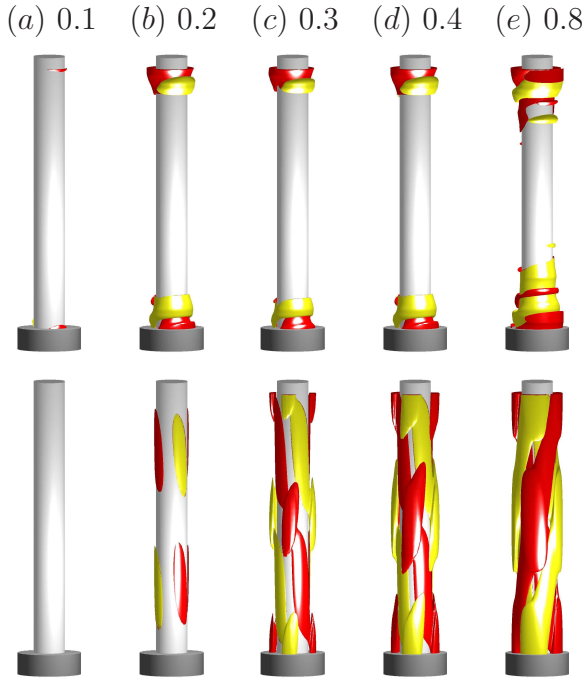

Fig. 1: Isosurfaces in differences of the azimuthal vorticity η, here $\Delta_2\eta = \eta(\lambda_2 \neq 0) - \eta(\lambda_2 = 0)$ for an left-winding (LW) characteristic flow at $Re = 60$, $s_x = 0.6$ and λ_2 as indicated; the top row is of the full solution (isolevel shown at $\Delta_2\eta = \pm 1$) and the bottom row is of the $m = 2$ contributions (isolevel shown at $\Delta_2\eta = \pm 0.02$).

⋆ **sebastian_altmeyer@t-online.de**

[1, 4] To come close to the realistic situation for ferrofluids, we investigate the effect of *elongational flow* incorporated by the symmetric part of the velocity gradient field tensor [1, 2], which could be scaled by a so-called *transport coefficient* λ_2 [1, 3]. Based on the hybrid finite - difference and Galerkin scheme, we study the flow of a ferrofluid in the gap between two concentric rotating cylinders subjected to either a transverse or an axial magnetic field with the transport coefficient. Under the influence of a transverse magnetic field with $\lambda_2 = 0$, we show that basic state and centrifugal unstable flows are modified and are *inherently three-dimensional* helical flows that are either left-winding or right-winding (Fig. 1) in the sense of

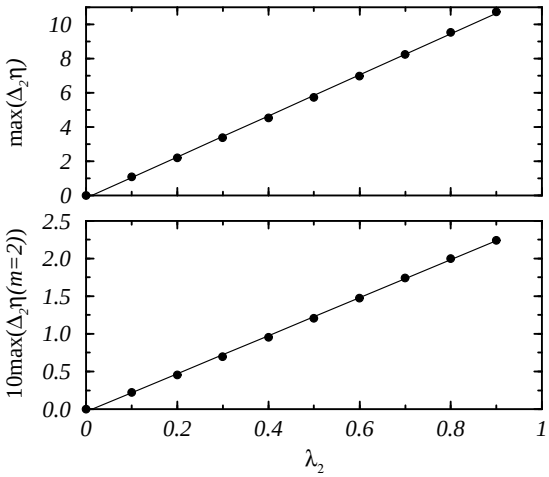

Fig. 2: Variation of $max[\Delta_2\eta]$ and $max(\Delta_2\eta(m = 2))$ for LW with λ_2 for $Re = 60$, $s_x = 0.6$ (c.f. Fig. 1). Lines are linear fits.

the azimuthal mode-2, which is in contrast to the generic cases. That is, classi-

cal modulated rotating waves rotate, but these flows do *not*. We find that under elongational flow ($\lambda_2 \neq 0$), the flow structure from basic state and centrifugal instability flows is modified and their azimuthal vorticity is *linearly* changed (Fig. 2). In addition, we also show that the bifurcation threshold of the supercritical centrifugal unstable flows under a magnetic field depends linearly on the transport coefficient (Fig. 3), but it does not affect the general stabilization effect of any magnetic field.

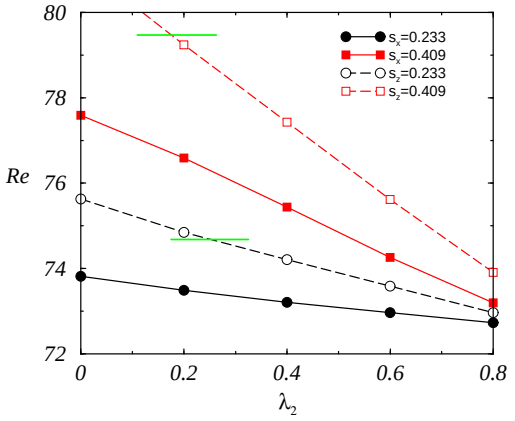

Fig. 3: Variation with λ_2 of the onsets for different field strengths s_x and s_z as indicated. Lines are linear fits. Points are just to guide the eyes; the numerical calculations are done for larger number of points. The both short horizontal lines indicate the experimental obtained onsets [4] ($Re_c(s_z = 0.233) = 74.68$ and $Re_c(s_z = 0.409) = 79.47$).

Comparing the onsets with experimental data [4, 3] we found best agreement for λ_2 about 0.2.

References

[1] H. W. Müller and M. Liu, *Structure of ferrofluid dynamics*, *Phys. Rev. E*, **64**, 061405 (2001).

[2] S. Altmeyer, Y. Do, and J. M. Lopez, *Effect of elongational flow on ferrofluids under a magnetic field*, *Phys. Rev. E*, **88**, 013003 (2013).

[3] S. Odenbach and H. W. M üller, *Stationary Off-Equilibrium Magnetization in Ferrofluids under Rotational and Elongational Flow*, *Phys. Rev. Lett.*, **89**, 037202 (2002).

[4] M. Reindl, and S. Odenbach, *Influence of a homogeneous axial magnetic field on Taylor-Couette flow of ferrofluids with low particle-particle interaction*, *Exp. Fluids*, **50**, 375 (2011).

Hardening transition and memory effects in a mesoscopic ferrogel model

M. A. Annunziata, A. M. Menzel, H. Löwen

Institute for Theoretical Physics II: Soft Matter, Heinrich-Heine University Düsseldorf, Universitätsstraße 1, D-40225 Düsseldorf, Germany.

Introduction

We concentrate on the mesoscopic characterization of two qualitatively different recent types of ferrogels [1]: in the first case, approximately spherical ferroparticles are embedded within a polymer gel network and free to reorient over long enough time scales; in the second case, however, the magnetic particles are crosslinked into the network via surface functionalization. The latter hinders free reorientation of the particles and imposes a sort of orientational memory – the magnetic particles remember their initial orientation after crosslinking.

Model

Our approach is mesoscopic in the sense that we resolve the single ferroparticles, but not single polymer chains. The ferroparticles are represented by hard spheres carrying dipolar moments. To mimic the elastic behavior of the polymer network, the centers of neighboring spheres are connected by harmonic springs. We introduce a route to include the orientational memory mentioned above into the model.

Results

So far, we have treated the model only in one spatial dimension [2]. These results will be important to test our later higher-dimensional theory. However, several features are already interesting from an application or experimental point of view. For example, with increasing magnetic moment, we find an elastic hardening transition for chain-like arrangements of the ferroparticles in the polymer network. Neglecting thermal fluctuations of the ferroparticles, this transition corresponds to a real phase transition that can be of first or second order. Furthermore, the orientational memory can lead to qualitatively different ground states of the chain-like arrangements: depending on the details of the memory, the dipolar moments can be arranged in a ferromagnetic fashion, in an antiferromagnetic-like way, or in the form of a spiral with a twist around the chain axis. We derived a corresponding phase diagram in terms of the orientational memory parameters.

Future work

Our work is currently extended towards higher spatial dimensions and more refined techniques to mimic the elastic behavior of the polymer network. We are starting to develop a theoretical framework in the form of a dynamical density functional theory.

Acknowledgments

This work has benefited from and is supported by the DFG via the SPP 1681.

References

[1] N. Frickel, R. Messing, A. M. Schmidt, J. Mater. Chem. **21**, 8466 (2011).

[2] M. A. Annunziata, A. M. Menzel, H. Löwen, J. Chem. Phys. **138**, 204906 (2013).

In vitro cell culture based analytical tools for nanoparticle-cell interactions

Franziska Bähring[1], Christian Bergemann[2], Andreas Hochhaus[1], Joachim H. Clement[1]

[1]*Abt. Hämatologie/Internistische Onkologie, Universitätsklinikum Jena, Erlanger Allee 101, 07747 Jena, Deutschland, franziska.baehring@med.uni-jena.de*
[2]*chemicell GmbH, Eresburgstrasse 22-23, 12103 Berlin, Deutschland*

Introduction

The interaction of magnetic core-shell nanoparticles with human cells is a complex process. There is general consent that physical and chemical characteristics of the nanoparticle core as well as chemical and physical properties of the cell surface are crucial. Furthermore, the biological specificities of the individual cell as well as the composition of cell clusters and tissues account to the consequences of cell-nanoparticle interaction. The wide-ranging applications of nanoscale hybrid materials require precise and standardized tools to pre-estimate the effects of core-shell nanoparticles on human cells.

Methods

Nanoparticles (core size ranging from 100 - 200 nm) with different types of shells were provided by chemicell GmbH. Human brain microvascular endothelial cells (HBMEC) were routinely cultivated with RPMI1640 + 10% FCS. Viability testing was performed with the CellTiter96® AQ_{ueous} One Solution Cell Proliferation Assay (Promega, Mannheim) or the PrestoBlue Cell Viability Assay (life technologies, Karlsruhe) as indicated. Furthermore the morphology of the cells was analyzed by phalloidin staining and fluorescence microscopy after nanoparticle addition.

The pure substances (polyethylenimine (PEI), starch (D)) were used in a 1/10 concentration because we calculate 10% w/w of the core/shell nanoparticles.

For studying the effects of the core/shell nanoparticles and the shell components on the HBMEC cells over a longer time period the xCELLigence System (RTCA DP) (Roche Applied Science, Mannheim) was used. Cells were seeded with a density of 20,000 cells per well. After 24 hours the cells were incubated with the core/shell nanoparticles or the substances for up to 72 hours. The incubation media remained on the cell cultures for the entire incubation time.

HBMEC were used for three-dimensional cell culture using the hanging drop method. 30,000 cells were cultured inverted in 20µl drops on the lid of a petri dish for 4 days. After transfer in agar-coated dishes the spheroids are ready to use within one day. The multicellular spheroids were incubated with various concentrations of nanoparticles for 3 hours. Viability was evaluated with the LIVE/DEAD® Viability/Cytotoxicity Kit (life technologies, Karlsruhe) and laser-scanning-microscopy.

Results

We could show previously that PEI-coated magnetic nanoparticles exhibit concentration-dependant cytotoxic effects on HBMEC cells demonstrated by viability assays and phalloidin staining. Studies on intracellular trafficking and metabolism of nanoparticles are facilitated by nanoparticles carrying a fluorescent dye. Therefore we used our standardized viability assays to check nanoscreenMAG/G-PEI and nanoscreenMAG/R-D nanoparticles for their cytotoxic potential [1]. The PEI-coated nanoparticles show a toxic effect starting between 25 and 50 µg/cm². Starch coated particles does not influence the viability of the cells at any concentration tested (Fig. 1). For long term observation we performed real-time cell analysis over a time-period of 72 hours with the highest concentration of 100 µg/cm². Under these condi-

tions the particles exhibit the same results as the CellTiter-Glo®-assay - the PEI-coated particles are cytotoxic, whereas particles with a starch shell are not.

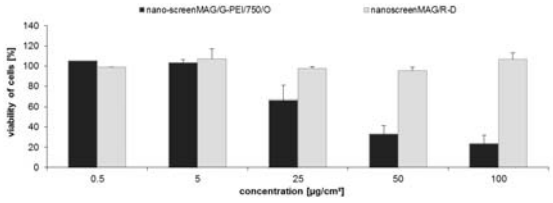

Fig. 1 Viability of HBMEC cells after incubation with two different fluorescence-labeled nanoparticles analyzed by CellTiter-Glo®-assay

For control we incubated HBMEC cells with PEI and starch alone for different time periods (3h and 72h).
The as yet presented data were obtained by using 2D cell cultures. In order to get closer to the situation in tissues we established a three-dimensional cell culture model. HBMEC cells are suitable for the generation of multicellular spheroids. Initially the viability of the 3D cell cultures in the presence of 0.5 µg/cm^2 up to 100 µg/cm^2 nanoparticles were tested. First preliminary estimations of the ratio of viable and dead cells reveal no explicit cytotoxicity of any core-shell nanoparticle in the three dimensional culture.

Conclusion

We could show that various cell-based assays are suitable to study the effects of magnetic core-shell nanoparticles, e.g. fluorescence-labelled nanoparticles. The expansion of the experimental settings towards 3D cell cultures will broaden the opportunities to analyse nanoparticle-cell interactions.

We thank Cornelia Jörke for expert technical assistance. This work was supported by the BMBF joint research project NanoMed, FKZ 03X0104D

[1] Bähring, F., Schlenk, F., Wotschadlo, J., Buske, N., Liebert, T., Bergemann, C., Heinze, T., Hochhaus, A., Fischer, D., Clement, J.H. 2013. Suitability of Viability Assays for Testing Biological Effects of Coated Superparamagnetic Nanoparticles. IEEE Transactions on Magnetics 49: 383-388

Estimation of the local elastic properties of gels by magnetization measurements using nickel nanorods as probes

P. Bender, A. Tschöpe, R. Birringer

Experimentalphysik, Universität des Saarlandes, 66041 Saarbrücken, Germany

1. Introduction

In recent years particle-based micro- and nanorheology became an emerging field of interest. In particular the investigation of the local structure of heterogenous networks such as physical hydrogels offers new inside into their microstructural makeup.
The present study focuses on the estimation of the local shear modulus of gelatine gels with nickel nanorods as magnetic phase via magnetization measurements. The nanorods were synthesized by electrodeposition of nickel into porous alumina templates, released into aqueous dispersion by dissolution of the alumina layer and further processed to gelatine-based ferrogels. With diameters below 42 nm they are ferromagnetic single-domain particles magnetized along the long rod axis [1]. Inside the gel the nanorods are mechanically linked to the polymer network and exhibit - without further pretreatment - isotropic orientation distribution [2]. However, applying an external homogenous magnetic field during the gelation process enabled the preparation of magnetically textured ferrogels, so called uniaxial ferrogels [3]. Depending on the ferrogels elastic compliance the nanorods can rotate in field direction in a homogenous magnetic field, working against the mechanical torque, which is caused by the shear deformation of the gel matrix. Such an elastic rotation results in characteristic deviations of the magnetization curve compared to mechanically hard ferrogels, where the particle orientation is fixed. This can be seen in figure 1, where the orientation-dependent magnetization curves of a mechanically hard ferrogel in the uniaxial state are shown together with the magnetization curve of a mechanically soft ferrogel perpendicular to anisotropy axes of the rods. In both gels nanorods with identical magnetic characteristics were dispersed. Therefore, the higher susceptibility of the soft ferrogel can be attributed to an elastic rotation of the rods in field direction. In this study four methods were developed which allow the estimation of the shear modulus of the surrounding gel matrix from the magnetization curves of mechanically soft ferrogels. In this presentation two of them are presented in detail.

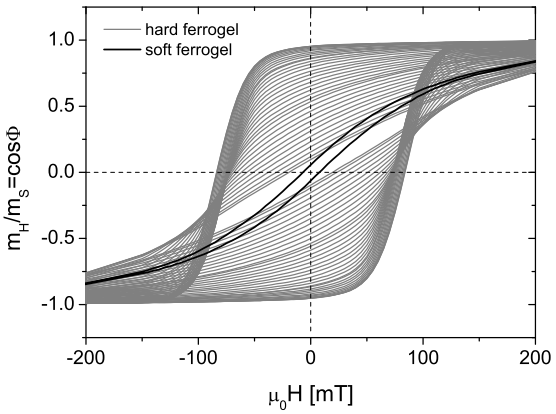

Figure 1: Orientation-dependent magnetization curves of the hard ferrogel ($\Theta = 0°$ - $90°$, $\Delta\Theta = 2.5°$) and the magnetization curve of the soft ferrogel perpendicular to the easy axis ($\Theta = 90°$).

2. Methods

Macroscopic rheological measurements of gelatine gels show that the shear modulus increases logarithmically with increasing gelation time [4]. In order to determine the time-dependent shear modulus G of the soft ferrogel several magnetization measurements were done after different gelation times ($t = 175 - 1473\,\mathrm{min}$, $\Delta t = 93\,\mathrm{min}$).

Method 1

In this method the initial susceptibility χ_0 of the magnetization curves of the soft ferrogel is analyzed. It can be shown that for $\Theta = 90°$

$$\chi_0 = \frac{M_S}{2K_s}\left(1 + \frac{6K_s \mathrm{lnn}}{4n^2 G}\right), \qquad (1)$$

where M_S is the saturation magnetization of the rods, K_s their shape anisotropy constant and n the aspect ratio. Thus, by measuring χ_0 as a function of gelation time the shear modulus G can be determined, when M_s, K_s and n are known.

Method 2

Here, the magnetization curves of the soft ferrogel and the hard ferrogel for $\Theta = 90°$ are transformed into $\Phi_{h,s}\,(\mu_0 H_{h,s}\mathrm{sin}\Phi_{\mathrm{h,s}})$-plots ($\Phi_{h,s}$ is the angle between the magnetic moments of the hard and soft ferrogel, and the external field). It can be shown that when the same magnetic torque $\mu_0 H_{h,s}\mathrm{sin}\Phi_{\mathrm{h,s}}$ acts on the rods in the hard and soft ferrogel, that the rotation angle ω of the rods in the soft ferrogel is $\omega = \Phi_h - \Phi_s$. Therefore, $\omega\,(\mu_0 H \mathrm{sin}\Phi)$ can be determined directly from the $\Phi\,(\mu_0 H \mathrm{sin}\Phi)$-plots and the shear modulus [3]

$$G = \frac{3\mathrm{lnn\,M_S}}{4n^2}\frac{\mu_0 H \mathrm{sin}\Phi}{\omega} \qquad (2)$$

can be calculated.

3. Results

In figure 2 the determined values for the time-dependent shear modulus of the soft ferrogel are shown. As can be seen, both methods result in nearly identical values for G and they are in very good agreement with the results of two other methods which are published in [2, 5] (method 4) and [3] (method 3), where the same ferrogel was analyzed. Furthermore, the observed logarithmical increase of G with increasing gelation time is in good agreement with macroscopic rheological measurements of gelatine gels [4].

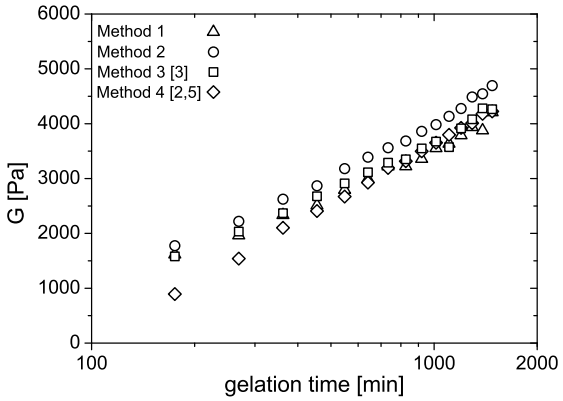

Figure 2: Shear modulus G of the soft ferrogel as determined with the four different methods.

References

[1] C.A. Ross et al., Phys. Rev. B 65, 144417 (2002).

[2] P. Bender, A. Tschöpe, and R. Birringer, JMMM 346, 152 (2013).

[3] P. Bender, A. Günther, A. Tschöpe, and R. Birringer, JMMM 323, 2055 (2011).

[4] V. Normand, S. Muller, J. Ravey, and A. Parker, Macromolecules 33, 1063 (2000).

[5] L. Roeder, P. Bender, A. Tschöpe, R. Birringer, and A. M. Schmidt, J. Polym. Sci., Part B: Polym. Phys. 50, 1772 (2012).

Microfluidic Flow Focusing - An Effective Method for the Production of Monosized Magnetic Microspheres

Mehrdad Bokharaei[1], Silvio Dutz[2,3], Urs O. Häfeli[1]

[1] *University of British Columbia, Faculty of Pharmaceutical Sciences, Vancouver, BC V6T1Z3, CANADA*
[2] *Institute of Photonic Technology, Department of Nano Biophotonics, Jena, Germany*
[3] *Ilmenau University of Technology, Institute of Biomedical Engineering and Informatics, Ilmenau, Germany*

Biodegradable microspheres made from the polyesters poly(lactic acid) (PLA), poly(lactic-co-glycolic acid) (PLGA) and poly(caprolactone) (PCL) can be made with highly uniform size distribution with a method called flow focusing. In this method, the polymer is dissolved in chloroform (phase d in **Fig. 1**) and pumped through an orifice. At the same time, a much higher (30x-100x) flow of an aqueous solution with a surface active agent (here polyvinyl alcohol in phase c) is pumped through the same orifice and "focuses" the stream of phase d. Due to pressure difference between the left channels and the right outlet in **Fig. 1**, the stream breaks up into monosized droplets. On the way out of the microfluidic chip, the solvent is partially extracted into the surrounding water phase, and single monosized microspheres form after complete solvent removal.

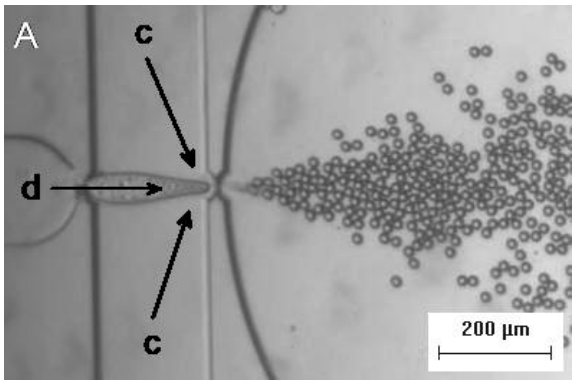

Fig. 1. Flow focusing produces identically sized droplets with dissolved polymer.

We have earlier shown that this method works well, that it can produce microspheres of between 2.8 µm and 50 µm with a standard deviation of less than 5% (**Fig. 2**), and that we even can use it for the delivery of ^{99m}Tc radiation to diagnose lung diseases [1]. In the current work, we have now additionally made the microspheres magnetic by encapsulating appropriately coated magnetic nanoparticles into the polymeric bulk phase. In this presentation, details of the coatings necessary for the preparation of magnetic microspheres and their magnetic characterizations will be discussed. Some hyperthermia data will also be discussed.

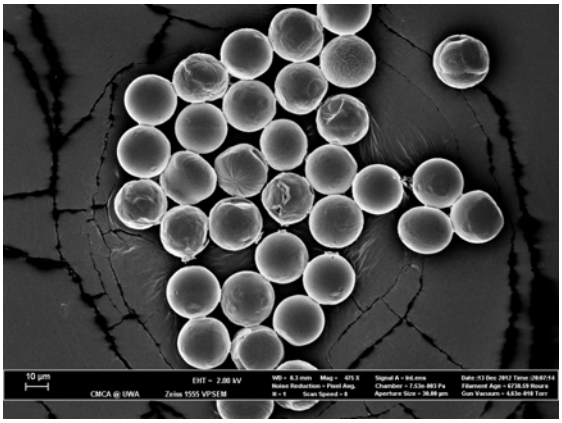

Fig. 2. Large magnetic PLA microspheres as seen by scanning electron microscopy.

Acknowledgments

This research was supported by a Canadian Institutes of Health Research (CIHR) and Natural Sciences and Engineering Research Council (NSERC) grant.

References

[1] Häfeli UO, Saatchi K, et al. (2010). Lung perfusion imaging with monosized biodegradable microspheres. Biomacromol 11, 561-567.

Soft magnetorheological elastomers: the influence of the powder composition on the controllable properties

D.Yu. Borin[1], G.V. Stepanov[2], S. Odenbach[1]

[1] *Technische Universität Dresden, Chair of Magnetofluiddynamics, 01062, Dresden, Germany*
[2] *Institute of Chemistry and Technology of Organoelement Compounds, Moscow, Russia*

The solid analogous of magnetorheological (MR) fluids are elastomers, in which the liquid carrier medium is replaced by a rubber or gel-like matrix (MREs) [1,2]. The most prominent property of these controllable elastomers is the MR effect. In the context of the elastomer it is an increase of elasticity in an external magnetic field. Physical properties of MREs are strongly correlated with their microstructure. Depending on the synthesis method, the spatial distribution of particles in the matrix can be either isotropic or anisotropic, if a magnetic field was applied during the cross-linking process. Using a sufficiently soft elastic matrix, for which the elasticity modulus does not exceed 200 kPa for vanishing magnetic field it is possible to obtain samples with an increase of the elasticity in an applied magnetic field up to several thousand percent [3]. Being once cured, conventional MREs based on carbonyl iron powder have certain properties which are controllable with an applied field. However, these characteristics can only be tuned by means of this external stimulus. Recently we proposed the use of a mixture of magnetic hard and soft powder, which enables the adjustment of the elasticity of MREs after they are cured [4].

In this work we report on the influence of the powder composition on the controllable mechanical properties of soft MREs. Quasi-static elongation-compression tests using a table-top machine equipped with an electromagnetic coil have been conducted. We have studied soft (modulus E_0~*50-200* kPa) and extra soft (modulus E_0~*10-30* kPa) samples of MRE filled with a soft magnetic powder, as well as samples based on hard magnetic powder and complex mixtures of both types of powder. Moreover, filler particles of spherical and irregular morphology have been used. MREs containing the magnetic hard powder were magnetized prior to the testing procedure in order to obtain a remanence magnetization. All characterized samples have almost the same concentration of magnetic powder; ϕ~85 wt.%. The iron powder with a spherical morphology has particles with a mean size of ~5 μm and the powder with an irregular morphology has particles with a mean size of ~35 μm. The used magnetic hard particles are made of FeNdB and have spherical as well as irregular geometrical form with a size distribution in the range of 5-70 μm. Studied MREs are cylinders with a height of 15 mm and a diameter of 15 mm. Exemplary results of the experiments are shown in figures 1 and 2. The absolute MR effect is $R_A=E_B-E_0$, where E_B and E_0 are moduli in an applied field B and for $B=0$ respectively. The relative MR effect is $R_R=(E_B-E_0)/E_0$. A maximal absolute effect is observed for the structured sample with an irregular powder. A giant relative effect is a feature of the samples with a very soft matrix. The addition of the magnetic hard powder decreases the observed effects. The modulus of the non-magnetized MRE with spherical FeNdB powder is rather not controllable with an external field, while the modulus of the non-magnetized sample containing magnetic hard powder of irregular shape can be effectively changed. The remanence magnetization of the samples based on FeNdB provides an adjustment of the initial modulus and modifies the range of the controllable properties. More details will be presented during the workshop.

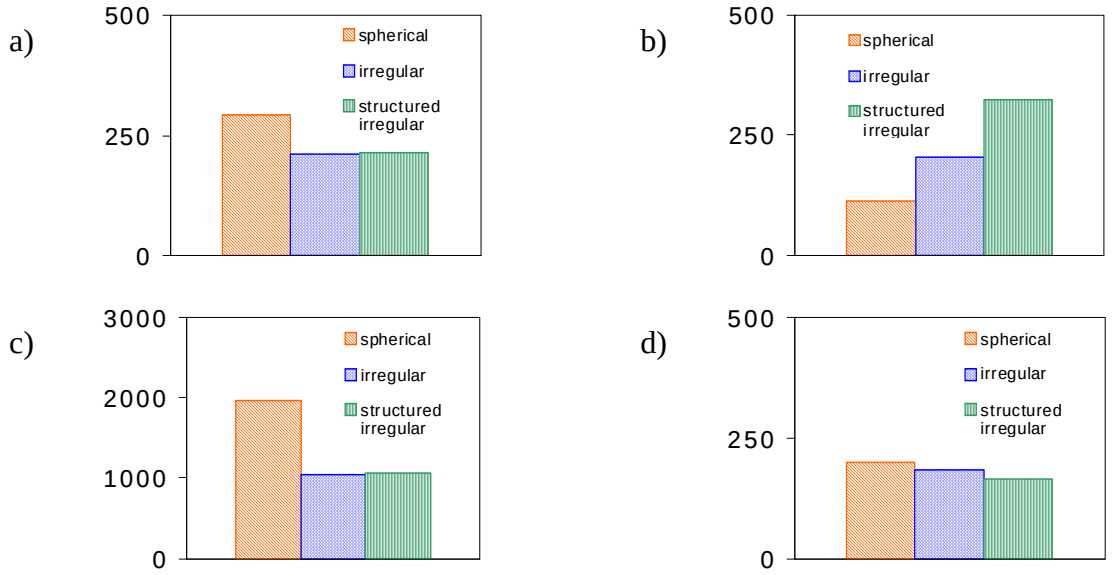

Figure 1. *MR effect for the MREs with magnetic soft powder (iron microparticles) of various morphologies given for the external magnetic field B=240 mT. Absolute effect R_A (kPa): a) for the extra-soft matrix (E_0<30 kPa); b) for the soft matrix (E_0~50-200 kPa). Relative effect R_A x100%: c) for the extra-soft matrix (E_0<30 kPa); d) for the soft matrix (E_0~50-200 kPa).*

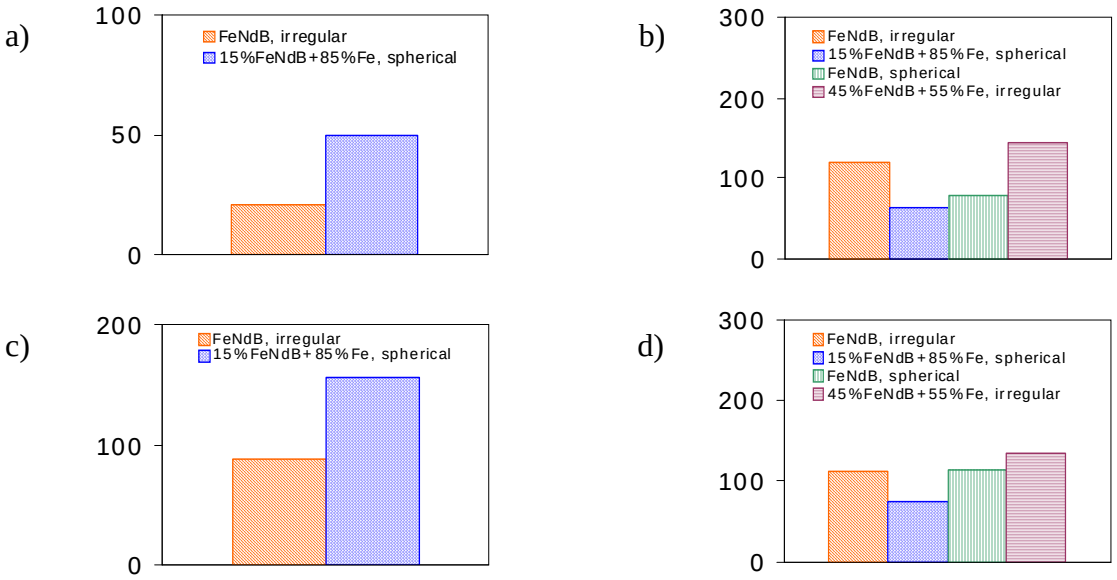

Figure 2. *MR effect for the MREs with magnetic hard and complex powder given for the external magnetic field B=240 mT. Absolute effect R_A (kPa): a) non-magnetized samples; b) samples magnetized at B=1.5 T. Relative effect R_A x100%; c) non-magnetized samples; d) samples magnetized at B=1.5 T.*

Acknowledgments

This project is funded by the European Union and the Free State of Saxony.
G.S. is grateful for the financial support to the Federal Agency for Science and Education of Russian Federation.

References

[1] Jolly M et al. 1996 J. Intell. Mater. Sys. Struct. 7.
[2] Kalio M 2005, VTT Publications
[3] Stepanov G V et al. 2007 Polymer 48.
[4] Borin D Yu et al. 2013 J. Phys. Conf. Ser. 412, 012040

Ferrofluids with Modified Ultra Small Magnetic Particles (USPIO-FF) as Options for Theranostics

N. Buske[1], N. Schelero[2], L. Dähne[2], J.R. Reichenbach[3], and S. Dutz[4,5]

[1] *Magneticfluids, Berlin, Germany*
[2] *Surflay Nanotec GmbH, Berlin, Germany*
[3] *Medical Physics Group, Center of Radiology, University Hospital Jena, Jena, Germany*
[4] *Department of Nano Biophotonics, Institute of Photonic Technology, Jena, Germany*
[5] *Institute of Biomedical Engineering and Informatics, Ilmenau University of Technology, Ilmenau, Germany*

Introduction

Multifunctional Ferrofluids (FF) have great potential for being simultaneously used in diagnostics and therapy, also known as theranostics. As a typical example one can combine Magnetic Resonance Imaging (MRI) for detection of cancer cells with therapy methods like drug targeting. For both applications the local particle and drug concentration at the target cells should be as high as possible to obtain a significant MRI signal and a high therapeutic effect.
In our study two different strategies were applied to improve the local particle concentration:

I) Exploiting the high half life time of USPIO particles in the blood circulation (up to 10h), enabling a long contact time of the particles towards the target cells
II) Creating an antigen-antibody interaction to the target cells by modifying the USPIO particle's CMD surface with specific antibodies.

Preparation

USPIO carboxymethylated dextran (CMD) magnetite particle FF were prepared in an one step process by aqueous co-precipitation in presence of an excess of CMD and further dialysis and filtering processes. Additionally, a combined centrifugation-dialysis process was used for FF purification and enrichment of the particle concentration up to 10 mg Fe/ml.
The as prepared aggregation stable USPIO-FFs were coated first with streptavidin and after that with biotinylated specific antibodies to establish an antigen-antibody-fixing.

Characterization

The hydrodynamic size, polydispersity index (PI) and Zeta-potential of the USPIO-CMD-FF were measured by dynamic light scattering (DLS). The core size was determined by transmission electron microscopy (TEM), from vibrating sample magnetometry (VSM) magnetization curves, and X-ray diffraction (XRD).
The amount of coupled and active streptavidine was determined by quantitative analysis of fluorescein-biotine coupling to the FF particles.
MRI relaxation times were determined at 1.5 T for different USPIO concentrations.

Results

Superparamagnetic behavior was confirmed by negligible coercivity and a relative remanence of 0.02.

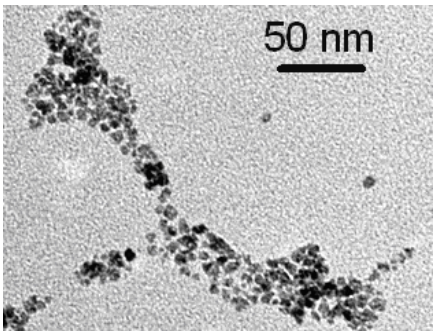

Figure 1: TEM image of USPIO-CMD particles.

The hydrodynamic diameter from DLS is on the order of 20 to 30 nm. Core size was determined to be 5 to 7 nm, see Figure 1.

The particles are suitable as contrast agents for MRI and show relaxation times similar to formerly commercially available products.
The chemisorbed values of marked streptavidin-biotin were determined and will be discussed in the poster.

Conclusions

Multifunctional, *in vivo* applicable USPIO-CMD-FFs modified with antibodies are potential candidates for application in theranostics by combining MRI with drug targeting.

Acknowledgments

The presented work was supported in the framework of the NIMINI-project No.: 01EZ0815. The USPIO-FF were prepared at Capsulution AG, Berlin, the antibody surface coating was performed at Surflay-Nanotec, Berlin. MRI experiments were performed by Ines Krumbein (Center of Radiology, University Hospital Jena).

Device for the measurement of the magnetic field angle dependent rheological properties of magnetorheological fluids (MRF) under translational oscillatory shear

E. Dohmen[1], M. Gude[1], W. Hufenbach[1]

[1] *Technische Universität Dresden, Institute of Lightweight Engineering and Polymer Technology, 01062, Dresden, Germany*

Magneto-active components are already in widespread use in industry and architecture. Experimentally verified characteristic data for magnetorheological fluids (MRF) is nevertheless required if reliable simulations are to be performed. At present, the majority of commercial rheometers are only able to measure the rheological properties of one field angle. Scientific investigations generally see modified Taylor cell [1] and capillary [2] viscosimeters used to measure the viscosity of ferrofluids in various magnetic fields.

Rheological data gathered under laboratory conditions characterized by highly homogeneous magnetic fields and precisely defined field angles is only partially applicable to practical applications in which a multitude of different field directions affect magnetic behaviour. The goal of this study is therefore to build and validate a testing device able to determine rheological properties across a number of field angles, thereby enabling the tailored design of MRF devices for practical scenarios.

The basic experimental setup is illustrated in Figure 1. A moving plate oscillates transversally between two fixed plates. The advantage of the two shear gaps is the minimization of transverse forces caused by magnetic attraction. The magnetic field is created by permanent neodymium (NdFeB) magnets, which can be revolved around the centre of the shear gaps. In order to ensure the continuous rotation of the magnets, the actuation of the moving shear plate is laterally offset. The mirroring of this double shear cell eliminates transverse forces. All four shear gaps are actuated simultaneously by a universal testing machine connected via a driving rod as illustrated in Figure 2.

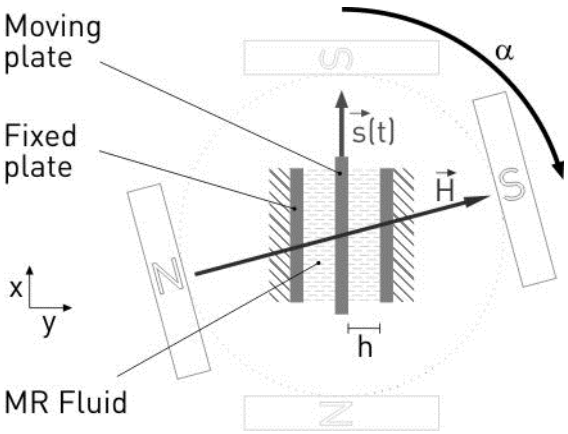

Figure 1: Schematic test setup. Shear gap h = 0.2 mm; H = 0.092 A/m.

Each of the four shear gaps has a plate area of 20 x 10 mm² and can be individually adjusted.

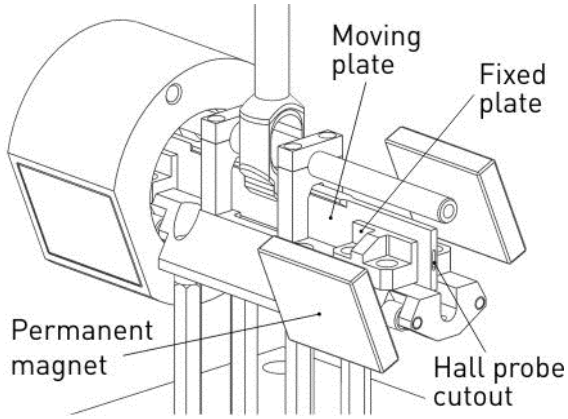

Figure 2: CAD model of test device.

A DynaMess dynamic testing machine was used to perform preliminary measurements

for silicon oil ElbeSil B500000 and Lord MRF-140CG both with and without a magnetic field. The values recorded for the MRF are collated in Figure 3.

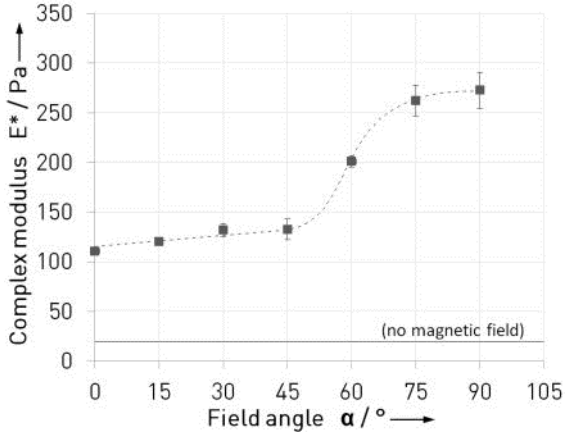

Figure 3: Complex modulus measured at various field angles α in a magnetic field (preliminary tests).

An AntonPaar MCR-502S rheometer was used to perform reference tests with the aim of validating the new field angle device. A 20 mm plate-plate geometry was selected for reference tests carried out using an AntonPaar MRD-170/1T magnetorheological device. Measurements without this optional device were performed using a 25 mm plate-plate geometry. The data gathered is compared in Figure 4.

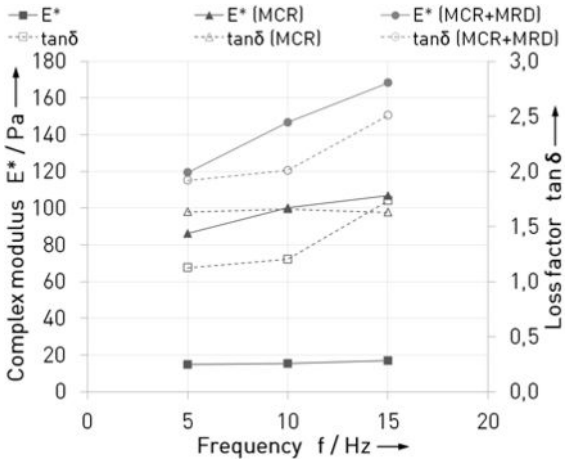

Figure 4: Comparison of the field angle device developed, the reference system (MCR) and the reference system with optional magnetorheological device (MCR+MRD) using the example of the complex modulus and loss factor measured for MRF-140CG at 5, 10 and 15 Hz.

A test series with and without the permanent magnets was carried out in order to rule out any magnetic interference in the measurements taken using the field angle device (Figure 5). The deviation of less than 5 % between the tests shows that neither the magnetic field applied nor the field angle exerts a significant influence.

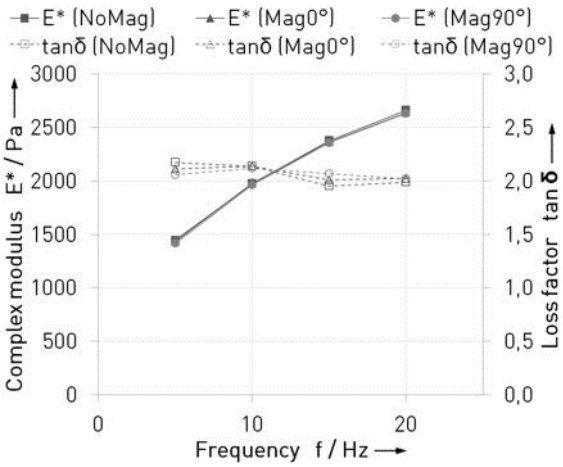

Figure 5: Influence of magnetic field and field angle on the measured data for silicon oil ElbeSil B500000.

Acknowledgments

The opportunity to perform measurements using the DynaMess testing machine at the Chair of Magnetofluiddynamics in Dresden and the technical assistance of Dmitry Borin are greatly appreciated.

References

[1] Ambacher, O.; Odenbach, S.; Stierstadt, K.: Rotational viscosity in ferrofluids. In: Zeitschrift für Physik B Condensed Matter 86 (1992), Nr. 1, pp. 29-32.

[2] Grants, A.; Irbītis, A.; Kroņkalns, G.; Maiorov, M.M.: Rheological properties of magnetite magnetic fluid. In: Journal of Magnetism and Magnetic Materials 85 (1990), Nr. 1-3, pp. 129-132.

Dynamic magnetic behaviour of DDM128 in agarose gel, gelatine and sugar matrix

D. Eberbeck, L. Trahms

Physikalisch-Technische Bundesanstalt, Berlin

Introduction

Magnetic nanoparticles (MNP) have found many applications in medicine, such as e.g. in magnetic drug targeting and hyperthermia and they are very promising tracer materials in newly developed Magnetic Particle Imaging (MPI). The efficiency of these applications strongly depends on the structure of applied MNP such as magnetic moment and magnetic anisotropy. However, in case of larger MNP a strong magnetic dipole-dipole interaction (DDI) can occur determined by the particle correlation within the given matrix (tissue, gels) [1]. Thus, DDI co-determines significantly the magnetic behaviour.

In present work we investigate the static and dynamic magnetic behaviour of MNP immobilised in a sugar matrix, agarose gel and gelatine. We apply different size bands of DDM128 (precursor of Resovist®), obtained by magnetic fractionation, in order to check the impact of the particle's magnetic moment.

Materials and methods

The MNP of DDM128 were size separated using a Miltenyi separation column applying a static magnetic field of 500 mT and 12 mT, respectively. Thus, the discharge of the column in 500 mT, assigned to D500, contains the smallest MNP while the eluate, E500, should comprises larger MNP, and the eluate of the 12 mT separation, E12, should be the fraction of the largest MNP. Diluted samples of DDM128, D500, E500 and E12 where immobilised in a sugar matrix by freeze drying, in agarose gel and in gelatine.

M(H) measurements were performed using a MPMS (Quantum Design), Magnetorelaxometry (MRX) was measured with a home-made SQUID-based device. M(H)- and MRX-data were analysed using the so called Moment Superposition Model (MSM) which describes the magnetisation and the relaxation of non-interacting magnetic moments by a superposition of contributions of MNP of different magnetic moments corresponding to the effective magnetic diameters d_m. This way we estimated the distribution of d_m and the effective magnetic anisotropy, respectively.

Finally, the nonlinear dynamic magnetic susceptibility were measured using a MPS-system (Bruker, MPS=Magnetic particle spectroscopy) at 25 kHz and 25 mT.

Results and discussion

Characterisation of MNP

Fitting the MSM with bimodal size distribution to the M(H) data, a distinct bimodality is obtained for DDM128 (Fig. 1), very similar to Resovist [2]. In contrast, the fraction of the smaller MNP, D500, clearly reveals a monomodal shape, matching TEM data (Fig. 1).

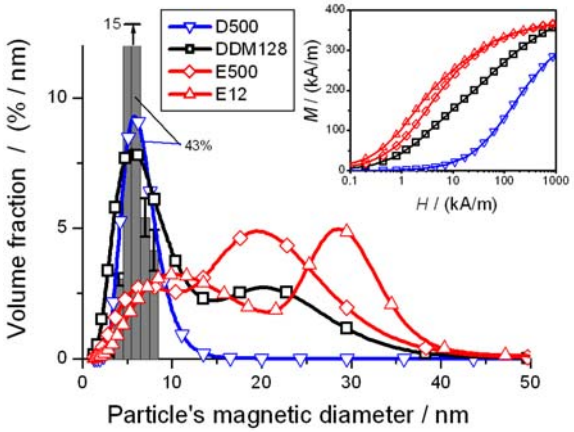

Figure 1: Distribution of effective magnetic diameters calculated fitting a bimodal distribution model to M(H)-data (inset). Bars: TEM data of D500.

As expected, the mean magnetic diameter of the large size fraction f_2 of E12 is larger than that of E500 (Fig. 1), also put in evidence by MRX-data. Interestingly, *both*

larger size samples, E500 and E12, maintain a bimodal magnetic size distribution with two fractions, f_1 and f_2, where the volume fraction of f_1, representing the smaller domains, is even larger in E12! Based on TEM observations we offer the following explanation of this finding: The two fractions f_1 and f_2 are attributed to multicore-MNP where each individual particle contains domains corresponding to small *and* large particles, where large domains (f_2-particles) may consist of either large grains or by exchange coupled small grains.

Influence of the matrix

The MNP of DDM128, E500 and E12 were embedded in a sugar matrix, in gelatine and agarose. The corresponding M(H) curves significantly differ from that of aqueous dispersions (Fig. 2). This is partly attributed to the cease of the Brownian motion. However, in gels this difference increased in comparison to the samples freeze dried in a sugar matrix. Hence, we conclude that there has to be an effect of DDI despite of the low iron concentration of about 1.5 mmol/L. That indicates that there are inhomogeneities in the particle distribution leading to closer distances between the MNP.

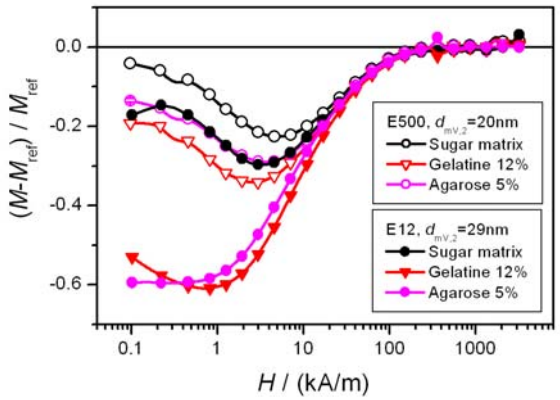

Figure 2: Normalised differences between of the magnetisation curves $M(H)$ of MNP in different matrices and corresponding aqueous MNP dispersions (M_{ref}).

This effect is much stronger in E12 compared to E500. This may be attributed to the larger magnetic moments (stronger interaction)MPS measurements on the same samples support these results: The amplitude spectra $A(k)$ and the phase curves $\phi(k)$ of all E500 and of E12 in sugar matrix are qualitatively roughly equal (Fig. 3) and the A_3 are about 20% below the A_3 of the aqueous dispersion. E12 in gelatine shows a steeper decay in A_k and a qualitatively different ϕ_k behaviour agreeing with M(H)-data which differ qualitatively, too (Fig. 2). On the other hand, E12 in agarose distinguishes qualitatively from E12 in sugar matrix only in A_k (also like M(H)) but not in ϕ_k (Fig. 3).

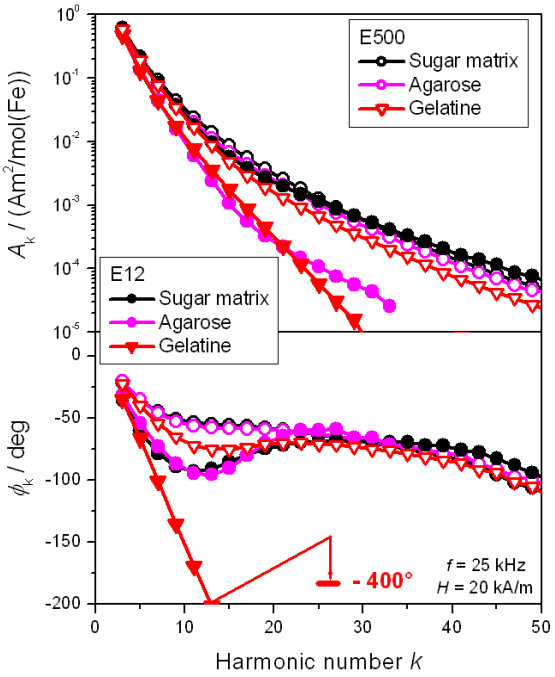

Figure 3: MPS-spectra of the Eluates of DDM128, E500 and E12, immobilised in indicated matrices.

Conclusion

Using different sensitive magnetic measurement techniques, we found evidence of a complex particle structure in preparations of multicore MNP and we could discriminate between 3 obviously qualitatively different MNP superstructures in different matrices.

Acknowledgments

We thank S. Gustafsson for provision of TEM-data. The research was supported by BMBF project FKZ-13N11092.

References

[1] D. Eberbeck, *EPJ* B, 10 (1999), 237-245.
[2] D. Eberbeck, F. Wiekhorst, S. Wagner, L. Trahms. Appl. Phys. Lett. **98** (2011), 182502.

Magnetic heating properties of $CoFe_2O_4$ in the Néel-Brown transition regime

M. Effertz[1], A. M. Schmidt[1*]

[1] *Department Chemie, Institut für Physikalische Chemie, Universität zu Köln, Luxemburger Str. 116, D-50939 Köln*
** E-mail: Annette.Schmidt@uni-koeln.de*

Magnetic heating of nanoparticles is of high potential for medical applications [1–3] as it offers novel treatment possibilities, like targeted thermal denaturation of cancer tissue. Magnetically heatable nanoparticles can also be used for drug delivery on demand.[4] For their reliability it is important to optimize their efficiency and thus to maximize their specific heating power and the relevant field parameters. It is of interest to analyze the magnetic heating properties of magnetic nanoparticles further with special emphasis on the Néel-Brown transition regime.

For medical purposes Fe_3O_4 is of primary interest, due to its biocompatibility. The limitation of it is, however, the low Specific loss Power (SLP) provided by these particles at medically possible magnetic field strengths. $CoFe_2O_4$ nanoparticles provide a higher SLP then Fe_3O_4 particles under the same conditions[4–6]. Biocompatibility can be achieved by encapsulating the $CoFe_2O_4$ particles in silica [7].

Aim of this work is to show the magnetic heating behavior of $CoFe_2O_4$ nanoparticles of different sizes and concentrations in dispersion as well as their dependency on the applied magnetic field.

To achieve this, different sizes of $CoFe_2O_4$ nanoparticles were synthesized by thermal decomposition of Co- and Fe oleylamine complexes [8] using a seed-grow procedure to increase particle size. We investigated the heating characteristics of $CoFe_2O_4$ NPs between 6 and 10 nm for concentrations up to 10 mg/ml at f=247 kHz. The SLP is obtained from initial slope of the heating curves [S] over multiple cycles and calculated by:

$$SLP = \frac{c_p}{\mu_{CoFe_2O_4}} \frac{dT}{dt}$$

With c_p : heat capacity of matrix, μ : volume percent of magnetic component, dT/dt : temperature change over time.

With increasing particle size, the SLP increased (Fig. 1). At diameters of 7.5 nm and higher, a linear increase of SLP with the particle diameter is observed, in good accordance with literature findings on Fe_3O_4 based single-domain-particles.[6]

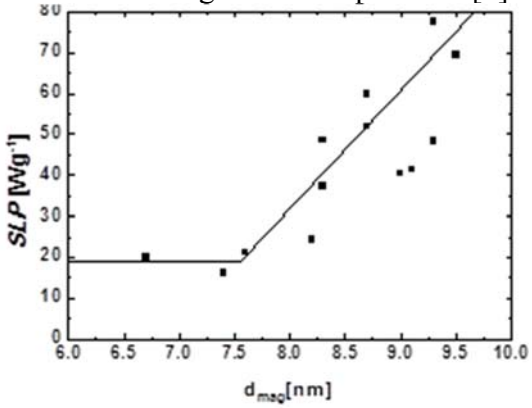

Fig. 1: SLP in dependence of d_{mag} for $CoFe_2O_4$-NPs in a 31 kAm^{-1} magnetic field.

The dependence of SLP on the applied magnetic field is nearly quadratic with deviations for higher fields and higher concentrations (Fig. 2). These deviations are as of yet unexplained, since according to literature such deviations should occur near the saturation magnetization, which is not reached at the applied fields.[6] A concentration dependence can be observed showing higher SLP for lower concentrations, which is counter intuitive in the case of ferromagnetic particles.

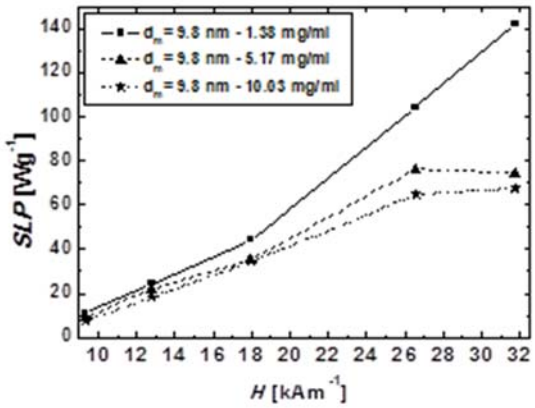

Fig. 2: SLP of $CoFe_2O_4$-NPs in dependence of magnetic field strength.

The SLP of $CoFe_2O_4$ NPs is dependent on the magnetic core diameter and a transition of constant SLP below d_{mag} = 7.5 nm and linear increase above is observed. The SLP of $CoFe_2O_4$ NPs is dependent on their concentration, with lower concentrations showing higher SLP.

Acknowledgments

We acknowledge the DFG within the framework of SPP1568 "self-healing Materials" for financial support.

References

[1] Q. a Pankhurst, J. Connolly, S. K. Jones, and J. Dobson, **Journal of Physics D: Applied Physics**, 36, (13), R167–R181, (2003).

[2] I. Hilger, R. Hergt, and W. a. Kaiser, **Journal of Magnetism and Magnetic Materials**, 293, (1), 314–319, (2005).

[3] D.-H. Kim, D. E. Nikles, D. T. Johnson, and C. S. Brazel, **Journal of Magnetism and Magnetic Materials**, 320, (19), 2390–2396, (2008).

[4] T. Gelbrich, G. U. Marten, and A. M. Schmidt, **Polymer**, 51, (13), 2818–2824, (2010).

[5] M. Veverka, P. Veverka, O. Kaman, a Lančok, K. Závěta, E. Pollert, K. Knížek, J. Boháček, M. Beneš, P. Kašpar, E. Duguet, and S. Vasseur, **Nanotechnology**, 18, (34), 345704, (2007).

[6] S. Dutz, R. Hergt, J. Mürbe, R. Müller, M. Zeisberger, W. Andrä, J. Töpfer, and M. E. Bellemann, **Journal of Magnetism and Magnetic Materials**, 308, (2), 305–312, (2007).

[7] Y.-H. Deng, C.-C. Wang, J.-H. Hu, W.-L. Yang, and S.-K. Fu, **Colloids and Surfaces A: Physicochemical and Engineering Aspects**, 262, (1)–(3), 87–93, (2005).

[8] S. Sun, H. Zeng, D. B. Robinson, S. Raoux, P. M. Rice, S. X. Wang, and G. Li, **J. Am. Chem. Soc**, 126, 273–279, (2004).

Hybrid magnetic-noble metal nanoparticles

M. Effertz[1], A. Bushmelev[1], A. M. Schmidt[1*]

[1] *Department Chemie, Institut für Physikalische Chemie, Universität zu Köln, Luxemburger Str. 116, D-50939 Köln*
** E-mail: annette.schmidt@uni-koeln.de*

The combination of magnetically and catalytically active components in a single nanoparticle is of great interest for the development of advanced catalytic systems based on magnetically manipulated nanoparticles with catalytic activity [1–5]. In addition, they may serve as nanoscale building blocks in advanced multifunctional nano constructed materials, for example as photonic crystals or metamaterial analogs.

A wide variety of nanoparticle shapes and sizes are described in literature, as collected for comparison by Cozzoli and Carbone.[6] The mechanisms underlying the formation of these hybrid particles are far from understood. The literature offers several examples for magnetic particles in combination with catalytically active components, however examples of magnetically blocked structures are rare. The high magnetic anisotropy in combination with oxidation stability predestines $CoFe_2O_4$ as the standard magnetic component, but other ferrites are also employed. The noble metal component is chosen from Au, Ag, Pt and Pd.

In this work we compare two ways of dumbbell synthesis: the growth of the noble metal component on $CoFe_2O_4$ seeds, and the growth of $CoFe_2O_4$ on noble metal seeds.[1] Their magnetic properties as well as hydrodynamic properties, are analyzed. While, after the optimization of the reaction conditions, a high fraction of $CoFe_2O_4$ seeds was decorated with a single Ag particle, the opposite approach results in virtually no free $CoFe_2O_4$ particles, and thus a high uniformity after processing. Depending on the reaction conditions, either spheroidal or cuboidal hybrids are obtained. By variation of the Pt/Co ratio during synthesis, particles of tailored size up to 40 nm are obtained (s. Fig 3b). The transfer of these hybrids to water is possible by using polyacrylic acid as transfer agent and stabilizer. All particles show superparamagnetic behavior in dispersion (s. Fig 2). Depending on the size of the magnetic component, the powders show magnetic hysteresis, with a remanence up to M_R/M_S=0.5. At a diameter of about 25 nm, the blocking size is reached as indicated by the high remanence (s. Fig 3a).

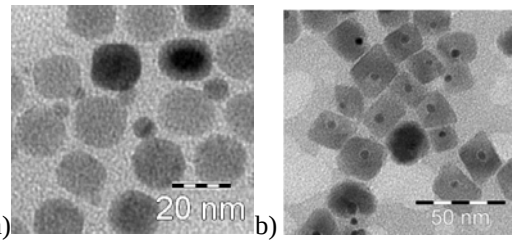

Fig. 1: TEM images of a) Ag@$CoFe_2O_4$ particles, b) $CoFe_2O_4$@Pt particles.

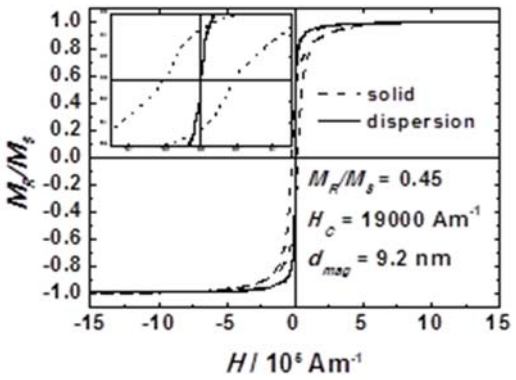

Fig. 2: Normalized magnetization curves for $CoFe_2O_4$@Pt-NPs, solid and in dispersion.

a)

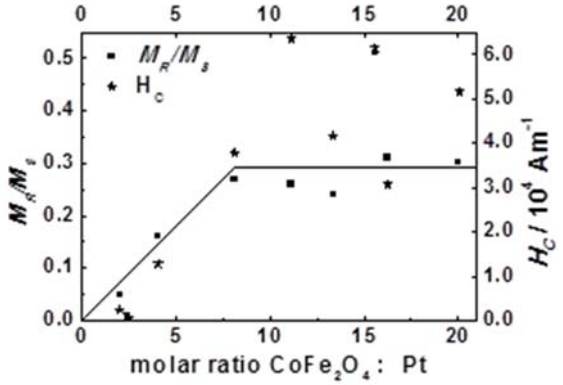

b)

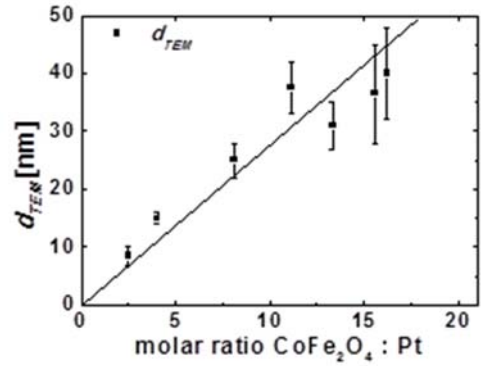

Fig. 3: a) Normalized remanence (M_R/M_S) and coercitivity (H_C) of $CoFe_2O_4$@Pt dumbbell particles synthesized using different Co / Pt ratios. b) d_{TEM} in dependency of ratio.

We demonstrate two robust methods for the preparation of ferromagnetic nanocatalysts with tunable properties.

Acknowledgments

We thank Dr. Belkoura and Dr. Roitsch, Universität zu Köln for TEM images. We acknowledge the DFG within the framework of NanoSciE+ (ERA) for financial support.

References

[1] C. Wang, H. Daimon, and S. Sun, **Nano Letters**, 9, (4), 1493–1496, (2009).

[2] Y. Mei, G. Sharma, Y. Lu, M. Ballauff, M. Drechsler, T. Irrgang, and R. Kempe, **Langmuir**, 21, (26), 12229–34, (2005).

[3] S. H. Joo, S. J. Choi, I. Oh, J. Kwak, Z. Liu, O. Terasaki, and R. Ryoo, **Nature**, 412, (6843), 169–72, (2001).

[4] B. Lim, M. Jiang, P. H. C. Camargo, E. C. Cho, J. Tao, X. Lu, Y. Zhu, and Y. Xia, **Science**, 324, (5932), 1302–5, (2009).

[5] R. Narayanan and M. a. El-Sayed, **Nano Letters**, 4, (7), 1343–1348, (2004).

[6] L. Carbone and P. D. Cozzoli, **Nano Today**, 5, (5), 449–493, (2010).

On the magnetization of dipole clusters

S. Förster[1], T. Friedrich[2], S. Mehdizadeh Taheri[1],
I. Rehberg[2], and S. Rosenfeldt[1]

[1] *Physikalische Chemie I, Universität Bayreuth, 95440 Bayreuth (Germany)*
[2] *Experimentalphysik V, Universität Bayreuth, 95440 Bayreuth (Germany)*

Introduction

Magnetic particles attract each other and form clusters. The shape of these clusters is particularly interesting when the magnetic particles are of uniform and regular shape. A macroscopic example is the toy sold as "magnetic cube puzzle" shown in Fig. 1. 216 spherical neodymium magnets of 5 mm diameter attract each other both in a seemingly disordered, and in the ordered arrangement of a simple cubic lattice.

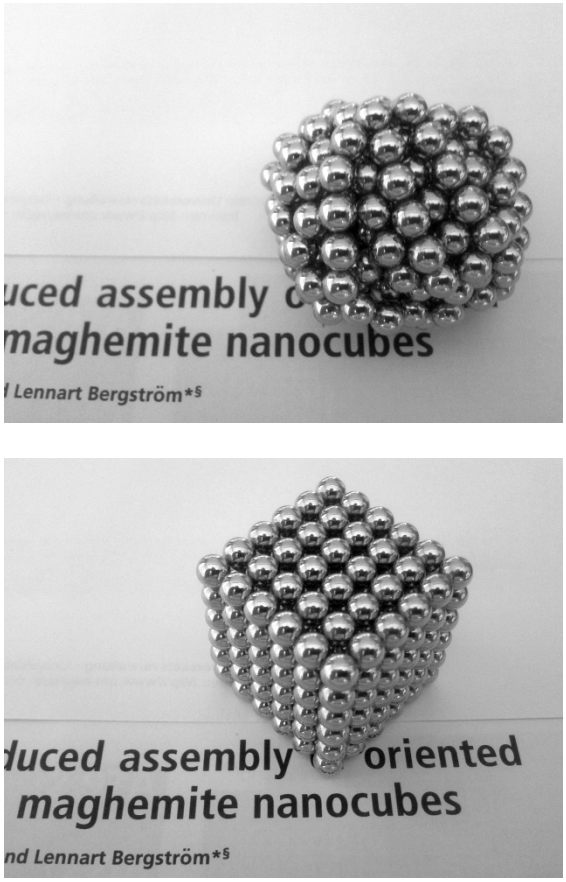

Figure 1: Photo of 216 spherical magnets in a disordered (above) and a simple cubic arrangement (below), located on the title page of Ref. [1] for proper focusing.

A nanoscopic example is provided by the self assembly of magnetic nano-cubes as described in Ref. [1], and discussed further in Ref. [2].

Method

In trying to understand the different shapes of clusters of spherical magnetic dipoles, and the self-assembly of magnetic nano-cubes we model both kinds of experiments by only considering the dipole-dipole interaction of point dipoles with magnetic moments $\vec{m}_i = m_0 \vec{e}_i$ of equal strength m_0 oriented along the individual unit vector $\vec{e}_i$. The interaction energy is then

$$U = \frac{\mu_0 m_0^2}{4\pi} \sum_{j>k} \frac{\vec{e}_j \cdot \vec{e}_k - 3\left(\vec{e}_j \cdot \vec{e}_{jk}\right)\left(\vec{e}_k \cdot \vec{e}_{jk}\right)}{\vec{r}_{jk}^{\,3}}$$

where r_{jk} is the distance between the two dipoles, and $\vec{e}_{jk}$ is the unit vector along the line joining the point dipoles labelled *j* and *k* [3].

The magnetic configuration of such three-dimensional arrangements of dipoles is obtained numerically, by allowing each dipole to adjust its orientation freely, while fixing the position within the three-dimensional lattice. The numerical method relaxes towards a local maximum of the binding energy within the 2*N*-dimensional configuration space, as established by *N* dipoles with 2 degrees of freedom, namely the polar and azimutal angle of their orientation.

Results

Figure 2 shows an example of the numerical calculation of the orientation of the vectors $\vec{e}_i$ obtained for 8 dipoles in a simple cubic arrangement.

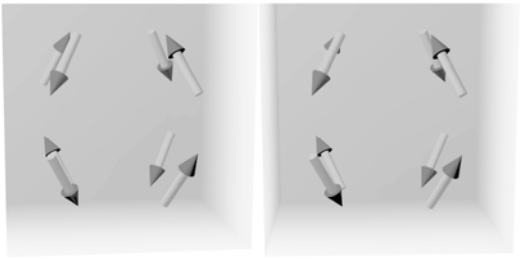

Figure 2: Stereoscopic image of a minimal energy arrangement of 8 dipoles in a simple cubic lattice.

As a side remark, we should mention that the configuration shown in Fig. 2 represents a local maximum of the binding energy, but it is not the only one. In this special arrangement of 8 dipoles there seems to be a continuum of frustrated states with the same energy.

Concerning the question, whether 1-, 2-, or 3-dimensional configurations are energetically favored, it turns out that increasing the number of interacting dipoles leads to a preference of the three-dimensional over the lower dimensional configurations. This is illustrated in Fig. 3.

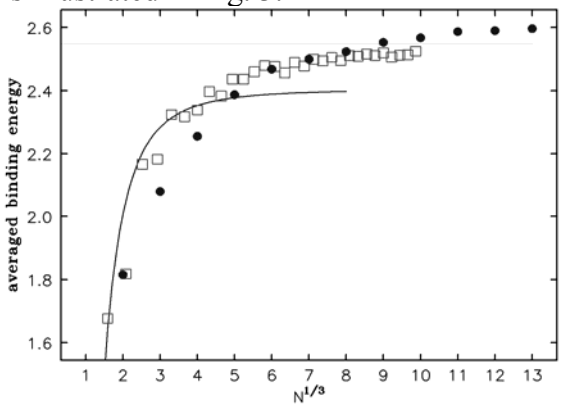

Figure 3: The binding energy of dipole clusters in 1d- (black solid curve), 2d- (open squares) and 3d-arrangement (solid circles). The horizontal grey lines indicate the asymptotic values for the 1d- and 2d-clusters.

For particle numbers above 100, it seems that a closed packing of the spheres is energetically favored over the simple cubic arrangement, so the configuration shown in the upper part of Fig. 1 should be preferred over the simple cubic arrangement. This is not in contradiction with the finding of a simple cubic lattice in Ref. [1]: The cubic shape of the nano-magnets does not allow for a close-packing arrangement of these dipols, but rather favors the simple cubic lattice, as discussed in Ref. [2].

Further experiments using different experimental techniques to reveal the dynamics of the self-assembly of these smallest magnets is currently under way [4].

Acknowledgments

It is a pleasure to thank Thomas Fischer and Reinhard Richter for stimulating discussions.

References

[1] A. Ahniyaz, Y. Sakamoto, and L. Bergström, PNAS **104**, 17570–17574 (2007).

[2] S. Disch, E. Wetterskog, R. P. Hermann, G. Salazar-Alvarez, P. Busch, T. Brückel, L. Bergström, and S. Kamali, Nano Letters **11**, 1651–1656 (2011).

[3] J. D. Jackson, Classical *Electrodynamics* (Wiley, New York, 2001).

[4] S. Mehdizadeh Taheri, S. Rosenfeldt, M. Michaelis, M. Drechsler, B. Förster, P. Böseke, T. Friedrich, I. Rehberg, and S. Förster, in preparation.

Directing Neurite Extension with Moveable Chemotaxis by NGF Release from Magnetic Nanospheres

R.J. Gilbert[1], J.M. Zuidema[1], C.G. Provenza[1], G.P. Desmond[1], S. Dutz[2,3]

[1] *Rensselaer Polytechnic Institute, Troy, NY, USA*
[2] *Department of Nano Biophotonics, Institute of Photonic Technology, Jena, Germany*
[3] *Institute of Biomedical Engineering and Informatics, Ilmenau University of Technology, Ilmenau, Germany*

Introduction

Following neural injury, regenerating axons must traverse through large gaps (within the peripheral nervous system) or through a glial scar environment (in the case of spinal cord injury). Many different modalities exist for directing axonal regeneration experimentally including aligned topography [1], electrical stimulation [2], or gradients of axon-extending ligands [3]. Specifically, gradient systems direct extending neurites in culture. However, one limitation in using gradient designs is that axons within such constructs may remain inside the construct and fail to migrate to distal targets. By designing moveable gradient systems, it may be possible to direct axonal extension into and through the injury site. Here, we present our development of a moveable chemotactic system facilitated by the combination of magnetic materials with chemokine-releasing polymers that preferentially direct neurite extension within proof-of-concept experiments.

Methods

Poly-L-lactic acid (PLLA) and oleic acid coated iron oxide nanoparticles (10 nm) were dissolved in a dichloromethane/ SPAN-80 solution. Nerve growth factor (NGF) in an aqueous solution was added to the PLLA solution and sonicated. An aqueous solution was added consisting of glycerine and Tween-80. After a final sonication step, the organic solvent was evaporated, the resulting magnetic nanospheres (MNS) washed, and then lyophilized. Scanning electron microscopy (SEM) was used for MNS imaging. NGF release from the MNS was characterized using a NGF ELISA. To assess the ability of the MNS to direct neurite extension, E9-stage chick dorsal root ganglia (DRG) were plated on aligned PLLA electrospun fibers. MNS were placed into the culture system and moved to one side of the DRG using magnets. Cultures persisted for two days, and explants were imaged using a beta-tubulin stain. Neurite extension was measured on both sides of the DRG and compared between groups.

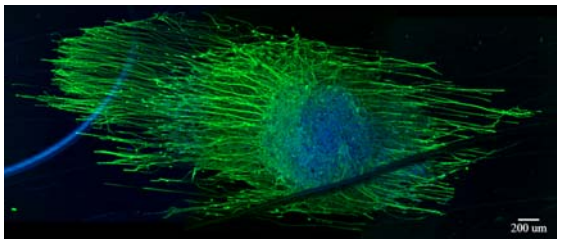

Figure 1: DRG cultured on aligned, electrospun fibers in which NGF nanospheres were placed to the left of the DRG.

Results

MNS were around 500 nm in diameter, and iron oxide nanoparticle pockets existed within the spheres. Using a NGF ELISA, NGF release from the MNS persisted up to 21 days. Interestingly, a specific concentration of MNS (100 NGF) was able to promote longer extension of neurites in the direction of the MNS (Figure 1).

Conclusions/Future Work

NGF-releasing spheres containing iron oxide nanoparticles were moveable within a culture situation, and longer neurites were measured extending towards the particles. Current work is examining the ability of the spheres to direct neurite outgrowth

while slowly moving the spheres away from the DRG.

Acknowledgments

Funding: NSF CAREER: 1150125. Students: Chris McKay, Chris Rivet, Nick Schaub, Nick Zaccor, and Susan Zheng

References

[1] Hurtado A., et al. Robust CNS regeneration after complete spinal cord transection using aligned poly-L-lactic acid microfibers. Biomaterials 32: 6068-79, 2011.

[2] Koppes A.N., et al. Neurite outgrowth is significantly increased by the simultaneous presentation of Schwann cells and moderate exogenous electric fields. J Neural Eng 8: 046023, 2011.

[3] Luo Y. and Shoichet MS. A photolabile hydrogel for guided three-dimensional cell growth and migration. Nat Mater 3: 249-53, 2004.

Magnetic drug targeting – Quantitative targeting results with blood

K.Gitter, S. Odenbach

TU Dresden, Institute of Fluid Mechanics, Chair of Magnetofluiddynamics, Measuring and Automation Technology, 01062 Dresden, Germany

Magnetic drug targeting

Magnetic drug targeting has been established as a promising technique for tumour treatment. Due to its high targeting efficiency unwanted side effects are considerably reduced, since drug-loaded nanoparticles are concentrated within a target region due to the influence of a magnetic field.

Details and setup

The artery-model, see Fig. 1, is a half-Y-branched glass tube (inner diameter d_i=1.6mm), where the branching tube is thought to supply the target area. This figure also shows the variation of magnet-positions and a scheme of the chosen cascade of measure-points. To obtain measure-data for one magnet-position, 1ml

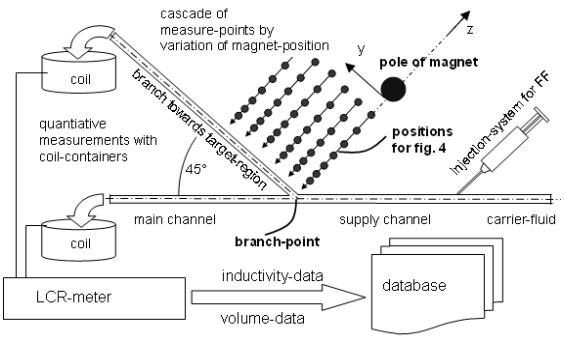

Fig. 1: Artery model with branch to tumour in 45° with a scheme of the chosen cascade of measure-points.

of ferrofluid with a volume-concentration of Φ=2.95 $\%_{vol}$ is injected during 10 minutes into the tube with the flow velocity of distilled water of v_{max} = 12.3mm/s. This leads to a Reynolds-number of Re=19.2, which is in the lower range for arterioles. In all experiments a comparably high concentration of injected ferrofluid of 2.95vol% is used. Such a considerably high concentration is chosen to enhance effects.

Quantitative data and magnet-system

Quantitative data is obtained by measurements of inductivity of calibrated coil-like containers capturing the outflow of each branch, as seen in fig. 1.
The magnetic field is generated by an arrangement of coils and pole pieces.

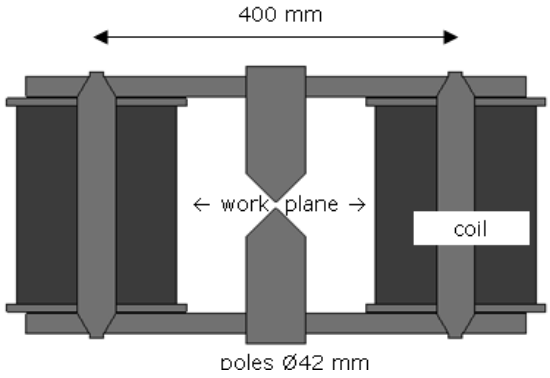

Fig 2: Controllable magnet-system. The work-plane is in the middle of two vertical poles.

The field in the work-plane in the middle of two vertical poles is generated by two coils around the side parts of a closed loop iron frame. Without active cooling this allows a maximum flux density of up to B_{max}=1.4 T and ∇B=80T/m at the poles.

Effects of the injection procedure

Our experimental investigations [1,2] and [3] have shown that the initial miscibility of even the water-based ferrofluid and water is low. Since in medical applications the ferrofluid will be injected close to an appropriate junction one cannot assume a homogeneous mixture approaching the branch-region. This has considerable consequences to the targeting process.

Injection into blood

In order to transfer the results to future medical applications the ferrofluid is injected into blood of sheep. The blood is stabilized with EDTA, which is a commonly used anticoagulant. The stability of the ferrofluid and blood mixture is promising. The mixture seems homogeneous and neither component shows clotting. Magnetic particles can easily be attracted and remixed.

Flow properties of blood

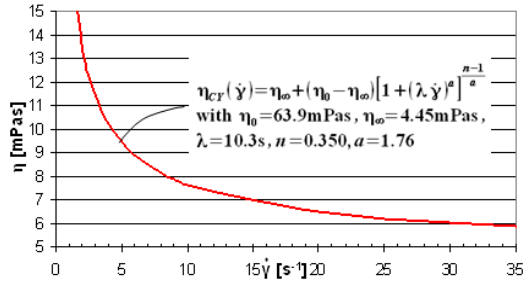

Fig. 3: Shear thinning behaviour of blood. Carreau-Yasuda viscosity model for human blood. Viscosity as function of the shear rate.

Fig. 3 shows shear thinning behaviour of human blood [4,5], which in a first step is also used as a model for the blood of sheep.

Results

Fig. 4 shows the targeting efficiency for an injection to water (diamonds) and for blood (triangles) as the percentage of ferrofluid that is targeted into the branch leading to the tumour. The x-axis is the distance of the magnet pole to the branch-point as seen in fig. 1.

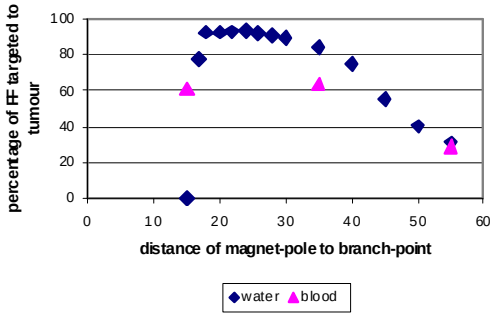

Fig. 4: Percentage of ferrofluid that is targeted towards the tumour for constant current of 0.5A and variation of the distance of the pole to the branch-point. Injection of ferrofluid with concentration of 2.95vol%. Diamonds (blood) and triangles (water).

For water a maximum yield of 93.5% is achieved. Nevertheless it can also be seen that a high magnetic volume force in the branch point leads to an accretion which inhibits the flow through the branch.

Such a behaviour was shown and discussed in previous works [1,2]. The targeting results for blood are lower than those of water which was expected with regard to the shear thinning flow properties of the blood, as seen in fig. 3. The measurement at point 15mm is interesting, since it shows a complete plug for water but still a yield of 61% for blood. Further measurements will lead to a better insight.

Outlook

The experiments in fig. 4 for blood are first results of a systematic investigation where many measure-points will be summarized in a targeting-map. A comparison of a map with blood to maps with water will contribute to a better understanding of the process of magnetic drug targeting.

Acknowledgments

The financial support by the Deutsche Forschungsgemeinschaft, grant OD18/13-3, is gratefully acknowledged..

References

[1] K. Gitter, S. Odenbach, JMMM, 323 (23), (2011).
[2] K. Gitter, S. Odenbach, JMMM, 323 (10), (2011).
[3] R. Ganguly, B. Zellmer, I.K. Puri, Phys. Fluids, (17) (2005).
[4] G.P. Galdi et al., Hemodynamical Flows: Modeling, Analysis and Simulation. Birkhauser Verlag, Berlin, (2008).
[5] K. Gitter, S. Odenbach, Magnetohydrodynamics, 40 (1) (2013).

Suppressing the Rayleigh-Taylor Instability in a tilted layer

A. Gómez-Ramírez[1], I. Rehberg[1], and R. Richter[1]

[1]*Experimentalphysik V, Universtät Bayreuth, 95440 Bayreuth (Germany)*

Introduction

The Rayleigh-Taylor-instability (RTI) takes place at the interface between two non-miscible liquids with different densities, when the denser liquid is placed on the top of a lighter one [1]. Because of this unstable energetic configuration, the interface between the two liquids loses its initial flatness, developing an interfacial pattern characterized by a group of wave numbers. Analyzing the topography of the interfacial pattern in 3D can provide a characterization of the dynamic evolution of the RTI. By utilizing a radioscopic technique [2] we can study the instability in 3D. Previous results obtained with this technique indicate that the RTI can be described as an imperfect subcritical Pitchfork bifurcation [3]. In this contribution, the factors which provoke the imperfection will be analyzed, taking special attention to the tilt of the experimental device.

Experimental methods

The two liquids used to carry out this work were a ferrofluid (FF, mark APG 512A from Ferrotec Co.) and a non-magnetic fluorinated fluid (Galden SVP). The use of the magnetic liquid (FF, lighter one) is suggested by Rannacher and Engel [4]. They present a model calculation which proposes that a magnetic field rotating in the plane of the interface between the two fluids (being one of them magnetic) can stabilize this interface. Previous work [3] has proven the feasibility of this approach. To perform an experiment, first the measurement cell is filled with the FF, second the rotating magnetic field (generated by means of two pairs of coils) is applied and eventually, the non-magnetic liquid is added. Afterwards, by switching off the rotating magnetic field the interface becomes unstable and the evolution of the RTI is recorded by means of the X-Ray detector. Figure 1 shows a schematic of the whole setup.

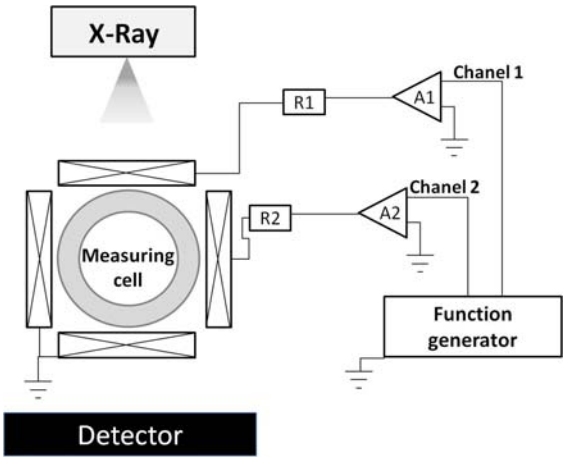

Figure 1. Schematic of the experimental setup.

Results

Figure 2 shows an exemplary radiogram obtained, and its 3D reconstruction. It was taken just before the liquids exchange their position, at the critical magnetic field (H_c) from which the interface becomes unstable. Analyzing pictures like those shown in figure 2 the amplitude of the peaks and valleys generated at the interface can be calculated. The height of the FF at each point of the interface can be modeled in cylindrical coordinates [3]:

$$h(r,\phi) = \sum_{n=0}^{\infty} \left[A_n J_n(k_c r) + B_n Y_n(k_c r) \right] \cos(n\phi + \alpha_n) \qquad (1)$$

where $h(r,\varphi)$ is the height of FF at the coordinates (r,φ), J_n and Y_n are the Bessel functions of first and second kind, respec-

tively. The capillary wave number is defined as $k_c = \sqrt{\Delta\rho\, g\, \sigma^{-1}}$, being $\Delta\rho$ the density difference between the two liquids employed, g the gravitational acceleration and σ the interfacial tension.

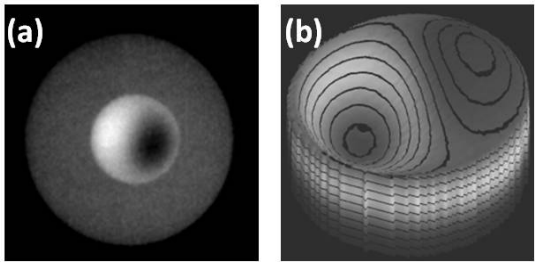

Figure 2. (a) Radiogram of the interface and (b) its 3D reconstruction.

Fitting the topography of the interface to the equation (1), the amplitude of the Bessel modes can be obtained for each magnetic field. At this point it should be mentioned that only the Bessel function of first kind is taken into account, because the one of second kind does not fit to the boundary condition. In figure 3 the amplitude of the first Bessel mode is plotted as a function of the rotating magnetic field for one of the experiments carried out.

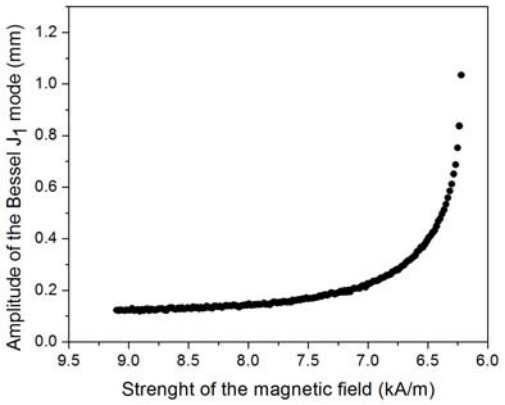

Figure 3. Amplitude of the Bessel mode J_1 as a function of the amplitude of the rotating magnetic field.

Experimental data like those shown in Figure 3 can be modeled as an imperfect subcritical Pitchfork bifurcation (eq. 2) using $\varepsilon = 1 - \frac{H^2}{H_c^2}$ as a control parameter.

$$A\varepsilon + \beta A^3 + b = 0 \qquad (2)$$

In this work, the origin of the imperfection (parameter b different from 0 in eq. 2) is investigated. It could be explained in terms of the tilt of the experimental device. So, in order to test this assumption, different measurements were performed by tilting the device. The results show the influence of the inclination on the imperfection.

Acknowledgments

A. Gómez-Ramirez acknowledges financial support by "Fundación Ramón Areces" through its post-doctoral fellow program.

References

[1] Lord Rayleigh, *Proc. Lond. Math. Soc.* **14**, 170–177 (1883); G. I. Taylor, *Proc. Roy. Soc. Lond. A. Mat.* **201** (1065), 192–196 (1950).

[2] R. Richter, J. Bläsing, *Rev. Sci. Instrum.* **72**, 1729–1733 (2001).

[3] A. Poehlmann, R. Richter, I. Rehberg, accepted for publication in *J. Fluid Mech. / Rapids* (2013).

[4] D. Rannacher, A. Engel, *Phys. Rev. E* **75** (1), 016311 (2007).

The influence of superparamagnetic nanoparticles on cell viability and intracellular signalling

Christine Gräfe[1], Franziska Bähring[1], Christian Bergemann[2], Florian Schlenk[3], Dagmar Fischer[3], Andreas Hochhaus[1], Joachim H. Clement[1]

[1]*Abt. Hämatologie/Internistische Onkologie, Universitätsklinikum Jena, Erlanger Allee 101, 07747 Jena, Deutschland, christine.graefe@med.uni-jena.de*
[2]*chemicell GmbH, Eresburgstrasse 22-23, 12103 Berlin, Deutschland*
[3]*Institut für Pharmazie, Abt. Pharmazeutische Technologie, Friedrich-Schiller-Universität Jena, Otto-Schott-Straße 41, 07745 Jena, Deutschland*

Introduction

The application of nanomaterials for various medical purposes is subject of current research. Due to their versatile beneficial features especially magnetic iron oxide nanoparticles (NP) are of high interest since amongst others they can be used in hyperthermal anti-tumour therapy and as contrast-enhancing agent in magnet resonance imaging. During their application in the human body NP get into direct contact with both targeted and non-targeted cells and might influence the cellular behaviour in different ways. Particularly the blood-brain barrier is a critical and sensitive interface. Therefore it seems to be an urgent need to investigate the NP influence on the barrier-forming cells.

Methods

Human brain microvascular endothelial cells (HBMEC) representing an important component of the blood-brain barrier, were cultured in RPMI1640 + 10% fetal calf serum. Long-term real-time cell analysis was performed with the xCELLigence system (Roche Applied Bioscience). Subconfluent cell cultures were exposed to 25µg/cm^2 NPs comprising coatings of different polymers, i.e. carboxymethyldextran (anionic), starch (neutral), and polyethylenimine (PEI, cationic). Cytological staining of the incubated cells visualized the interaction between NPs and cells. Particles' effects regarding the viability were analysed by flow cytometry. Prominent intracellular signalling pathways and target genes were studied by both immunoblotting and gene expression analysis via quantitative PCR.

Results

Cytological staining confirms that NPs interact with HBMEC and especially cationic PEI-coated particles accumulate at the cellular surface. Flow cytometry shows that viability of HBMEC is not affected by neutral or anionic NPs. In contrast, cationic NPs reduce cell viability by 25%. Additionally, the positively charged PEI NPs attenuate pro-proliferative signalling via MAPK p44/42 and strengthen the inhibition of anti-proliferative GSK-3β. A two-fold increase of phospho-AKT after incubation with cationic particles seems to trigger survival cascades supported by a more than 100-fold increase in c-fos transcription. PEI polymers alone show similar but less pronounced effects. Interestingly, long-term real time cell analysis reveals that HBMECs seem to be capable for recovery from the treatment with cationic NPs.

Conclusion

We show that neutral, anionic and cationic iron-oxide nanoparticles interact with blood-brain barrier forming HBMECs. Especially cationic PEI-coated NP affect various intracellular signalling pathways, whereby the consequences for the individual cell and the integrity of the tissue remain to be further investigated.

This work was supported by the BMBF joint research project NanoMed, FKZ 03X0104D

Magneto-optical measurement of the rotational relaxation of nickel nanorod colloidal dispersions in AC magnetic fields

Micha Gratz, Daniel Kaiser, Andreas Tschöpe and Rainer Birringer

Universität des Saarlandes – FR 7.2 Experimentalphysik – 66123 Saarbrücken, Germany

In microrheology, the motion of colloidal particles is analyzed to obtain rheological properties of the surrounding matrix. Nickel nanorods are ferromagnetic single domain particles [1] with a distinct optical anisotropy and therefore suitable for microrheological investigations by magneto-optical measurements [2,3].

In the present work we investigated the magneto-optical response of nickel nanorod colloidal dispersions in AC magnetic fields.

The nanorods were prepared by pulsed electro deposition of nickel into nanoporous AAO-templates [4]. Dissolution of the alumina layer in dilute NaOH with polyvinylpyrrolidone (PVP) for steric stabilization followed by separation and purification resulted in a stable aqueous dispersion of the nanorods.

Alternating magnetic fields with different field amplitudes and frequencies were applied to the nanorod colloidal dispersion. The amplitude and the phase shift of the oscillating optical transmission were determined using a lock-in amplifier algorithm. The experimental results were analyzed by comparison with numerical solutions of the Fokker-Planck equation of rotational diffusion in AC magnetic fields [5]. From the second moment of the orientation distribution function $\langle\cos^2\theta\rangle$, the time-dependent optical transmission was calculated and the amplitude and phase shift were retrieved using the same lock-in algorithm.

A characteristic relaxation frequency ω_C of the nanorods was defined by the phase shift of 45°. Figure 1 shows the ratio ω_C/ω_B of the simulation, where ω_B is the Brownian relaxation frequency, as function of the normalized field amplitude $\zeta_a = m\mu_0 H_0/k_B T$. In the limit of low field amplitudes, the ratio ω_C/ω_B converges towards a value of 1.225 and increases for higher field amplitudes.

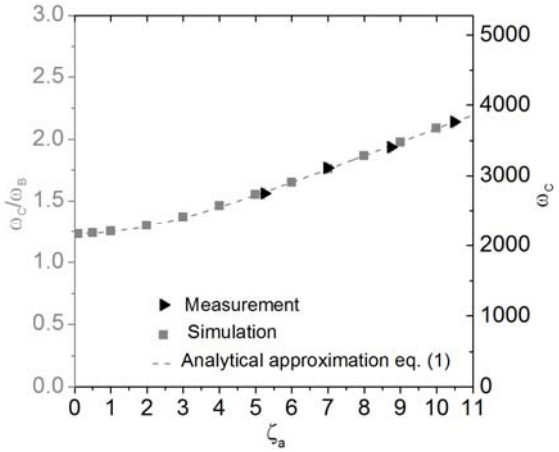

figure 1: Normalized characteristic frequencies ω_C/ω_B from numerical simulation with approximation by eq. (1) and the measurements of ω_C as function of ζ_a.

The simulation results could be approximated by the analytical expression

$$\frac{\omega_C}{\omega_B} = 1.225(1 + 0.04\zeta_a)^{0.328}. \qquad (1)$$

An excellent matching between the experimental and the theoretical results is achieve by rescaling the measured characteristic frequencies ω_C with the Brownian relaxation frequency $\omega_B = 1767\text{s}^{-1}$. This result is close to the value of $\omega_B = 1812\text{s}^{-1}$ obtained independently by AC magnetization measurements [1].

We employed the AC magneto-optical measurement of the Brownian rotation relaxation to investigate the interaction between nickel nanorods and gelatin molecules in solution above the gelation tem-

perature. Figure 2 shows the measured relaxation frequency ω_B as function of the total amount of gelatin.

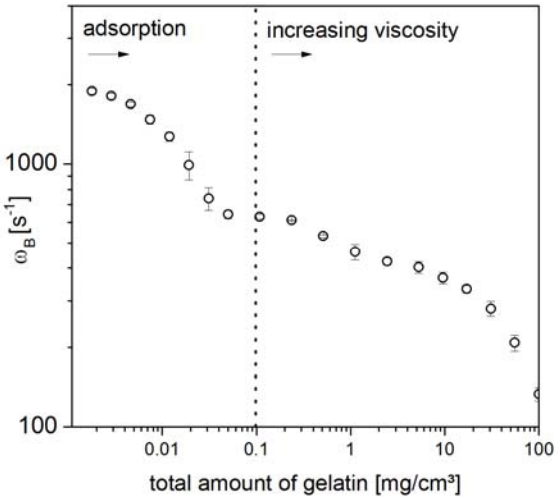

figure 2: Brownian relaxation frequency ω_B as function of total amount of gelatin in the sol state (T = 41°C).

Above a concentration of 0.1 mg/cm³ the decrease in ω_B is caused by the increasing viscosity of the surrounding matrix. By contrast, at lower concentrations the viscosities of the solution can be assumed to be virtually constant, so that the decrease of ω_B must be due to the adsorption of gelatin on the nanorods.
Figure 3 shows the thickness D of the adsorbed gelatin layer as function of the total amount of gelatin as determined by the model of Tirado et al. [6].

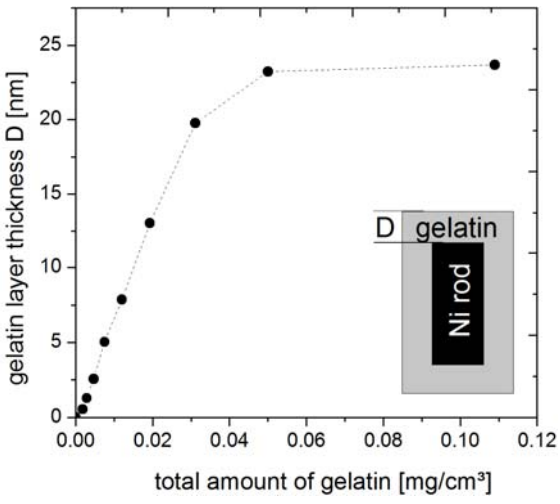

figure 3: Gelatin layer thickness D as function of total amount of gelatin.

Up to the concentration of ~ 0.12 mg/cm³, D increases until it saturates at ≈ 24 nm. The presence of the adsorbed gelatin layer on the nanorods was confirmed by SEM (fig.4a/b).

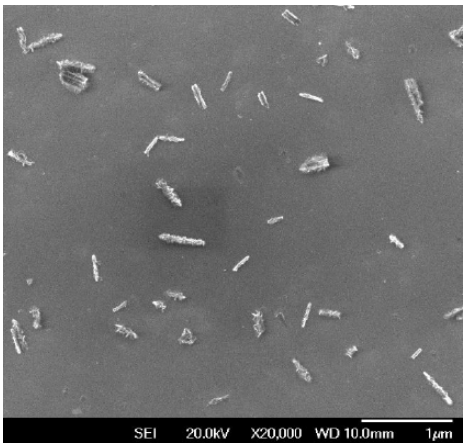

figure 4a: SEM image of nickel nanorods.

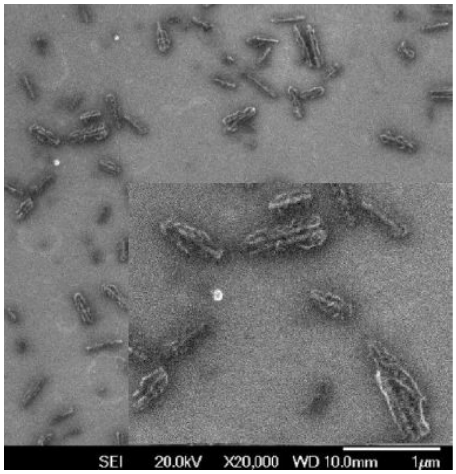

figure 4b: SEM image of gelatin coated nickel nanorods.

References

[1] Ross et al., Phys. Rev. B65, 144447, (2002)
[2] A.Günther et al., J. Phys. Condens. Matter 23, 325103 (2011)
[3] S. Schrittwieser et al., DOI: Small 2013, 10.1002/smll.201300023
[4] Masuda, Japan, Journal of Applied Physics, 35, L126 (1996)
[5] T. Yoshida and K. Enpuku, Japanese Journal of Applied Physics 48 (2009)
[6] M. M. Tirado et al., Journal of Chemical Physics 73, 1986 (1980).

Motion of magnetic particles in elastomeric materials

T. Gundermann, S. Günther, D. Borin, S. Odenbach

Technische Universität Dresden, Chair of Magnetofluiddynamics, 01062 Dresden, Germany

By composition of soft magnetic particles with an elastomeric matrix it is possible to develop a new kind of smart material. The physical properties of this new class of magnetoactive composite materials are of great interest on further applications in technology.
E.g. the mechanical properties of this composite material can be changed active and reversibly by applying a magnetic field. An essential reason for the property changes is an internal magnetodipolar striction, i.e. a change of the local positions of the particles.
A possibility to determine these particles and their local position in a magneto active composite is given by micro-computed tomography (µ-CT) [1, 2, 3].
The main interest of the current study has been an observation of the magnetic field dependent motion of individual particles from their initial positions inside an elastomeric matrix. For this purpose a µ-CT system has been combined with a sample holder coupled with two permanent magnets, enabling the investigation of the micro-structure under influence of an external homogeneous magnetic flux density of approximately 200 mT [3].
In the experimental investigations samples based on carbonyl iron particles with a mean size of $d \approx 40$ µm have been investigated. The particles have been dispersed in a soft polymeric matrix supplied by Wacker Corp. Germany. The basic matrix components were mixed with a high-viscosity softener. This leads to a reduction of the sedimentation rate during the polymerization process and to an isotropic particle distribution inside the elastomeric matrix.

The investigations were performed on a µ-CT system with an acceleration voltage of 160 kV. After the characterization of the sample in its initial state, i.e. without external stimuli, it has been subjected to the magnetic field and its internal structure has been once more studied by µ-CT.
The investigations provided as a result 3D images of the sample. Further, these 3D images were analyzed with image processing software. Here, a threshold was set to distinguish the particles from the matrix. Also, the particles where separated by using a watershed algorithm. Finally the particles could be characterized by geometrical properties like particle center, volume, surface area, main axes and circularity. This process leads to the possibility to recover particles in different CT-Images of the same sample.
As a result a comparison of the macroscopic change of the sample structure and the particle displacement could be undertaken.

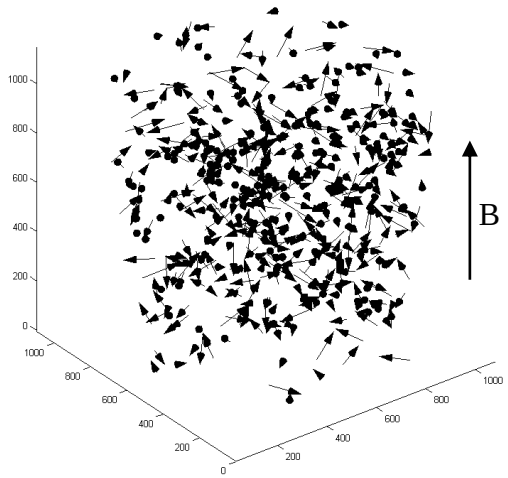

Figure 1: Displacement of the center of the particles inside the cylindrical sample and under the influence of a homogeneous magnetic field, shown is 20% of all particles, values are in pixel.

The resolution of the µ-CT in this investigation of samples with a size of d = 4 mm and h = 4 mm corresponded to 1 pixel = 3.2 µm.
Fig.1 shows the particle movement of a sample with a particle quantity of 2 wt.%. This resolution shows a particle movement that looks like a statistically random allocation of the arrows.
Zooming into the sample and comparing the movement in smaller volumes, the results show a particle movement that leads to the formation of chain like structures (Fig. 2).
The particle displacement observed here is larger than the macroscopic deformation of the sample. This finding leads to the conclusion that the particles in this kind of MR-elastomer can move relative to the matrix with small influence on the matrix deformation only.
It also leads to the assumption that the elastic moduli in the elastomer do not show a homogeneous distribution.

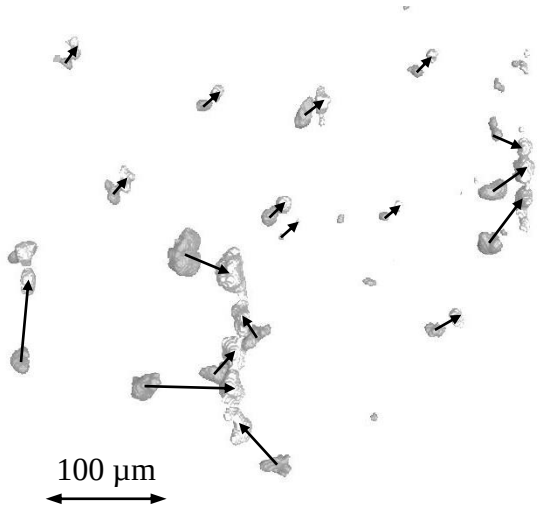

Figure 2: Structure formation of the particles, dark grey: sample without magnetic field, light grey: sample within magnetic field.

Acknowledgments

This project is founded by the European Union and the Free State of Saxony

References

[1] D. Günther, D. Yu Borin, S. Günther, and S. Odenbach, Smart Mater. Struct. **21** 015005 (2012)
[2] T. Borbath, S. Günther, D. Yu Borin, Th. Gundermann and S. Odenbach, Smart Mater. Struct. **21** 105018 (2012)
[3] Th. Gundermann, S. Günther, D. Yu Borin and S. Odenbach, J. Phys.: Conf. Ser. **412** 012027 (2013)

Investigation of the temperature distribution during magnetic heating treatment using polyurethane-ferrofluid-phantoms

F.Henrich[1] and S. Odenbach[1]

[1] *Chair of Magnetofluiddynamics, Measuring and Automation Technology, Technische Universität Dresden, Dresden 01062, Germany*

Heating treatment is an important approach in several medical therapies. Heat is used e.g. for muscle relaxation but is also proposed for the treatment of cancer. This is enabled by the fact that cancer cells are more heat-sensitive then healthy cells [1]. In this respect a possible treatment in the cancer therapy is the magnetic heating treatment. Magnetic nanoparticle are injected into the tumor and by the application of an alternating magnetic field the particles heat up due to remangetization losses (Brownian and Néelian relaxation) [2, 3].

The temperature distribution inside the tumor and in the surrounding tissue is important for a successful treatment. At the current state of research the investigation of the respective temperature profile in a tumor is not possible or only with great difficulties. To enable an investigation and therefore to optimize the treatment polyurethane-ferrofluid-phantoms were build.

Polyurethane Bectron PU4526 (ELANTAS Beck GmbH) was used to build the phantoms. It has a similar thermal conductivity coefficient (0.6 W/(mK)) as human tissue (0.63 W/(mK)) [4], therefore the heat distribution in and around a tumor can be investigated with the help of the phantoms.

Four phantoms with different designs were built. All phantoms are cylindrical and include an area which is enriched with ferrofluid (APG 513A). These parts have a magnetic particle concentration of 13 mg/ml.

Three of the phantoms have one enriched sphere with different diameters (5, 10 and 15 mm) (figure 1(a)). The fourth phantom has two enriched spheres with a respective diameter of 10 mm (figure 1(b)).

To measure the temperature inside these phantoms thermocouples (type T) were used. The exact position of the spheres and the thermocouples was measured with the help of X-ray tomography.

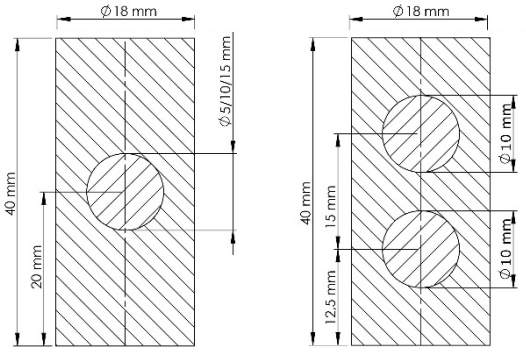

(a) (b)

Figure 1: technical drawing of the phantom enriched with (a) one sphere, (b) two spheres.

During the measurements with an applied magnetic field the phantoms were placed inside a water bath with a temperature of 37 °C to ensure constant environmental conditions. The magnetic field strength was varied between 4.39 and 8.71 kA/m. The frequency of the magnetic field was 284 kHz.

Based on the results of the measurements three-dimensional finite element method models were created for the respective phantoms. In figure 2 the measured and simulated temperatures at different magnetic field strengths for the phantom with the 10 mm sphere are depicted.

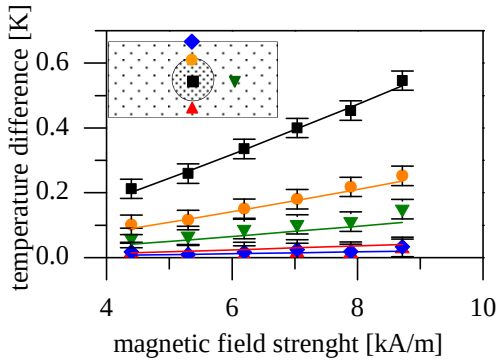

Figure 2: Comparison of the measured (symbols) and simulated (lines) temperature differences in the phantom with 10 mm sphere which is enriched with magnetic particles.

In the center of the sphere the highest temperature difference could be detected, whereas the temperature difference decreases when approaching the phantoms border. The obtained temperature difference rises with increasing magnetic field strength.

The measured and simulated temperature profiles in each phantom showed an agreement.

A comparison of the simulated temperature profile in the phantoms with one sphere is shown in figure 3.

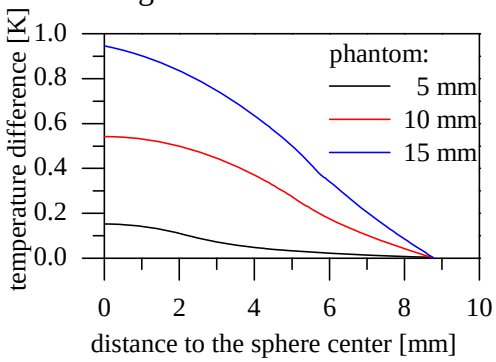

Figure 3: Simulated temperature profiles inside the phantoms at a magnetic field strength of 8.71 kA/m

The phantom with the largest sphere shows the highest temperature differences, whereas the phantom with the smallest ferrofluid-enriched sphere shows the lowest.

In figure 4 the simulated temperature profile in the phantom with the two spheres is depicted. It can be observed, that the temperature profiles of the spheres overlap in the central area. The simulated and measured temperatures for this phantom reveal the same behavior.

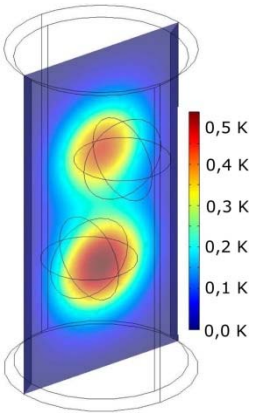

Figure 4: Simulated temperature profile for the phantom with two enriched spheres.

It was possible for all phantoms built in this experimental study to achieve an agreement for the measured and simulated temperatures.

This enables a theoretical predication of temperature profiles in tumors and surrounding tissue for the potential cancer treatment and therefore an optimization of e.g. the respective ferrofluid-concentrations. The agreement of measurements and simulations furthermore enables simulating complex cases without building phantoms for each setting.

Acknowledgments

These studies are supported by the (DFG-OD 18/16-1). We would like to thank ELANTAS Beck GmbH as well for providing the elastomer.

References

[1] P. Wust, B. Rau, P. Schlag, (2006) Prinzipien der Hyperthermie in Kombination mit Strahlentherapie und Chemotherapie; Berlin: Springer

[2] W. F. Brown (1963) Thermal Fluctuations of a Single-Domain Particle Phys Rev;130 (5):1677–86.

[3] L. Néel (1949) Théorie du trainage magnétique des ferromagnétiques en grains fins avec applications aux terres cuites. Ann Géophys;5:99–136.

[4] H. Hensel, K.D. Bock (1955), Durchblutung und Wärmeleitfähigkeit des menschlichen Muskels. Pflügers Archiv European Journal of Physiology, 260(5): 361-367

Properties of low temperature dipolar hard sphere fluid

S. Kantorovich[1,2], L. Rovigatti[3], J.M. Tavares[4], F. Sciortino[3], A. Ivanov[2]

[1] *University of Vienna, Sensengasse 8, 1090, Vienna, Austria*; [2] *Ural Federal University, Lenin av. 51, 620000, Ekaterinburg, Russia*; [3] *University of Rome, La Sapienza, p-le A. Moro 5, 00185, Rome, Italy*; [4] *Instituto Superior de Engenharia de Lisboa - ISEL, Rua Conselheiro Emidio Navarro 1, P-1950-062, Lisbon, Portugal*

Introduction

In this contribution we investigate the low-temperature, low-density behaviour of dipolar hard-sphere (DHS) particles, aiming at: (i) describing the DHS fluid in terms of a network of chains and rings held together by branching points (defects) of different nature; (ii) developing a theory describing the drop of initial magnetic susceptibility observed for low temperature.

Branching

We introduce a systematic classification of inter-cluster connections based on their topology, and analyse the geometric and thermodynamic properties of each class, as extracted from state-of-the-art equilibrium Monte Carlo simulations. We find that the relevant contribution to inter-cluster interactions is provided by (rare) three-way junctions and by four-way junctions arising from parallel or anti-parallel locally linear aggregates. Other defects are intra-cluster or associated to low cluster-cluster energies, suggesting that these defects play a significant role in the thermodynamic description of the self-assembly processes of (DHS). Fig.1 shows the defects analysed and compared in our work [1].

Initial susceptibility

We investigate via simulations, mean-field and density functional theories the magnetic response of a DHS fluid at low temperatures and densities, in the region of strong association [2]. The proposed parameter-

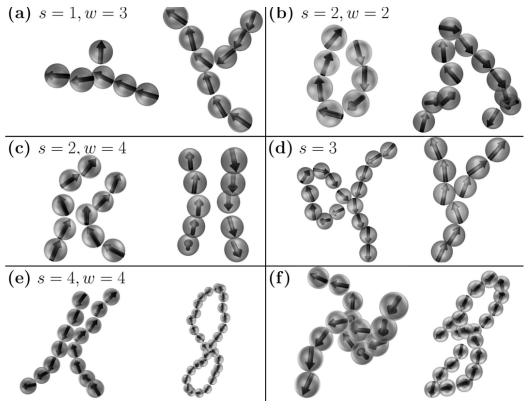

Figure 1: (a) Two $s = 1$, $w = 3$ defects. (b) $s = 2$, $w = 2$ defects stemming from intra-cluster interactions. (c) $s = 2$, $w = 4$ defects forming when two linear structures are close to each other resulting in weak intercluster interaction. (d) $s = 3$ defects with $w = 4$ (left, similar to those with s and w even) and $w = 3$ (right, defective Safran junctions). (e) $s = 4$, $w = 4$ defects originating from the chains, rings or part of chain-like structures interactions. (f) Defects with a mixed nature. Left: a $s = 5$, $w = 3$ defect which can be seen as a combination of a intra-cluster defect and a Three Way Junctions. Right: a $s = 4$, $w = 5$ defect coming from a $s = 4$, $w = 4$ defect and a $s = 2$, $w = 2$ defect.

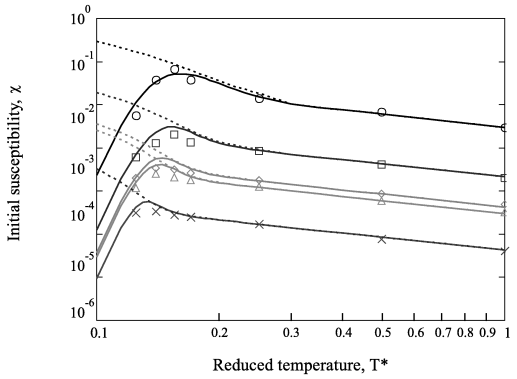

Figure 2: Initial magnetic susceptibility as a function of T^* for various volume fractions Theoretical results: solid lines. Simulation data: circles, $\varphi = 3.67 \cdot 10^{-3}$; squares, $\varphi = 2.62 \cdot 10^{-4}$; diamonds, $\varphi = 5.24 \cdot 10^{-5}$; triangles, $\varphi = 3.67 \cdot 10^{-5}$; crosses, $\varphi = 5.24 \cdot 10^{-6}$. The maximum of χ shifts towards lower T^* with decreasing φ. Dashed lines: initial magnetic susceptibility obtained in theory assuming that only chains and no rings.

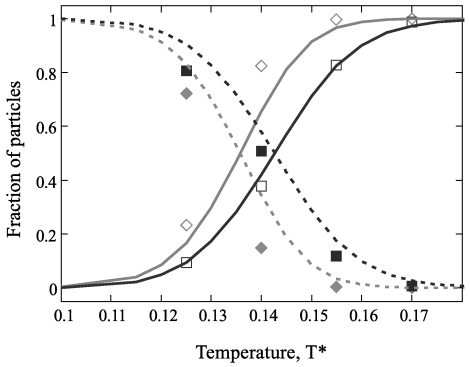

Figure 3: Fractions of particles aggregated in rings and chains as a function of T^* for two different densities. Simulation data: open squares, fraction of particles in chains; filled squares, fraction of particles in rings ($\varphi = 2.62 \cdot 10^{-4}$); open diamonds, chains; filled diamonds, rings ($\varphi = 5.24 \cdot 10^{-5}$). Theoretical results for the same densities (lines): solid, chains; dashed, rings. In both cases particle redistribution from chains to rings in the narrow range $0.13 < T^* < 0.15$ is evident.

free theory is able to capture both the density and temperature dependence of the ring-chain equilibrium and the contribution to the susceptibility of a chain of generic length. The theory predicts a nonmonotonic temperature dependence of the initial (zero field) magnetic susceptibility χ (see, Fig. 2), arising from the competition between magnetically inert particle rings and magnetically active chains (see, the redistribution of particles presented in Fig. 3). Monte Carlo results closely agree with theoretical ones.

For higher densities, branched structure could also be characterised by a closed magnetic dipole moment, and might also lead to the drop of the magnetic susceptibility. We are confident that the presented theoretical predictions will motivate further experiments at low densities and temperatures (at which the carrier might still be liquid [3, 4]).

Acknowledgments We thank: RFBR Grant 12-02-12063-ofi-m; RFBR grant mol-a-ved 12-02-33106; Ministry of Science and Education RF 2.609.2011; FWF START-Projekt Y 627-N27; RFBR grant mol-a 12-02-31330.

References

[1] L. Rovigatti, S. Kantorovich, A. O. Ivanov, J. M. Tavares, and F. Sciortino *J. Chem. Phys.* accepted (2013);

[2] S. Kantorovich, A. O. Ivanov, L. Rovigatti, J. M. Tavares, and F. Sciortino, *Phys. Rev. Lett.* **110**, 148306 (2013);

[3] A. Lebedev, *Colloid Journal* 72, **815** (2010);

[4] A. Lebedev and S. Lysenko, *J. Magn. Magn. Mater.* **323**, 1198 (2011).

Phenomenological analysis of magnetic nanoparticle size distributions with temperature dependent magnetorelaxometry

C. Knopke[1], F. Wiekhorst[1], N. Löwa[1], S. Wagner[2], J. Schnorr[2] L. Trahms[1]

[1]*Physikalisch-Technische Bundesanstalt, Berlin, Germany*
[2]*Charité, University Medicine Berlin, Berlin, Germany*

Abstract

The effectiveness of biomedical applications of magnetic nanoparticles (MNP) crucially depends on the knowledge about the magnetic characteristics of the MNP used. By aggregation through the interaction with the biomolecular environment the MNP can considerably change their magnetic behavior [1]. Applying temperature dependent magnetorelaxometry (TMRX) we examined these magnetic behavior changes due to enforced MNP aggregation in the presence of a high salt concentration.

Introduction

MRX is a sensitive tool for the specific and quantitative detection of MNP in biological systems [2] which denotes the decreasing magnetic moment of the MNP after the removal of an external field. Normally, the measurements are conducted at room temperature allowing for MNP detection even in in-vivo animal models. Including the temperature as a further parameter, TMRX reveals the underlying energy barrier distribution of the MNP [3], although the extraction of distribution parameters from TMRX curves is a major challenge. The energy barrier distribution is mainly dependent on MNP size and crystal structure but may also be influenced by interactions between the MNP. In medical applications of MNP mainly two effects may alter their magnetic behavior: the size selective MNP uptake by cells/organs changes the MNPs magnetic behavior as well as MNP interactions due to aggregation. To investigate the influence of the aggregation we compared the TMRX spectra of original MNP with those of MNP aggregated by the presence of sodium chloride to break up the colloidal stability.

Methods

MNP samples: We used two fractions of different size distribution (F2, F7) of citrate coated iron oxide MNP (Charité Berlin). Out of both fractions two samples of the original MNP suspension (30 µl, c_{Fe} = 0.1 mol/l) were prepared together with two MNP samples where additionally 30 µl 1 mol/l sodium chloride solution had been added leading to the enforced MNP aggregation clearly visible after 30 min. Of each sample pair one sample was kept in a fluid state while one sample was immobilized by freeze drying after addition of 30 µl mannitol(c_{mannit} = 50 mmol/l) solution.

Measurement devices: We used two different MRX timing regimes, the common MRX device employed solely for room temperature measurements uses a magnetizing duration of t_{mag}=1 s and a data acquisition interval 450 µs ... 0.5 s denoted hereafter as *short timing regime*. For the TMRX measurements we utilized a conventional SQUID magnetometer (MPMS-XL, Quantum Design). At fixed temperatures between 5 K and 350 K the sample was magnetized for 460 s followed by a data acquisition interval of 40 min referred to as *long timing regime*. These increased timing parameters were required by the control of the apparatus. Both devices operate with a magnetizing field of 800 A/m (1 mT) for the measurements. To obtain a TMRX spectrum the relaxation moment amplitude was determined as the decline of the magnetic moment within a fixed time interval normalized to the iron content X_{Fe} of the sample

$$\Delta M = \frac{m_{t=1.5min} - m_{t=40min}}{X_{Fe}} \qquad (1)$$

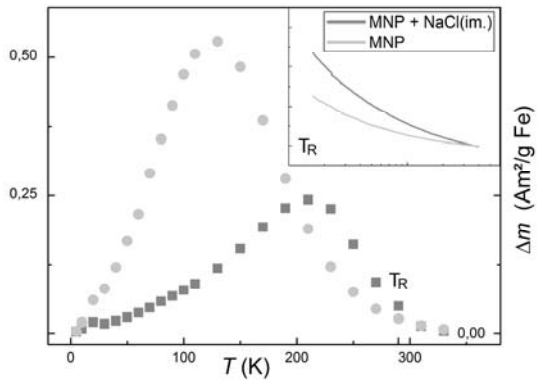

Figure 1. TMRX spectra of original and aggregated MNP(F2). Inset: MRX Relaxation curve at T_R for long timing regime of original and aggregated immobilized MNP.

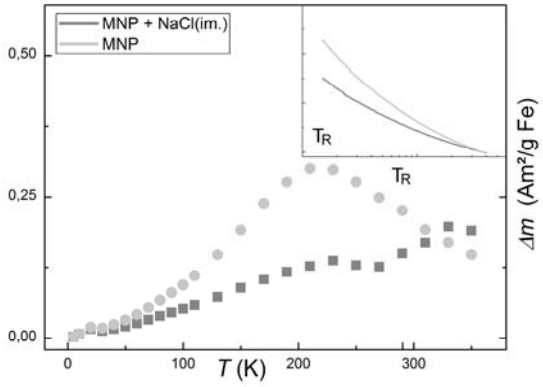

Figure 2. TMRX spectra of original and aggregated MNP(F7). Inset: MRX Relaxation curve at T_R for long timing regime of original and aggregated immobilized MNP.

Results

The shapes of the relaxation curves of the immobilized MNP measured at T_R (Inset of Fig. 1 & 2) exhibit only moderate changes due to aggregation. In sample F2 containing the smaller MNP fraction the relaxation amplitude increased after aggregation while for sample F7 containing the larger MNP fraction the relaxation amplitude slightly decreased. In both fractions the fast relaxation of the original MNP in the fluid state drastically slows down by aggregation (with relaxation times similar to immobilized MNP). Considerably more pronounced becomes the effect of aggregation manifest in the TMRX spectra (Fig. 1 & 2), where the relaxation amplitude is plotted as a function of temperature for the long timing regime. The original MNP fractions F2 and F7 exhibit a pronounced maximum at different temperatures below room temperature (T_{max}(F2) = 130 K, T_{max}(F7) = 210 K). The aggregation leads in both fractions to a decrease in amplitude and a shift of T_{max} towards higher temperatures by about 100 K. In fraction F7 containing larger MNP the maximum at 210 K still remains resulting in a bimodal distribution. So, the apparent differing relaxation behavior changes of F2 and F7 after aggregation measured at room temperature can be explained by the different displacements of the maxima as recovered by the TMRX spectra.

Discussion

TMRX expands the reliability to detect changes in the magnetic behavior of room temperature MRX measurements. Although TMRX is excluded from in-vivo applications of MNP it becomes a valuable tool to investigate the influence of aggregation and thus the interaction of MNP with their biomolecular environment. In the same way changes in the size distribution due to uptake and internalization by a biological system can be documented. For a further more quantitative description the particular timing regime has to be taken into account. Additionally a dedicated magnetorelaxometry device is presently under construction to enable TMRX measurements at the short timing regime.

Acknowledgement

This work was financially supported by the DFG research program TR408/5-2.

References

[1] D. Eberbeck, et al. *Journal of Physics: Condensed Matter*, vol. 18, no. 38, pp. S2829–S2846, Sep. 2006.

[2] F. Wiekhorst, et al. *Magnetic Particle Imaging*,1st ed., Springer, pp. 301-305, 2012

[3] E. Romanus, et al. *Nanotechnology*, vol. 18, no. 11, p. 115709, Mar. 2007.

MicroCT imaging reveals intratumoral distribution of magnetic nanoparticles and enables optimized therapy planning

S. Kossatz[1], M. Stapf[1], R. Ludwig[1], H. Dähring[1], I. Hilger[1]

[1]*Institute for Diagnostic and Interventional Radiology I, Jena University Hospital – Friedrich Schiller University Jena, Bachstraße 18, D-07740 Jena, Germany*

Background

Tumor cells and tumors can be effectively killed by thermal stress, also called hyperthermia [1]. This promising approach has already been tested in clinical studies. There, a lack of the ability to deposit cytotoxic temperatures homogeneously in the tumor area to reach all tumor cells led to unsatisfactory results. Hyperthermia can be optimized by using magnetic fluids, like for example iron oxide magnetic nanoparticles (MNP), which are deposited directly in the tumor, and which produce heat when placed inside of an alternating magnetic field (AMF). Up to date, intratumoral injection of the magnetic material is the state-of-the-art because it readily leads to sufficient amounts of magnetic material to induce hyperthermic temperatures above 43°C in the tumor. However, after intratumoral injection naturally the magnetic material will be heterogeneously distributed, leading to intratumoral temperature gradients. Especially regions of temperature underdosage, where the temperatures are in the sub-lethal range, pose a problem to therapeutic efficiency because surviving cells can form a new tumor.
A thorough characterization of intratumoral MNP distribution could enhance the effects of hyperthermia by the identification of regions where MNP are absent and should be re-injected and the identification of regions where MNP are close to non-tumor tissue or spine, where very high temperatures should be avoided.

Aim

In this study, we tested if intratumoral distribution of iron oxide MNP can be determined via microCT imaging and how the distribution influences the therapy outcome.

Methods

We used athymic nude mice bearing subcutaneously implanted breast cancer xenografts derived from the cell line MDA-MB-231. MNP were produced by Liquids Research Limited (Bangor, UK) by means of the co-precipitation technique [2] and were coated with dimercapotsuccinymid acid. Intratumoral injection of MNP was performed by slow bolus injection of 0.25 mg Fe / 100 mm^3 tumor. Mice were then imaged using a microCT Scanner (TomoScope Synergy Twin, CT-Imaging GmbH, Erlangen, Germany) using a low radiation dose protocol (29s, 65kV) under isoflurane anesthesia. MNP distribution and volume were analyzed with the Imalytics Research Software (Philips Technologie GmbH, Aachen, Germany). For hyperthermia treatment, the tumor of anesthetized animals was placed inside the coil of an alternating magnetic field (AMF, H = 15.4 kA/m, f = 435 kHz) for 60 min and tumor surface temperature was additionally monitored using an infrared thermography camera. Photographs of animals were taken before and two days after magnetic hyperthermia treatment.

Results

MNP had a core diameter of 12 nm, a hydrodynamic diameter of 77 nm and a specific absorption in rate in water of 900 ± 22 W/g Fe. After intratumoral application, nanoparticles became clearly visible in the

microCT (Figure 1) and the extent of heterogeneity in distribution could be analyzed. Proximity to non-tumor tissue and the spine could also be measured. During in vivo magnetic heating tumor surface temperature was controlled to be between 42 and 50°C. Tumor regression as observed macroscopically correlated clearly with MNP distribution. Especially in the tumor regions farthest from MNP tumor growth was not influenced. On the other hand in regions where MNP were observed in microCT hyperthermic temperatures were achieved and led to tumor decay.

Conclusion

By monitoring MNP distribution after intratumoral injection, planning and outcome of magnetic hyperthermia therapy can be improved. Known regions of MNP undersupply can be reached by increasing AMF power. Safety of the treatment can be improved by avoiding high temperatures in regions where MNP are close to non-tumor structures.

Figures

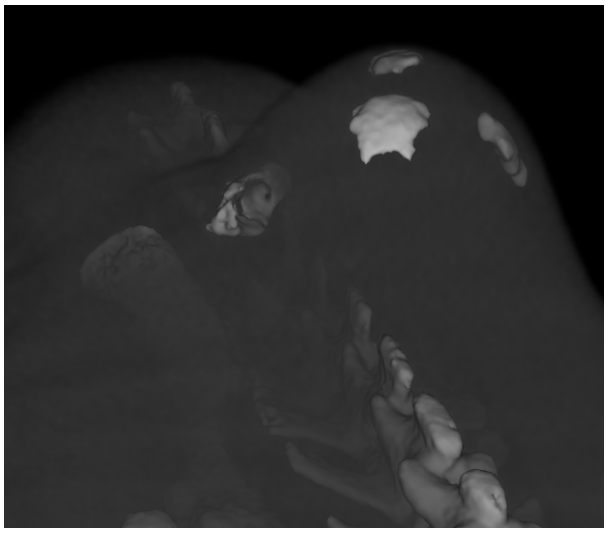

Figure 1: MNP Distribution after intratumoral injection into a tumor bearing mouse. 3D reconstruction of data acquired using an in vivo micro CT. Reconstruction was conducted with Imalytics Software.

Acknowledgments

The described work was carried out within the project “Multifunctional Nanoparticles for the Selective Detection and Treatment of Cancer” (Multifun), which is funded by the European Seventh Framework Program (FP7/2007-2013) under grant agreement no. 262943. We thank S. Burgold, Y. Ozegowski and J. Göring for animal handling. We acknowledge Liquids Research Limited, Deiniol Road, Bangor, Gwynedd, United Kingdom for providing the magnetic material.

References

[1] Hilger I, Rapp A, Greulich K-O, Kaiser WA. Assessment of DNA damage in target tumor cells after thermoablation in mice. Radiology. 2005 Nov;237:500–6.

[2] Reimers, G.W. and S.E. Khalafalla, US Bureau of Mines, Tech. Prog. Rep. 59, 1972.

Influence of Silica-Encapsulation on the Hydrodynamical Properties of Ni Nanorods

F. Krämer, D. Pieter, P. Bender, A. Tschöpe, R. Birringer

Experimentalphysik, Universität des Saarlandes, 66123 Saarbrücken

Ni nanorods are ferromagnetic particles with distinct optical anisotropy. Protected by an organic surface layer (Polyvinylpyrrolidone: PVP), the nanorods can be dispersed in aqueous colloidal suspension. By applying external magnetic fields, the nanorods can be forced into an oscillating motion which can be detected by optical transmission measurements. Analysis of the rotational dynamics allows the extraction of information regarding viscoelastic properties of the matrix and hydrodynamic parameters of the nanorods. However, the organic surface layer does not provide a geometrically and chemically well defined particle-matrix-interface. Hence, theoretical models for their rotation diffusion behavior like the Tirado Model [1, 2] show significant discrepancies in both the mean relaxation frequency of the rods and the width of its distribution.
As an alternative, we explore the potential of Ni nanorods with an inorganic silica shell.

1 Synthesis

The rods were synthesized by current-pulsed electrochemical deposition of Ni into porous alumina templates as described by Masuda [3, 4]. During the dissolution of the alumina matrix, the PVP adsorbed at the rod surfaces and served as steric stabilizer in the resulting colloidal dispersion. Starting with this fluid, the Stöber process was used to produce silica encapsulated Ni nanorods [5]. These were dispersed in water again to obtain a colloidal dispersion.

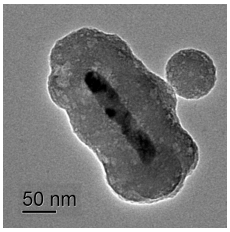

Figure 1: TEM micrograph of a typical silica encapsulated nanorod. The crystalline structure of the Ni core can be observed through the amorphous silica shell.

2 Characterization

First, the rods were characterized by transmission electron microscopy (TEM) to obtain their size distribution (Fig. 1). This revealed a diameter of the PVP coated rods of $25 \pm 4\,\mathrm{nm}$, a length of $135 \pm 30\,\mathrm{nm}$ and a mean thickness of the silica shell of $120\,\mathrm{nm}$. Following the Tirado Model, the relaxation frequency $\omega_c(l, d)$ of every single rod observed in the TEM was calculated through its length l and diameter d

$$\omega_c = \frac{3m\mu_0 H_0}{\pi\eta l^3}\left(\ln\left(\frac{l}{d}\right) + k(l,d)\right)$$

where m is the rods' magnetic moment , $\mu_0 H_0$ the absolute value of the external field, η the viscosity and $k(l, d)$ a correction term. This revealed a logarithmic normal distribution

$$f(\omega_c) = \frac{1}{\omega_c\sigma\sqrt{2\pi}}\exp\left(\frac{-\ln^2\left(\frac{\omega_c^0}{\omega_c}\right)}{2\sigma^2}\right)$$

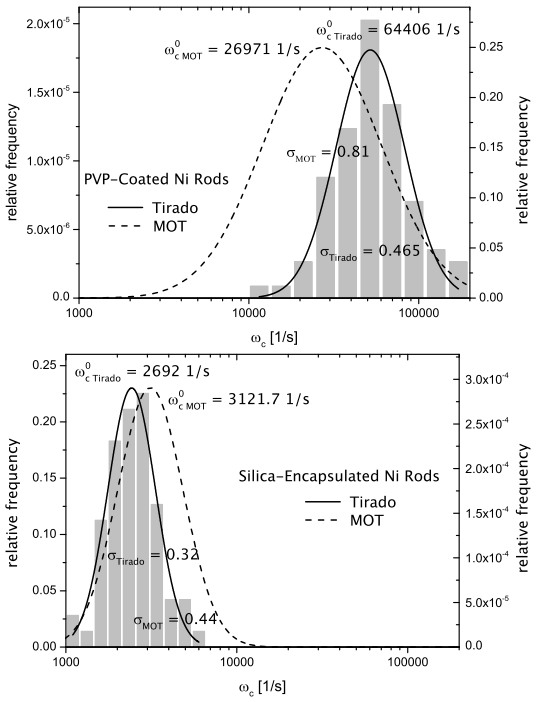

Figure 2: Distributions of relaxation frequencies expected using the Tirado model and from the MOT measurements.

of the relaxation frequencies ω_c for both samples with the silica encapsulated rods and with PVP-coated rods (Fig. 2).

Experimental values for the relaxation frequencies of the rods with and without the silica shell were obtained from Magneto-Optical Transmission measurements (MOT) in an oscillating magnetic field. The optical anisotropy of the rods was used to measure the time-dependent rotation angle of the nanorods from which the frequency-dependent phase shift between the rods and the driving external magnetic field was retrieved. This phase shift was analyzed for the distribution function of the rods' relaxation frequencies. Fig. 2 compares the distribution of the relaxation frequencies for both samples obtained by the MOT measurements to the ones expected by the Tirado model.

3 Results

The silica encapsulated rods show lower relaxation frequencies with a more narrow distribution due to their change in length and diameter compared to the PVP coated rods. With respect to the values expected by the Tirado model, the MOT measurements of the rods with the PVP layer show large discrepancies in the mean relaxation frequency ($\frac{\omega^0_{c,\mathrm{Tirado}}}{\omega^0_{c,\mathrm{MOT}}} \approx 2.4$) and the width of its distribution ($\frac{\sigma_{\mathrm{Tirado}}}{\sigma_{\mathrm{MOT}}} \approx 0.57$). The silica encapsulated rods agree much better with the theoretical model: $\frac{\omega^0_{c,\mathrm{Tirado}}}{\omega^0_{c,\mathrm{MOT}}} \approx 0.9$ and $\frac{\sigma_{\mathrm{Tirado}}}{\sigma_{\mathrm{MOT}}} \approx 0.73$, respectively. This indicates a geometrically much better defined particle-matrix-interface, as desired.

4 Outlook

For further experiments, the silica encapsulated rods can be functionalized for dispersion in a wide range of matrices to provide new model systems for the investigation of particle-matrix-interactions.

References

[1] M.M. Tirado and J.G. de la Torre, JCP **73**, 1986 (1980)

[2] M.M. Tirado, C.L. Martinez and J.G. de la Torre, JCP **81**, 2047 (1984)

[3] H. Masuda, Jpn. J. Appl. Phys. **35** (1996), L126-L129

[4] K. Nielsch et al, Adv. Mat. 2000; 12 No.8; 582

[5] V. V. Hardikar und E. Matijevic, Journal of colloid and interface science 221, 133-136 (2000)

Anisotropy in thermal conductivity in ferrofluids

M. Krichler, S. Odenbach

Chair of Magnetofluiddynamics, Measuring and Automation Technology, TU Dresden, 01062 Dresden

Introduction

In ferrofluids two main peculiarities can be found, with the first being the ability to attract the fluid with an external magnetic field gradient and the second being the magnetic driven interaction between the particles which is the cause for material changes in viscosity and sound propagation [1]. Our experimental investigation shows that also the thermal conductivity in ferrofluids can be subject of large changes in the presence of a magnetic field and that these changes are anisotropic.

Experimental Setup

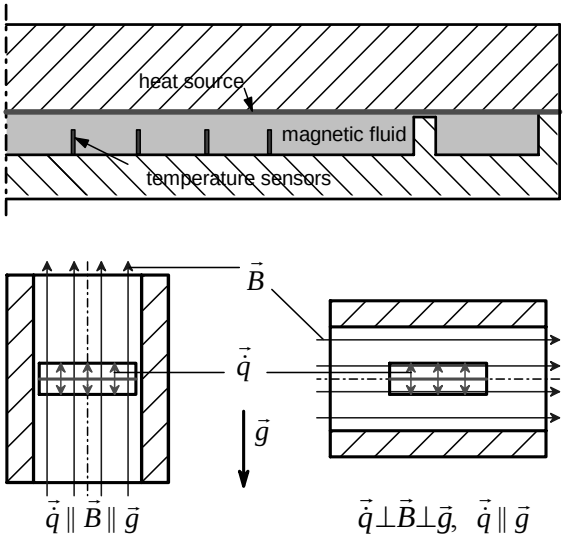

Figure 1: sketch with a cross-sectional view of the planar measurement device (upper side) for thermal conductivity measurements embedded in a helical coil for parallel alignment of magnetic field an heat flux (left side) an for perpendicular alignment (right side)

We have performed thermal conductivity measurements [2] in ferrofluids with a magnetic field applied parallel or perpendicular to the heat flux direction. The measuring device operates according to the plane heat source method to guarantee an uniaxial heat flux.
The 15 investigated ferrofluids differ in volume concentration, particle size distribution, viscosity and surfactant length. With a regularization method [3] we obtained the particle size distributions from magnetisation measurements. In general the mean diameter is about 9 nm.

Results

We found that in all examined liquids an impact of a magnetic field on heat flux can be seen. For a parallel alignment of heat flux and magnetic field the thermal conductivity is increased, and decreased for perpendicular alignment (Fig.2). This is in qualitative accordance with [4]. The quantity of increase for parallel alignment was always bigger than the quantity of decrease for perpendicular alignment. We did not find a good correlation of the measured changes with the volume fraction weighted interparticle interaction parameter

$$\lambda_w^* = \sum_i \varphi_i \lambda_i^* , \quad \lambda^* = \frac{\mu_0 M_0^2 V}{24 k_B T} \left(\frac{d}{d+2s} \right)^3 . \quad (1)$$

The index i denotes the fraction of each particle size d of the particle size distribution. Instead we graph the changes in thermal conductivity as function of a combined term of volume concentration and interparticle interaction parameter $\varphi^2 \lambda_w^*$. For an initial increase of this parameter up to 50 the changes in thermal conductivity increase. But for a further increase of $\varphi^2 \lambda_w^*$ the changes in thermal conductivity begin to decrease again. We believe the reason for these two different behaviours can be

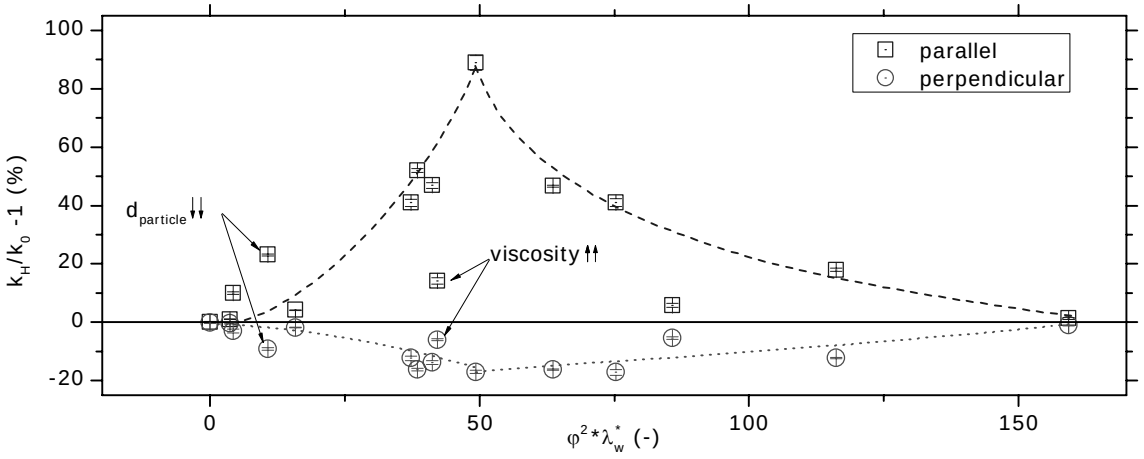

Figure 2: relative change in thermal conductivity at H = 40 kA/m as function of $\varphi^2*\lambda^*_w$ for parallel and perpendicular alignment of heat flux and magnetic field. Lines are just a guide for the eye.

found in two different mechanisms of interparticle interaction. For low values of the combined interaction parameter we believe that the small particles dominate the interaction between the particles. These have an increased movement parallel to the magnetic field [5]. With a further increasing combined interaction parameter more structure formation occurs which on the one hand increases the heat flux along those chainlike structures but on the other hand reduces the particle motion parallel to the magnetic field [6,7] which reduces heat transport via diffusion. At a certain level of the combined interaction parameter both mechanisms take place resulting in the largest measured changes in thermal conductivity. However the almost vanished change in thermal conductivity at a value of $\varphi^2\lambda^*_w \approx 160$ is astonishing and not completely understood yet. One possible explanation is that large clusters of particle are formed which have a small aspect ratio.

Conclusion

The measured changes in thermal conductivity in ferrofluids under a magnetic field are influenced by the volume fraction of suspended particles. We also believe the changes are subject to the impact of two different mechanism, heat bridging alongside chainlike structures and the change in diffusivity parallel to the magnetic field as function of the particle size.

Acknowledgments

Financial support by *Deutsches Zentrum für Luft- und Raumfahrt* under grant number DLR 50 WM 0639 and 50 WM 1235 is gratefully acknowledged.

References

[1] W.E. Isler, D.E. Chung, Ultrasonic Symposium Proc. IEEE Cat. #**78**CH 1344-ISU (1978) 409

[2] M. Krichler, S. Odenbach, J Magn. Magn. Mater **326** (2013) 85

[3] T. Weser, K. Stierstadt, Z. Phys. B: Con. Mat. **59** (1985) 253

[4] E. Blums, A. Cebers, M.M. Majorov, Magnetic Fluids, de Gruyter, Berlin, New York 1997

[5] J.C. Bacri, A. Cebers, A. Bourdon, G. Demouchy, B.M. Heegard, B. Kashevsky, R. Perzynski, Phys. Rev. E **52** (1995) 52

[6] J. Jordanovic, S. Jäger, S.H.L. Klapp, Physical Review Letters **106** (2011) 038301

[7] P. Ilg, M. Kröger, Phys. Rev. E **72** (2005) 031504

Magnetic Particle Spectrometer with up to 100 kHz drive frequency

C. Kuhlmann, T. Wawrzik, M. Schilling, F. Ludwig

Institut für Elektrische Messtechnik und Grundlagen der Elektrotechnik, TU Braunschweig, Hans-Sommer-Str. 66, 38106 Braunschweig

Introduction

Magnetic iron oxide nanoparticles can be used as tracer for a new imaging modality called "Magnetic Particle Imaging" (MPI) [1]. Recent studies have shown that an increase in the drive field frequency may be necessary to avoid nerve stimulation [2].
In order to evaluate the MPI performance of nanoparticles, a magnetic particle spectrometer (MPS) can be used.We have shown that a variation of the drive field frequency of such a spectrometer is very beneficial for particle characterization [3]. On the other hand, if particle properties are known, a combination of spectra at different drive frequencies can be used to deduce particle mobility [4]. Applications could be binding assays or the investigation of the particle interaction with the surrounding matrix.
In order to characterize nanoparticles for future generations of MPI systems, an extended frequency range up to 100 kHz is required. We have constructed an improved magnetic particle spectrometer that can utilize discrete drive field frequencies of 10 kHz, 25 kHz, 50 kHz and 100 kHz and therefore allows one to evaluate the MPI performance of nanoparticles at all commonly used MPI drive field frequencies. The amplitude of the excitation field can be as high as 25 mT (rms) which exceeds the drive field amplitudes of all current MPI systems and therefore allows one to study a wide set of parameters.

System setup

The MPS system consists of a solenoidal drive coil that generates the pure sinusoidal magnetic field which is applied to the nanoparticle suspension. The nonlinear particle magnetization curve leads to the generation of higher harmonics of the drive frequency which are measured using a gradiometric detection system.
In order to allow particle characterization under the influence of a static magnetic field, the system can be equipped with additional coil pairs perpendicularly to the drive field. These coils serve to imitate the gradient field used in MPI for spatial encoding. A second system of detection coils allows one to record the particle response in these directions as well.

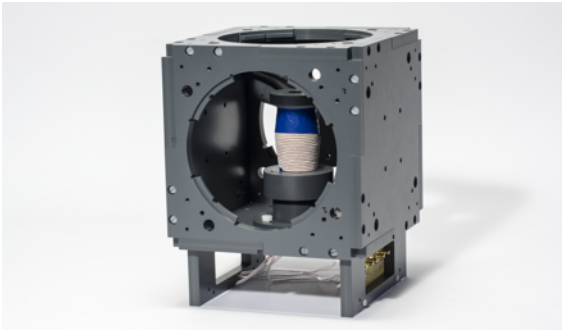

Front view of the MPS coil system showing the drive coil in the center.

Measurements

We have used the system to measure the response of magnetic nanoparticles at different drive field frequencies. We measured the response of a 150 µl sample of UW-1 particles from the Krishnan Labs, University of Washington, USA, in comparison to a 150 µl sample of FeraSpin^{TM} R particles from nanoPET GmbH, Berlin, Germany. FeraSpin

particles are a replacement for Resovist® which is the standard tracer for MPI. Measurements were performed at 25 kHz, 50 kHz and 100 kHz with 25 mT (rms) field amplitude. We examined a mobile, as well as a freeze-dried sample to identify the contributions of the Brownian and the Néel process.

Results

The data has been normalized to the iron concentration of the sample to allow better comparison.
Results show that the mobile sample of UW-1 generates approximately 9 to 12 dB higher detection signals for the same iron concentration while the steepness of the harmonic decay is also marginally smaller.

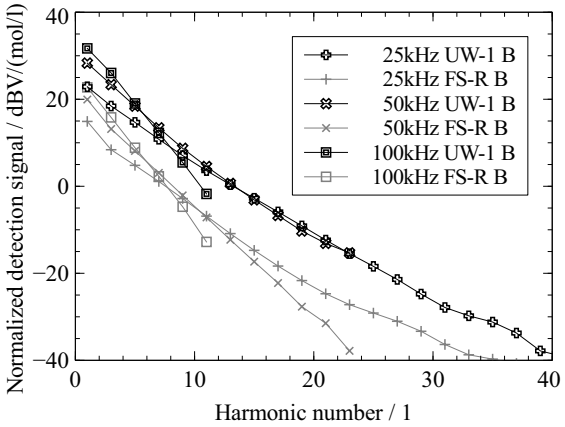

Results obtained from mobile samples of UW-1 and FeraSpin-R particles. The detection signal was normalized to the particle concentration of 26 mM *for UW-1 and* 50 mM *for FS-R particles.*

The freeze-dried sample of UW-1 shows a much smaller detection signal compared to FeraSpin, due to the large core size of 20 nm compared to the approx. 5 nm crystallite size of FeraSpin. Therefore the UW-1 particles exhibit a larger Néel time constant and cannot follow the drive field in their immobilized state, while the response of freeze-dried FeraSpin particles shows only minor differences compared to the mobile sample.
Both particle types show a similar harmonic decay which increases with the drive frequency. This counteracts the frequency-proportional gain due to Faraday's law when using coils as a detection system. Therefore, higher harmonics fall below the amplitudes of their equivalents at lower drive frequencies beyond a certain point.

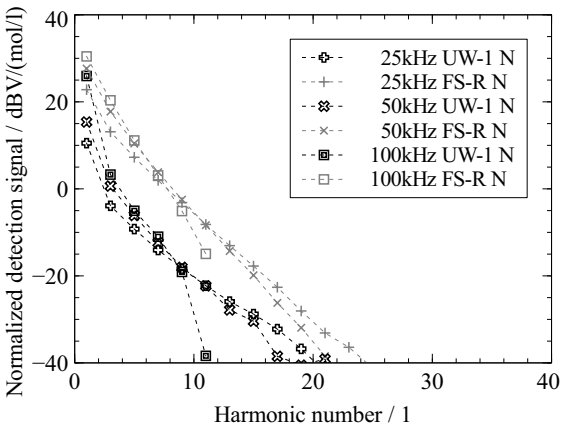

Results of the immobilized samples of UW-1 and FeraSpin-R

Although both particles have proven to be suitable for MPI at 100 kHz drive field frequency due to the rich spectrum of harmonics, further investigations are required.

Acknowledgments

Funding by BMWi under FKZ KF3061201UW2 is gratefully acknowledged.

References

[1] Gleich, B. and Weizenecker, J., Nature **435** (2005) 1214.

[2] Schmale, I. et al., in *Magnetic Particle Imaging (IWMPI), 2013 International Workshop on*, online, 2013.

[3] Ludwig, F. et al., Biomed. Eng. (2013) (in press)

[4] Wawrzik, T. et al., in *Magnetic Particle Imaging (IWMPI), 2013 International Workshop on*, online, 2013.

Retarding the Growth of the Rosensweig Instability: Theory and Experiment

A. Lange[1], C. Gollwitzer[2], I. Rehberg[2] and R. Richter[2],

[1] *TU Dresden, Institute of Fluid Mechanics, Chair of Magnetofluiddynamics, Measuring and Automation Technology, 01062 Dresden, Germany*
[2] *Experimentalphysik V, Universität Bayreuth, D-95440 Bayreuth, Germany*

Introduction

The Rosensweig or normal field instability [1] is observed in a horizontal layer of magnetic fluid (MF) with a free surface, when a critical value B_c of the vertically oriented magnetic induction is surpassed. The growth rate of this instability is both accessible to an experimental observation and a theoretical calculation, it provides a quantitative test of our understanding of the dynamic behaviour of these polarizable liquids. Up to now, no quantitative agreement between theory and experiment of this viscosity-dependent parameter has been observed. Thus, we provide here measurements in a highly viscous fluid, and discuss the results using refinements of the theoretical description.

System

Whereas so far the growth rate of the emerging Rosensweig pattern has been measured utilizing ferrofluids with $\eta = 4.2 \times 10^{-3}$Pa s [2, 3] and 52×10^{-3}Pa s [3] we are tackling here the growth process in a MF which is a thousand times more viscous than the first one. Such a MF is being created by cooling the commercially available viscous magnetic fluid APG E32 (Ferrotec Co.) in our setup by means of Peltier elements [4]. The viscosity has been measured in a temperature range of $-5\ ^\circ\mathrm{C} \leq \theta \leq 20\ ^\circ\mathrm{C}$, using a commercial rheometer (MCR 301, Anton Paar). At room temperature, the magnetic fluid with a viscosity of $\eta = 2\,\mathrm{Pa\,s}$ is 2000 times more viscous than water. The viscosity data can be nicely fitted with the Vogel-Fulcher law $\eta = \eta_0 \exp\left[\psi/(\theta - \theta_0)\right]$ with $\eta_0 = 0.48\,\mathrm{mPa\,s}$, $\psi = 1074\,\mathrm{K}$, and $\theta_0 = -107.5\ ^\circ\mathrm{C}$. For the present measurements, we chose a temperature of $\theta = 10\ ^\circ\mathrm{C}$, where the viscosity amounts to $\eta = 4.48\,\mathrm{Pa\,s}$.

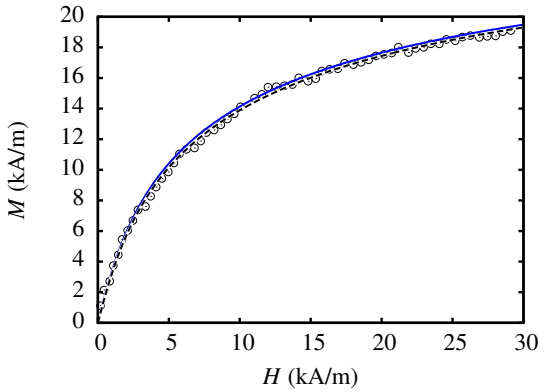

Figure 1: Magnetization curve of the magnetic fluid APG E32. The symbols show the measured data at $\theta = 20\ ^\circ\mathrm{C}$. The dashed line is a fit with the model by [5]. The solid line shows an evaluation of the model at $\theta = 10\ ^\circ\mathrm{C}$.

The magnetization curve has been determined using a fluxmetric magnetometer (Lakeshore Model 480) at a temperature of $\theta = 20\ ^\circ\mathrm{C}$ (Fig. 1). For a comparison with the pattern formation experiments, this curve is extrapolated to $\theta = 10\ ^\circ\mathrm{C}$ by the modified mean field model [5].

Results

The experimentally determined growth rates

are compared with the calculated ones, where the nonlinear magnetization curve is taken into account (for details see [3]). The former are indicated as black squares in Fig. 2. The growth rates show very small errors and a nearly perfect linear dependence on the magnetic induction B. Both features motivate a linear fit, indicated by the dashed line, to extract the critical induction with a value of $B_{\mathrm{c,\,exp}} = 11.23\,\mathrm{mT}$ (vertical black solid line). This experimentally determined critical induction is 7% above the theoretical one, $B_{\mathrm{c,\,theo}} = 10.52\,\mathrm{mT}$, based on the material parameters. According to the uncertainties of the different material parameters, it seems reasonable to consider the surface tension σ as the only fit parameter. By using a value of $\sigma = 38.7\,\mathrm{mN/m}$ the theoretically calculated critical induction equals the experimental one. The resulting growth rates are shown in Fig. 2 as a solid line. A comparison with the experimental data reveals a systematic deviation.

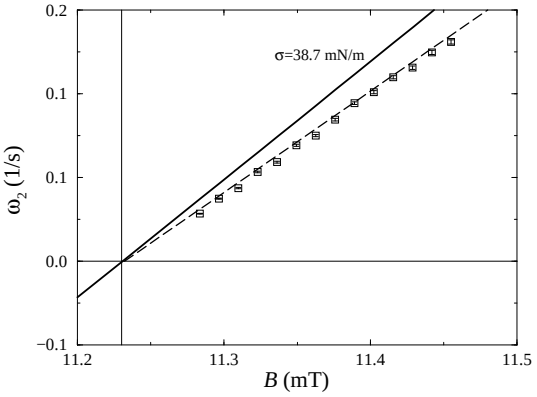

Figure 2: The growth rates ω_2 as a function of B. The symbols with error bars represent the measured data. The dashed line shows a linear fit to the experimental growth rates resulting in $B_{\mathrm{c,\,exp}} = 11.23\,\mathrm{mT}$ (vertical line). The solid line shows the theoretical growth rates for $\sigma = 38.7\,\mathrm{mN/m}$.

Using the surface tension as a fit parameter to match the values of ω_2 instead, entails a rescaling of B by $\hat{B} = (B - B_{\mathrm{c,\,i}})/B_{\mathrm{c,\,i}}$,

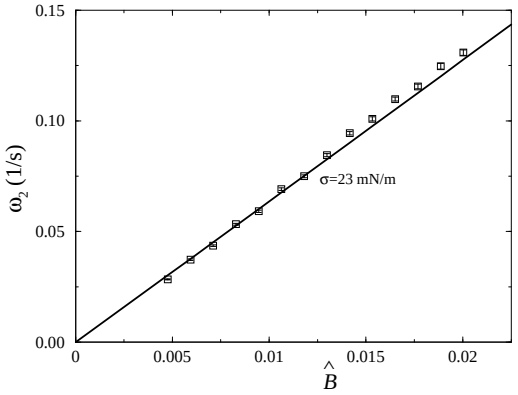

Figure 3: The growth rates ω_2 as a function of $\hat{B}$. The symbols with error bars represent the measured data. The solid line indicates the theoretical growth rates for $\sigma = 23\,\mathrm{mN/m}$.

where $B_{\mathrm{c,\,i}}$ is the critical induction of the corresponding data set. A least square fit yields $\sigma = 23\,\mathrm{mN/m}$ (solid line). Now the experimentally determined rates can be well described by the theory, see Fig. 3.
Since the fit value of σ differs from the value of the *static* surface tension measured in advance of the experiments, the relation between growth rates and the *dynamic* surface tension will be discussed in our contribution in more detail.

References

[1] M. D. Cowley and R. E. Rosensweig, J. Fluid Mech. **30**, 671 (1967).

[2] A. Lange, B. Reimann and R. Richter, Phys. Rev. E **61**, 5528 (2000).

[3] H. Knieling, R. Richter, I. Rehberg, G. Matthies and A. Lange, Phys. Rev. E **76**, 066301 (2007).

[4] C. Gollwitzer, I. Rehberg, R. Richter, New J. Phys. **12**, 093037 (2010).

[5] A. O. Ivanov and O. B. Kuznetsova, Phys. Rev. E **64**, 041405 (2001).

Dynamics and Self-assembly of α-Fe_2O_3 Ellipsoids

J. Lebert[1], M. Kundt[1], A. Schmidt[1,*]

[1] *Institut für physikalische Chemie, Universität zu Köln, Luxemburger Straße 116, D-50939 Köln*

Dispersions of rodlike particles are known to show liquid-crystalline behaviour at high concentrations. This phenomenon is caused by the self-assembly of the interacting rods within the dispersant. A theoretical model on the phase-transition from a disordered isotropic to an ordered liquid-crystalline phase has first been published by Onsager in 1949. [5] If the particles possess a magnetic component, particle-particle as well as particle-field interactions give rise to an additional contribution to the phase behavior.

For the low concentration regime without particle-particle interaction the hydrodynamic properties of anisotropic particles like rods or prolate ellipsoids can be easily characterized by depolarized dynamic light scattering (DDLS). [1,2] The rotational and translational diffusion properties of elongated particles are highly affected by their shape, size and aspect ratio, and can be described based on several theoretical models. The most common are propably the ones of Tirado and Torre [3] as well as Perrin. [4]

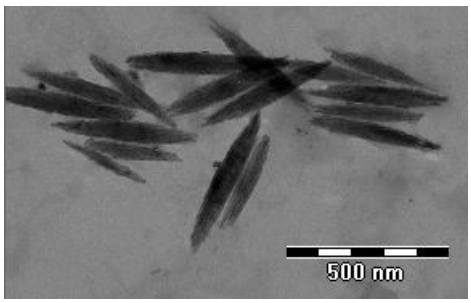

Fig. 1: TEM image of α-Fe_2O_3 ellipsoids.

In the present work, we employ α-Fe_2O_3 ellipsoids with aspect ratios up to about 7. Due to a canted antiferromagnetism, the ellipsoids show a magnetic easy axis perpendicular to their long axis. They show superparamagnetic behaviour in dispersion.

The particles are decorated by different surface functionalizations to prevent agglomeration; citrate and poly(oligo-ethyleneglycol)methylethermethacrylate, respectively. Colloids of these particles are analyzed in respect to their diffusional and rotational behaviour, their magnetic properties and formation of liquid-crystalline phases.

The results for the translational (D_{trans}) and rotational (D_{rot}) diffusion coefficients for hematite ellipsoids from DDLS agree with theoretical values calculated according to the Tirado-Torre model in the regime of low concentration.

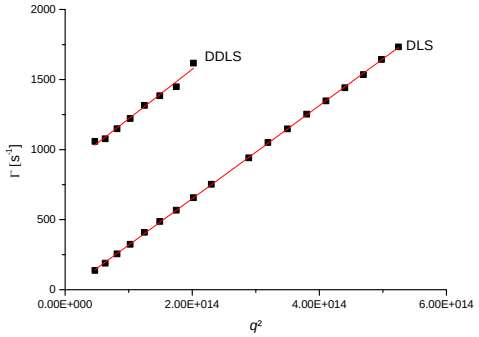

Fig. 2: Dynamic light scattering and depolarized dynamic light scattering measurement for hematite ellipsoids with aspect ratio 6.2.

The dynamics in an alternating magnetic field are analyzed via AC-susceptometry.

Polarization microscopy is used to detect the self-assembly of the ellipsoids, since optical birefringence is characteristic for liquid crystals. In a second step an external magnetic field is applied to induce particle

assembly and to obtain field strength dependent phase diagrams.

References

[1] D. Lehner, H. Lindner, O. Glatter, *Langmuir* **2000**, 1689–1695.

[2] H. Matsuoka, H. Morikawa, H. Yamaoka, *Colloids and Surfaces A: Physicochemical and Engineering Aspects* **1996**, *109*, 137–145.

[3] M. M. Tirado, C. L. Martínez, J. G. de la Torre, *The Journal of Chemical Physics* **1984**, *81*, 2047.

[4] F. Perrin, *Journal de Physique et le Radium* **1936**, *7*.

[5] L. Onsager, *Ann. N.Y. Acad. Sci.* 51, 627-659, **1949**

Spatial reconstruction of magnetic nanoparticle distribution using a non-negativity constraint

M. Liebl[1], U. Steinhoff[1], F. Wiekhorst[1], A. Coene[2], J. Haueisen[3], L. Trahms[1]

[1] *Physikalisch-Technische Bundesanstalt, 10587 Berlin, Germany*
[2] *Department of Electrical Energy, Systems and Automation, Ghent University, 9000 Ghent, Belgium*
[3] *Institute of Biomedical Engineering and Informatics, Ilmenau University of Technology, 98693 Ilmenau, Germany*

Introduction

Magnetic nanoparticles (MNP) are promising tools for novel cancer treatment approaches [1], e.g. as nanovehicles to deliver drugs in magnetic drug targeting. An essential prerequisite for the development of these approaches is a quantitative knowledge of the MNP distribution inside a body. Magnetorelaxometry (MRX) is a non-invasive method for the quantification of the MNP content inside biological samples [2]. Using a multi-sensor setup device a spatially resolved quantification of multiple MNP accumulations becomes feasible [2,3]. Furthermore, by sequentially applying different inhomogeneous excitation fields a spatial encoding of the MNP in a sample was achieved that increased the spatial resolution of the reconstruction, as suggested theoretically in [4,5,6]. Based on experimental MRX data measured by the PTB 304 SQUID-magnetometer we compare a minimum-norm estimation using a truncated singular value decomposition (denoted as TSVD-MNE) [5,6] and a nonnegative least squares (NNLS) algorithm [7] for the reconstruction of a known MNP distribution.

Methods

The experimental setup is shown in fig. 1. We used a compact volume phantom assembled of 54 individual gypsum cubes of 1 cm^3 volume, containing 12 cubes with with 5±0.07 mg MNP amount as shown in fig. 2. Alongside the phantom 48 planar spiral coils were mounted providing inhomogeneous magnetizing fields. The relaxation amplitudes ΔB_{meas} were calculated as the difference of the relaxation signals $\mathbf{B}(t)$ (measured by 171 sensors) between two fixed time instants

$$\Delta B_{meas} = B_{t_1=100\,\mathrm{ms}} - B_{t_2=1.5\,\mathrm{s}} \qquad (1)$$

Forward Problem: We divide the sample volume into K voxels and aim to determine the MNP amounts $X_{\mathrm{MNP},k}$ of each voxel. In case of small magnetizing fields the partial magnetic flux density B_k at the sensor location $\mathbf{r}_s$ resulting from the relaxation of MNP within the kth voxel is proportional to $\chi_{\mathrm{MRX}} \circledcirc \mathbf{H}_k \circledcirc X_{\mathrm{MNP},k}$. The relaxation susceptibility χ_{MRX} is MNP specific and was determined separately by a conventional MRX measurement of a single MNP containing cube.

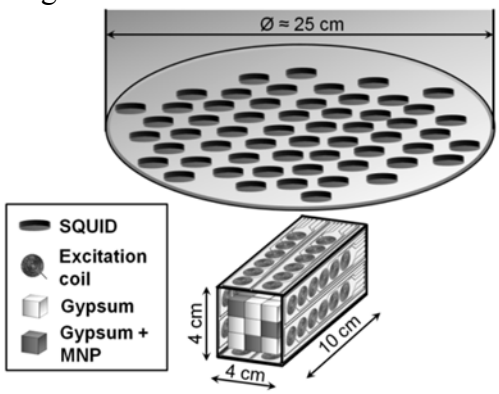

Figure 1: Sketch of the measurement setup used for MRX with inhomogeneous magnetizing of the MNP phantom showing the PTB 304 SQUID device, arrangement of magnetizing coils and 54 gypsum cubes (12 MNP loaded).

Thus the magnetic flux density is given by

$$\Delta B_k = \frac{\mu_0}{4\pi}\left[\left(\frac{3\cdot\mathbf{n}^{\mathrm{T}}(\mathbf{r}_k\mathbf{r}_k^{\mathrm{T}})}{|\mathbf{r}_k|^5} - \frac{\mathbf{n}^{\mathrm{T}}}{|\mathbf{r}_k|^3}\right)\cdot\mathbf{H}_k\,\chi_{\mathrm{MRX}}\right] X_{\mathrm{MNP},k} \qquad (2)$$

with $\mathbf{n}$ being the normal vector of the sensor orientation and $\mathbf{H}_k$ the magnetizing field in the kth voxel. The right hand side of eq. 2 can be separated into geometry

parameters and source parameters to $\Delta B_k = \mathbf{L} \odot X_{MNP,k}$. The total relaxation amplitude ΔB follows by superposition of the field contributions of all voxels

$$\Delta B = \sum_k L_k X_{MNP,k} = \mathbf{L} \cdot \mathbf{X}_{MNP} \qquad (3)$$

Using multiple magnetizing coils and multiple sensors, $\Delta\mathbf{B}$ becomes a vector and $\mathbf{L}$ is a matrix of dimension ($N_{sensors} \odot N_{coils} \times K$).

Inverse Problem: The MNP content $X_{MNP,k}$ in each voxel can then be determined [5,6] applying a minimum norm estimation employing the Moore-Penrose pseudoinverse $\mathbf{L}^+ = (\mathbf{L}^T\mathbf{L})^{-1}\mathbf{L}^T$ calculated by a TSVD

$$\mathbf{X}_{MNP,est} = \mathbf{L}^+ \Delta\mathbf{B}_{meas} \qquad (4)$$

Alternatively, eq. 4 can be also solved by an active set NNLS algorithm [7] until a set of $\mathbf{X}_{MNP,est}$ is found that satisfies the constraints $\mathbf{X}_{MNP,est \geq 0}$.

Results

The results obtained by both estimations are shown together with the nominal MNP distribution in fig 2. For both algorithms the reconstructed total MNP amount is close to the nominal amount of MNP. The TSVD-MNE reconstructed in some voxels negative MNP amounts and resulted in a total MNP content about 10 % below the nominal value. As expected, less deviation (3 %) was found for the NNLS reconstruction.

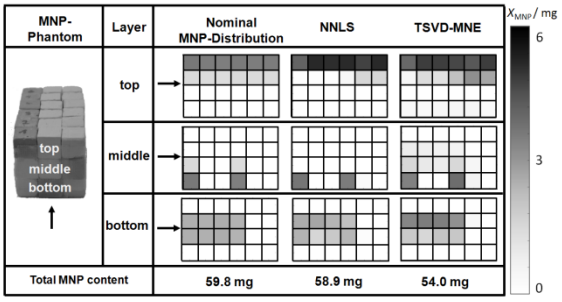

Figure 2: Nominal MNP cube distribution over each of the 3 layers of the phantom and reconstructed MNP amounts by NNLS and TSVD-MNE. The total MNP amount of the phantom is given in the bottom line. (negative MNP content is neglected)

Discussion

We investigated the quantitative imaging of an MNP distribution using sequential MRX with inhomogeneous magnetization [5,6]. We demonstrated that it is experimentally possible to reconstruct distributed MNP content in the milligram/cm^3 range within a volume of 54 cm^3. We also showed that the NNLS method can improve the quality of the reconstruction.

Acknowledgement

This work was financially supported by the DFG research programs "Magnetische Nanopartikel für die Krebstherapie" TR408/4-3 and "Magnetische Nanopartikel für die Zelluläre und Molekulare MR-Bildgebung" TR408/5-2.

References

[1] Q. A. Pankhurst et. al.: Applications of magnetic nanoparticles in biomedicine, J. Phys. D: Appl. Phys., vol. 36, pp. R167-R181, 2003.

[2] F. Wiekhorst et al.: Magneto-relaxometry Assisting Biomedical Applications of Magnetic Nanoparticles, Pharm. Res., vol. 29(5), pp. 1189-202, 2012.

[3] D. Baumgarten et al.: Magnetic nanoparticle imaging by means of minimum norm estimates from remanence measurements, Med. Biol. Eng. Comp., vol. 46, pp. 1177-1185, 2008.

[4] N. G. Sepulveda et al.: Magnetic susceptibility tomography for three dimensional imaging of diamagnetic and paramagnetic objects, IEEE Trans. Magn., vol. 30, pp. 5062-5069, 1994.

[5] U. Steinhoff et al.: Bildgebung magnetischer Nano-partikel basierend auf Magnetorelaxometrie mit sequentieller Aktivierung inhomogener Anregungsfelder, Biomed. Tech., vol. 55(1), pp. 22-25, 2010.

[6] G. Crevecoeur et al.: Advancements in magnetic nanoparticle reconstruction using sequential activation of excitation coil arrays using magnetorelaxometry, IEEE Trans. on Magn., vol. 48, pp. 1313-1316, 2012

[7] C. L. Lawson et al.: Solving Least Squares Problems, Prentice Hall., Chapter 23, p. 161, 1974.

Synthesis of iron oxide particles for magnetic fluids by ultrasonic aerosol assisted pyrolysis

J. Linke[1], M. Domaschke[1], S. Odenbach[1]

[1] *Institute of Fluid Mechanics, Chair of Magnetofluiddynamics, Measuring and Automation Technology, 01062 Dresden, Germany*

Introduction and Background

The physical properties of magnetic fluids depend significantly on the size, shape and composition of the dispersed magnetic phase. Equidimensional magnetite (Fe_3O_4) particles for example, are considered single-domain for mean diameters $d_m \lesssim$ 50-80 nm, with superparamagnetic characteristics for $d_m \lesssim$ 25-30 nm and magnetically non-interacting for $d_m \lesssim$ 10-13 nm [1, 2]. Hence control of the particle size distribution is a key requirement when synthesizing and studying magnetic fluids. For this ultrasonic aerosol assisted pyrolysis (UAAP) [3] offers a versatile synthesis route to tailor-made iron oxide particles.

UAAP Method for Particle Synthesis

Precursors for the UAAP are dilute solutions of formic acid and water-soluble iron salts, for instance chlorides, nitrates, citrates or gluconates. Figure 1 illustrates the experimental set up and the respective stages of the UAAP process.

The precursor solution is nebulized by six piezoceramic transducers (HM-2412, Honda Electronics, Japan) at 2.4 MHz to gain a fine aerosol with small droplet sizes. The aerosol is then fed into a vertical hot wall furnace where the droplets react to form solid iron oxide particles. The heated zone is 400 mm long and 55 mm in diameter. After the reaction, the particles are cooled and separated from the carrier gas flow in two gas washers with formic and oleic acid at pH3. The optimum absorbing capacity of the gas washers is at a carrier gas flow of 15 STL/min which is equivalent to an aerosol yield of approx. 115 ml water/h.

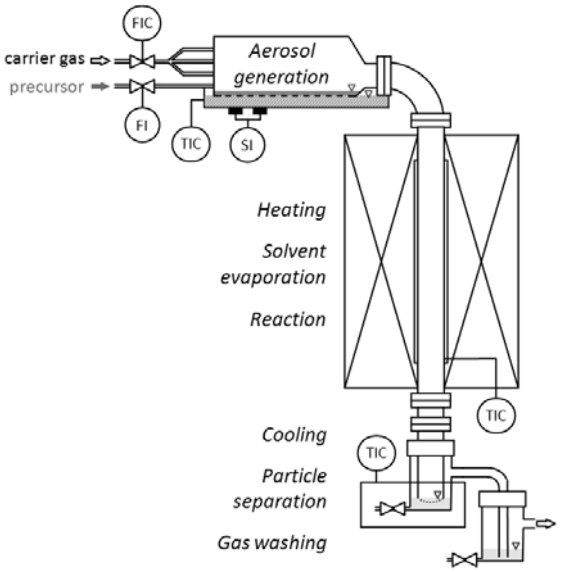

Fig. 1: Schematic plan of the UAAP set-up with process stages and monitoring points.

Results and Discussion

Crucial process parameters for the UAAP are the choice of the carrier gas, the reaction temperature and the concentration and composition of the precursor solution.
Common carrier gases are nitrogen or argon with hydrogen or ammonia as reducing agents. A cost-efficient alternative would be air. However, the oxygen contained in air oxidizes the iron salts to yield rust (α-Fe_2O_3). To avoid oxidation several co-precursor were tested to bind the oxygen. Formic acid was found to be a suitable co-precursor to enhance the yield of magnetic iron oxides (Fe_3O_4, γ-Fe_2O_3), undergoing the following possible reactions:

I) $2\ HCOOH \rightarrow 2\ CO_2 + 2\ H_2$
$2\ H_2 + O_2 \rightarrow 2\ H_2O$

II) $2\ HCOOH \rightarrow 2\ CO + 2\ H_2O$
$2\ CO + O_2 \rightarrow 2\ CO_2$

The addition of formic acid almost doubles the yield of magnetic iron oxides in UAAP from iron-(II) chloride. For other iron salts the yield of magnetic iron oxides was also increased above the level found in the synthesis from iron-(II) chloride without formic acid, summarized in figure 2. The maximum yield of magnetic oxides was reached at a reaction temperature of 700±20 °C.

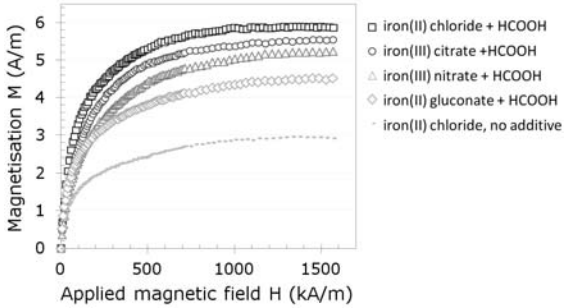

Fig. 2: Magnetisation of iron oxide particles grown from 0.3 mmol/kg iron salts with and without formic acid, HCOOH.

According to Lang [4] the droplet size of aerosols generated by ultrasound depends on the ultrasonic frequency f and the density ρ_ℓ and surface energy σ_ℓ of the atomized liquid. Assuming that each droplet reacts to give one spherical particle, the theoretical particle diameter d_p can be estimated by:

$$d_p \approx 0.34 \cdot \left(\frac{4 \cdot \pi \cdot \sigma_\ell \cdot c_\ell \cdot M_p}{\rho_p \cdot \rho_\ell \cdot f^2} \right)^{1/3}$$

with M_p the molar mass and ρ_p the density of the particle and c_ℓ the concentration of precursor salt.

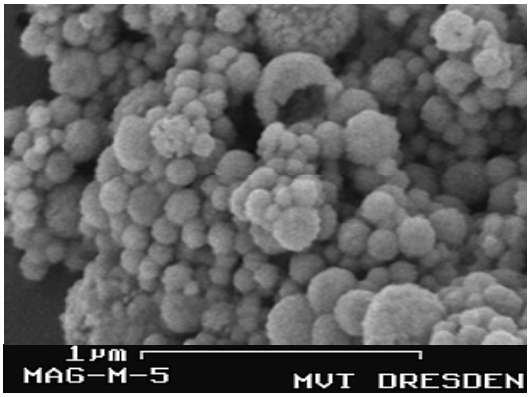

Fig. 3: Scanning electron microscopy image of iron oxide particles grown by UAAP from iron-(II) chloride and formic acid.

Particles grown in air are spherical but have a rougher surface than particles grown in inert gases (fig. 3). Their geometric diameter, given in figure 4, is larger than the expected theoretical diameter or the magnetic size determined from the initial magnetisation curve. This indicates that the air grown particles are multi-domain and hollow due to rapid precipitation at the droplet surface where the precursor is in contact with the reactive carrier gas. These particles would be ideal candidates for applications requiring large surface areas, e.g. waste water treatment or catalysis.

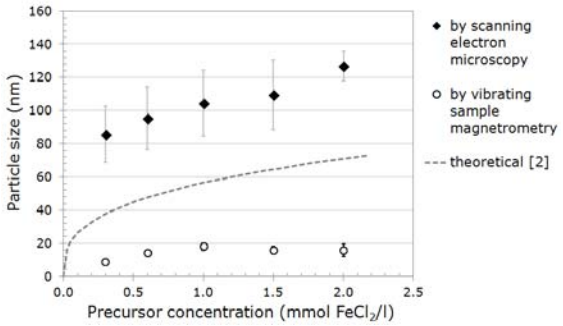

Fig. 4: Particle size in dependence of the precursor salt concentration for UAAP with iron-(II) chloride and formic acid.

Outlook

Future work will focus on UAAP particle growth with variation of the residence time and mixtures of nitrogen and air to obtain suitable particles for the synthesis of magnetic fluids. Further, it would be interesting to investigate reaction pathways to incorporate medical tracer materials into the particles during UAAP.

Acknowledgment

We thankfully acknowledge the funding of this project (OD-18/18-2) by the DFG.

References

[1] D. J. Dunlop, Phys. Earth Planetary Interiors 26 (1), 1981.
[2] M. Moskowitz, S.K. Benerjes, IEEE Trans. Magn. MAG-15, 1241, 1979.
[3] J. H. Bang, K.S. Suslick, Adv. Mater. 22, 1039-1059, 2010.
[4] R. J. Lang, J. Acoust. Soc. Am. 34 (6), 6-8, 1962.

First-order reversal curve (FORC-) analysis of magneto-active composite materials with mixed magnetic phases

J. Linke[1], T. Richter[1], S. Odenbach[1]

[1] *Institute of Fluid Mechanics, Chair of Magnetofluiddynamics, Measuring and Automation Technology, 01062 Dresden, Germany*

Introduction

A standard method for magnetic characterisation is the measurement of major hysteresis loops, i.e. the magnetisation in dependence of an applied magnetic field. These magnetisation curves present bulk averages. By contrast, the first-order reversal curve (FORC) method is based on a set of minor partial hysteresis loops. They provide information of the switching field distribution and local interaction fields between particles or grains. This allows the exploration of magnetic interactions in more complex composite materials.

Magneto-active Elastomers (MAEs)

MAEs consist of magnetic particles embedded in a non-magnetic elastomeric matrix [1]. The MAE samples were prepared from mixtures of carbonyl iron (~5 µm size) and NdFeB particles (~50 µm) in a 18 m% of silicon methyl-vinyl rubber and cross-linking agent (SIEL^{TM}). The mixtures were degassed before curing at 70-80°C for 3 hours. The MAE samples were characterised in a Lakeshore 7400 vibrating sample magnetometer.

First-order reversal curve method

Prior to measuring each FORC the magnetic field is first increased to saturation, then decreased to the so-called reversal field H_r. Starting from this reversal field the FORC is recorded as the magnetisation M when the applied magnetic field H_a is increased back to saturation. The reversal field H_r is changed for each FORC covering the field range from positive to negative saturation as illustrated in figure 1. The FORCs are fitted with a second-order polynomial function using the processing package FORCinel [2] to derive the final FORC distribution:

$$\mu(H_r,H_a) = -\frac{1}{2}\frac{\partial^2 M(H_r,H_a)}{\partial H_r \partial H_a} \qquad \text{(I)}$$

The FORC distribution $\mu(H_r,H_a)$ is plotted with an axis transformation so that the horizontal axis relates to the coercive field distribution H_c and the vertical axis to the interaction field distribution H_u.

$$H_c = \frac{H_r - H_a}{2},\ H_u = \frac{H_r + H_a}{2} \qquad \text{(II)}$$

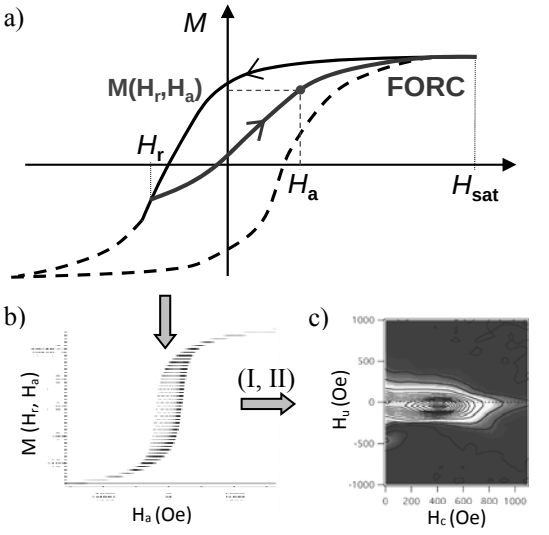

Fig. 1: a) FORC measurement protocol, b) FORCs, c) FORC distribution µ

Results and Discussion

NdFeB is magnetically hard, it has a high coercive resp. switching field (±75 kA/m). By contrast, carbonyl iron is magnetically

soft, it has a low coercive field, as shown in figure 2, meaning that the magnetic polarisation of the iron particles can be switched already by low magnetic fields.

When the two materials are mixed, the magnetically soft iron particles respond to the stray field of the neighbouring NdFeB particles. In FORCs with a negative reversal field larger than the coercive field of NdFeB, -75 kA/m < H_r < 0, the moments of the NdFeB particles are still positively magnetised. They can switch the negatively magnetised iron moments which relates to a negative interaction field distribution in the FORC distribution. Figure 3 shows the FORC distribution of an MAE sample with 35 vol% carbonyl iron in H_u, H_c space and its projection onto the FORCs.

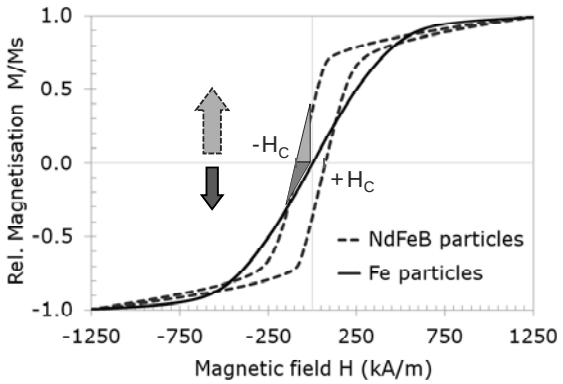

Fig. 2: Magnetisation curves of the pure materials. At low negative fields the materials behave differently, NdFeB is still positively magnetised, Fe negatively.

Theoretical studies by Panagiotopoulos [3] based on Preisach hysterons demonstrate that the interaction field distributions of the hard and soft phase in mixed systems shift with increasing interaction strength. The distribution of the soft phase shifts towards lower H_u and the distribution of the hard phase towards lower H_c values. These shifts could also be observed in the MAEs with increasing carbonyl iron content. However, the origin of the additional features that appear in MAEs with high iron loading and their relation to the elastic properties of the matrix is still unclear. Furthermore, theoretical studies for multidomain systems are still lacking.

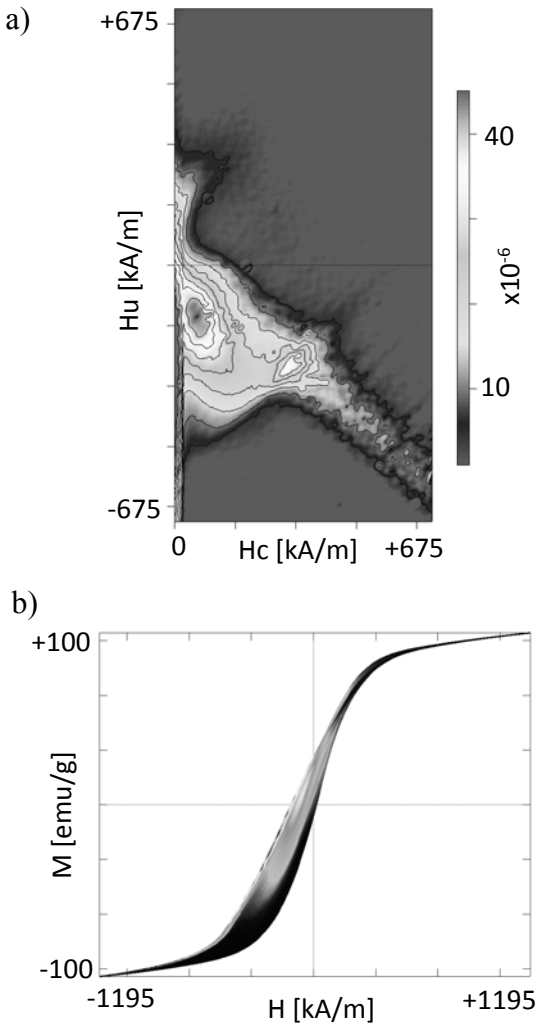

Fig. 3: Exemplary FORC distribution of a MRE sample with 35 vol% carbonyl iron in the magnetic phase: a) in H_u, H_c space, b) projection onto the FORCs.

Outlook

Future work will focus on understanding the role of the elastic matrix during magnetisation processes in MAEs, by varying the cross linking in the polymer and by studying temperature dependent FORCs.

References

[1] D. Borin, G. Stepanov, S. Odenbach, J. Phys.: Conf. Ser. 412, 012040, 2013.

[2] R. J. Harrison, J. M. Feinberg, Geochem. Geophys., Geosys. 9 (5), Q05016, 2008.

[3] I. Panagiotopoulos: J. Mag. Mag. Mat. 323 (16), 2148-2153, 2011.

Agglomerated Magnetite Crystals for Magnetic Particle Imaging

N. Löwa[1], S. Dutz[2], N. Buske[3] and L. Trahms[1]

[1]*Physikalisch-Technische Bundesanstalt, Berlin, Abbestraße 2-12, 10587 Berlin*
[2]*IPHT Jena, Albert-Einstein-Straße 9, D-07745 Jena*
[3]*Magneticfluids, Köpenicker Landstraße 203, 12437 Berlin*

Introduction

Magnetic Particle Imaging (MPI) is a promising novel medical imaging technique allowing the background-free localization of magnetic nanoparticles (MNP) with high temporal and spatial resolution [1]. In principle, it is based on the nonlinear magnetization response of MNP exposed to an external oscillating magnetic field. To this end, the properties of the used MNP are of fundamental importance for MPI image quality. So far, the clinical approved MRI contrast agent Resovist® is the mostly used MNP sample for MPI. Measurements revealed that a minority of aggregates (consisting of primary crystallites) within the fluid are responsible for Resovist®'s preferential performance [1,2]. Quite likely, this configuration is of crucial significance for MNP suitable for MPI. Anyhow, defining optimal particle properties for MPI are of special interest and recently of great debate [2,3].
The present article reports on preparation and characterization of aqueous ferrofluids (FF) containing specially designed MNP to be used as tracers for MPI. We used magnetic measurements (susceptometry, *M(H)*; magnetic particle spectroscopy, MPS), Transmission Electron Microscopy (TEM), Dynamic Light Scattering (DLS) and X-Ray Diffraction (XRD) to characterize the obtained MNP regarding size, structure, and magnetic properties.

Materials and Methods

Preparation

Following the example of Resovist®, stable clusters of small primary particles were prepared. For this, a hydrosol of clustered positively charged magnetite nanoparticles without any organic components was fractionated by ultracentrifugation and the sediment was discarded. The MNP in the supernatant were used as an intermediate to subsequently prepare carboxymethylated dextran-coated negatively charged MNP.

Measurement

For all size distributions, derived from XRD and *M(H)*, we assumed spherical particles with diameters d obeying a lognomal function $f(d)$. Based on these considerations, we estimated the diameter of the mean volume d_V and the dispersion parameter σ.
Saturation magnetization M_S and size distribution of effective magnetic domain diameters (i.e. effective magnetic core size) were estimated from *M(H)* data, according to [2]. The measurements were performed with a commercial susceptometer (MPMS, Quantum Design). In addition, we obtained the core size distribution, in terms of crystallite sizes, analyzing the shape of the XRD intensity distribution by using an X-ray diffractometer (X'Pert Pro MPD). Furthermore, the hydrodynamic diameter of the MNP was measured by DLS using the Zetasizer 3000 (Malvern Instruments, UK).
To evaluate the performance of the MNP as MPI tracer we used a magnetic particle spectrometer (MPS-3, Bruker) which can also be considered as a 0-dimensional MPI system. In this study, all MPS measurements were performed with 25 mT magnetic field amplitude and an excitation frequency of 25 kHz.

Results and Discussion

The estimated core size distribution parameters for the MNP hydrosol and the

coated MNP estimated by XRD are $d_{V,\mathrm{XRD}}$=8.5 nm and 8.5 nm as well as σ_{XRD}=0.36 and 0.37, respectively. Furthermore, the magnetic size distributions derived from *M(H)* data $d_{V,\mathrm{M\text{-}H}}$=6.4(1) nm and 6.4(1) nm / $\sigma_{\mathrm{M\text{-}H}}$ =0.537(4) and 0.531(5), respectively, are similar to those of the core size distributions from XRD. In contrast to Resovist®, neither for the core sizes nor for the magnetic sizes no bimodal distribution was found.

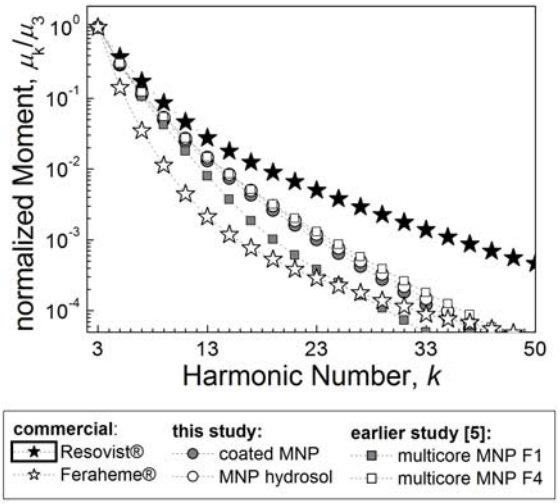

Figure 1: MPS measurement (25 mT, 25 kHz, results normalized to 3rd harmonic amplitude) of coated MNP (grey circles), MNP hydrosol (open circles) and the commercially available systems Resovist® (filled stars) and Feraheme® (open stars). For comparison, data for more compact multicore MNP (squares) of a previous study (prepared following a different route [5]) are shown.

The saturation magnetization M_S of the MNP hydrosol and the coated MNP, being 441(2) kA/m and 417(2) kA/m, respectively, were about 20% higher than for Resovist®.

DLS of the samples result in hydrodynamic diameter of $d_{V,\mathrm{DLS}}$=97 nm for the MNP hydrosol and $d_{V,\mathrm{DLS}}$=109 nm for the coated MNP. The difference in the sizes derived from DLS and XRD is an indication for the presence of clusters. The prepared clusters show a size of nearly twice the diameter of aggregates found in Resovist® ($d_{V,\mathrm{DLS}}$=45(7) nm [4]).

MPS signals of the investigated samples (normalized to their 3rd harmonic amplitude) are shown in Fig. 1. To be eligible for MPI application a tracer should produce many harmonic components (i.e. spectrum with low degree of decrease). As can clearly be seen, both samples exhibit a spectrum with similar slope but stronger than for Resovist®. The absolute signal amplitudes, normalized to the respective iron content, were about 20% less than Resovist® for the third harmonic and even less for higher harmonics. Compared to Feraheme® (an approved formulation of small single core MNP) the prepared clusters show higher MPS signal amplitudes until the 23rd harmonic and one order of magnitude higher when normalized to iron content.

Conclusion

As the measurement results show, clusters of small primary particles were prepared. Both, core size distribution and magnetic properties were not significantly influenced by the coating procedure. Compared to Resovist®, no second fraction of not clustered single cores could be identified from XRD and *M(H)* data. The MPS signals of the coated MNP and the MNP hydrosols were similar and in the order of Resovist® but exhibiting a steeper decay for higher harmonics. Probably, this problem can be solved by optimization of the packing density of the clusters - influencing exchange and dipole-dipole interactions between single cores by this way.

References

[1] B. Gleich, J. Weizenecker. *Nature* 435, 1214-17 (2005).

[2] D. Eberbeck, F. Wiekhorst, S. Wagner, L. Trahms. *Appl. Phys.* 98, 182502 (2011).

[3] R. M. Ferguson, A. P. Khandhar, K. Krishnan. *Appl. Phys.* 111, 07B318 (2012).

[4] D. Eberbeck, M. Kettering, C. Bergemann, P. Zirpel, I. Hilger, L. Trahms. *Appl. Phys.* 42, 405002 (2010).

[5] S. Dutz, D. Eberbeck, R. Müller, M. Zeisberger. In: Magnetic Particle Imaging, *Springer Proceedings in Physics* 140, 78-83 (2012).

Efficient drug-delivery using magnetic nanoparticles – biodistribution and therapeutic effects in tumour bearing rabbits

S. Lyer[1], R.Tietze[1], S. Dürr[1], T. Struffert[2], T.Engelhorn[2], M. Schwarz[2], A. Dörfler[2], E. Eckert[3], T. Göen[3], S. Vasylyev[4], W. Peukert[4], F. Wiekhorst[5], L. Trahms[5], C. Alexiou[1]

[1] *Department of Oto-Rhino-Laryngology, Head and Neck Surgery, Section for Experimental Oncology & Nanomedicine (SEON), Else Kröner-Fresenius-Stiftung-Professorship, University Hospital Erlangen, Germany*
[2] *Department of Neuroradiology, University Hospital Erlangen, Germany*
[3] *Institute and Outpatient Clinic of Occupational, Social and Environmental Medicine, University of Erlangen-Nuremberg, Germany*
[4] *Institute of Particle Technology, University Erlangen-Nuremberg, Germany*
[5] *Physikalisch-Technische-Bundesanstalt, Berlin, Germany*

Introduction

Iron-oxide-based nanoparticles, are good candidates for personalized delivery of cancer therapeutics, as they have magnetic properties, enabling a region-specific accumulation by external magnetic fields and in addition to that real-time tracking using established imaging techniques [1].
For a preclinical animal model aiming to a translation into the clinics treatment scheme has to be set up, which has to fulfil several important requirements. These prerequisites include the particle composition, the mode of administration and the capabilities for performing proper diagnostics and analytics before and after the treatment of the animals.
Particle design and mode of application are influencing each other very strongly.
E.g. for intravenous administration, sophisticated particles must be used to avoid premature metabolic trapping. **[2]**. Intraarterial (i.a.) administration near the tumour, like it is done in Magnetic Drug Targeting (MDT) [3], prevents nanoparticles from being captured and cleared before reaching the tumour. Therefore compounds without complicated chemistry can be used in MDT. This has the advantage of particles that are easier to control, offer a good batch to batch stability and show high efficiency with low side effects

Here, we describe magnetically directed SPION drug delivery in a rabbit tumour model. We developed a new nanoparticulate drug-carrier-system and built up a unique preclinical intervention-unit consisting of a C-arm cone beam CT for angiographic imaging and a strong electromagnet for the *in vivo* investigation of MDT in animal trials. The present work does express an advanced preclinical setting including synthesis of the nanoparticle core, drug loading and extensive in-vivo investigations for biodistribution (29 animals) and therapeutic effects (38 animals) under imaging guided modalities, performed in an integrated study design.

Methods

SPIONs were synthesised according to an alkaline precipitation protocol, coated with lauric acid and loaded with the chemotherapeutic Mitoxantron (MTO). For the animal experiments the particles were filtered through a 0.22 µm sterile syringe filter.
Particles were routinely tested for size distribution and zeta potential. Selected samples were analysed with TEM. MTO-loading of the particles was measured with HPLC-UV.
Biodistribution of MTO in tissue was analysed with HPLC-UV, too. Biodistribution of SPIONs was quantified with Magnetorelaxometry.

Tumour bearing New Zealand White rabbits were treated once with 5% or 10% MTO compared to one normal i.v. dose. For the biodistribution study (29 animals) the animals were sacrificed 24h after performing MDT and organs and tissue were taken for further analysis. The animals of the treatment groups were observed for a maximum of 16 weeks after MDT.
Angiographical imaging was done with an Artis zee floor®-System (Siemens Healthcare, Forchheim, Germany) using a standard contrast agent with an iodine concentration of 350mg/ml.

Results

TEM-images of the nanoparticles showed tight clusters of raw particles successfully being prevented from agglomerating by using the organic surface coating. MTO was spherically positioned around monodispersed SPIONs and encapsulated inside larger (80-120 nm) substructures. SPIONs used for the animal studies had a hydrodynamic diameter of less than 200nm, a zetapotential of -24 to – 30mV and a payload of up to 130µg/ml MTO.
Four conditions were tested for the biodistribution studies. Systemic application of MTO alone led to high accumulation in liver (14%) and kidneys (78%) of the detected amount and low concentration in the tumour region (TR) (<1%). Using SPION-MTO administered i.v. the MTO-content in the TR remained low whether or not a magnetic field was applied onto the tumour, but a shift of MTO from the kidneys to the liver could be detected.
However, i.a. administration of MTO-SPIONs plus an external magnetic field led to superior enrichment of MTO (57.2%) in the TR. The levels of MTO in the liver (14.4%) and kidneys (15.2%) were considerably lower than were seen after i.v. administration.
In the therapy groups (TG) treated with 5%- and 10%-MTO-MDT (n = 30), nine animals (30%) had complete tumour remissions 5-16 weeks after administration, and another eight animals showed slower tumour growth with increased survival [4].

Discussion

The basic intention of MDT is to achieve superior drug enrichment in the treated tissue in comparison to other modes of application. The data demonstrate that with the newly developed nanoparticle-system, efficient targeting of a chemo- therapeutic agent to solid tumours *in vivo* and effective treatment of those is possible with MDT.
This could be shown with dramatically reduced doses of only 5% or 10% MTO in a combined *in vivo* study (67 rabbits), representing the largest animal study describing the biomedical effect of MDT, to date.
We are now working towards translation into clinical practice for the treatment of solid tumours, by implementing catheter-based administration procedure for MDT and a GMP-conform particle-fabrication.

Acknowledgments

German Research Foundation (AL552/3-3), Else Kröner-Fresenius Stiftung (Bad Homburg v. d. H.), Germany; Federal Ministry for Education and Research (FKZ:01EX1012B); Emerging Fields Initiative of the University Erlangen-Nuremberg; Forschungsstiftung Medizin University Hospital Erlangen, Germany; Bavarian Ministry for Environment and Health (74-U8793-2012/7-35); Margarete Ammon Stiftung, Munich, Germany.

References

[1] Mikhaylov G, et al. Ferri-liposomes as an MRI-visible drug-delivery system for targeting tumours and their microenvironment. Nat Nanotechnol 2011;6:594-602
[2] Maldiney T, et al. Effect of core diameter, surface coating, and PEG chain length on the biodistribution of persistent luminescence nanoparticles in mice. ACS Nano 2011;5:854-62
[3] S. Lyer, et al.: Visualisation of tumour regression after local chemotherapy with magnetic nanoparticles - a pilot study. Anticancer Res 30: 1553-1557, 2010
[4] Tietze R, et al, Efficient drug-delivery using magnetic nanoparticles - biodistribution and therapeutic effects in tumour bearing rabbits. Nanomedicine: NBM 2013; xx:1-11

Magnetic spatial forcing of a ferrofluid layer

F. J. Maier[1], I. Rehberg[1], R. Richter[1]

[1]*Experimentalphysik V, Universität Bayreuth, 95440 Bayreuth, Germany*

Introduction

In two-dimensional pattern-forming systems with broken up-down symmetry, hexagonal patterns are normally preferred near the onset of pattern formation, as summarized in [1]. One famous example is the Rosensweig instability at an interface between ferrofluid and air subjected to a normal magnetic field [2]. However, stripes may become the preferred pattern when the amplitude of some spatially periodic resonant forcing is sufficiently large [1]. Experiments regarding these circumstances have been performed using a thin layer of ferrofluid forced by an array of current carrying wires [3]. Here we continue these experiments with an improved setup.

Experimental setup

An aluminium vessel with a length of 41.0 cm and a width of 5.5 cm is filled with 55 ml ferrofluid (EMG909 from Ferrotec Corporation), creating a layer with a thickness of about 2.5 mm. The vessel is mounted in the center of a Helmholtz pair of 40 cm diameter coils which serves to create a magnetic induction $\mu_0 H_0$. In this way, a "magnetic ramp" [4] is generated along the length of the vessel. This ramp reduces finite size effects of the stripe-like patterns. Additionally, a spatially modulated magnetic field is created by an electric current flowing through a wire array machined from an aluminium plate with a thickness of 2 mm. A part of this array is shown in Fig. 1, also containing a plot of the normal magnetic induction $\mu_0 H_z$, measured at a distance of 2 mm from the array's surface at a current of $I = 30\,\mathrm{A}$.

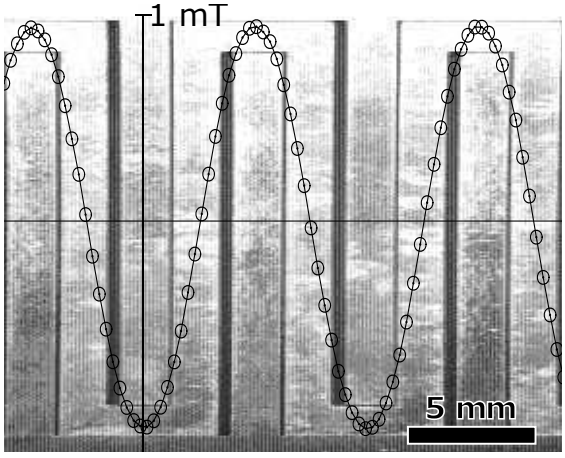

Figure 1: Picture of the aluminium wire array (vertically sqeezed to 25%), superimposed with a plot of the normal component of the corresponding magnetic induction.

The wavelength of the modulation has been selected to be 9.6 mm, which is close to the critical wavelength $\lambda_c = 2\pi\sqrt{\frac{\sigma}{\rho g}}$ of EMG909. The array is mounted below the vessel, providing a spatially modulated normal component of the magnetic induction throughout the ferrofluid layer. The resulting surface profile of the ferrofluid layer is recorded via X-ray absorption. For details of this method see Ref. [5].

Results

With the vessel being longer than the diameter of the Helmholtz coil, the ferrofluid is pulled to the middle due to the Kelvin force when the current in the coil is turned on, resulting in a bigger fluid height in the detected area than originally prepared. Additionally applying the modulated magnetic field, a periodic surface modulation with its

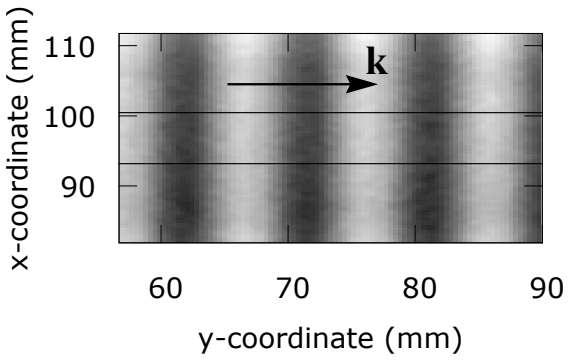

Figure 2: Brightness-encoded height profile of the ferrofluid layer subjected to a homogeneous induction of $\mu_0 H_0 = 19.5\,\mathrm{mT}$ and a spatially modulated induction with amplitude $\mu_0 H_\mathrm{z} = 0.96\,\mathrm{mT}$.

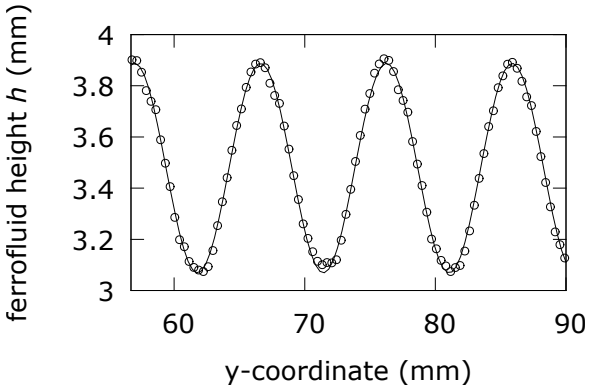

Figure 3: Height modulation of the surface, extracted from the marked area in Fig. 2. The open circles mark the experimental data, the solid line stems from a fit by a sinusoidal function.

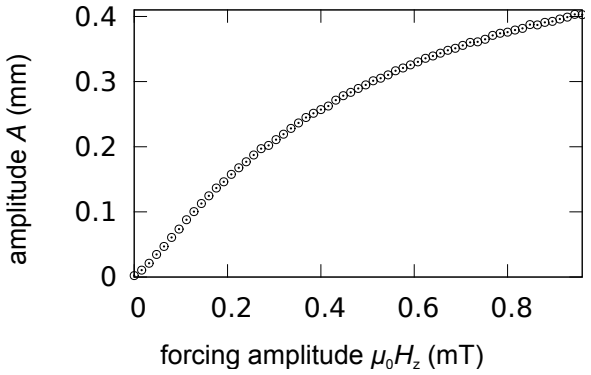

Figure 4: Amplitude of the height modulation versus the forcing amplitude $\mu_0 H_\mathrm{z}$ at a homogeneous induction of $\mu_0 H_0 = 19.5\,\mathrm{mT}$.

wave-vector **k** pointing along the y-axis emerges as seen in Fig. 2. Averaging over multiple rows (indicated by the horizontal black lines in Fig. 2) improves the SNR. The result of this procedure is shown in Fig. 3. A fit of the form $h(y) = A \cdot \sin(ky + \varphi) + c$ matches the data and yields the wavenumber k of the wire array, as well as the amplitude A of the height modulation. Extracting A for different forcing amplitudes $\mu_0 H_\mathrm{z}$ at the bottom of the vessel at a constant homogeneous magnetic induction of $\mu_0 H_0 = 19.5\,\mathrm{mT}$ results in Fig. 4. As one can see, A monotonously increases with the forcing amplitude $\mu_0 H_\mathrm{z}$. We will present a series of curves for different values of $\mu_0 H_0$. A quantitative description of these curves is the aim of current investigations.

Acknowledgments

F.J.M. is grateful to Thomas Friedrich for an excellent introduction to the experimental setup, and all authors would like to thank him for fruitful discussions.

References

[1] R. Peter, M. Hilt, F. Ziebert, J. Bammert, C. Erlenkämper, N. Lorscheid, C. Weitenberg, A. Winter, M. Hammele, and W. Zimmermann, Phys Rev. E, **71**, 046212 (2005).

[2] M. D. Cowley and R. E. Rosensweig, J. Fluid Mech., vol. **30**, no. 4, pp. 671-688 (1967).

[3] Th. Friedrich, A. Lange, I. Rehberg, R. Richter, Magnetohydrodynamics, Vol. **47**, No. 2, pp. 167-173 (2011).

[4] H. Knieling, I. Rehberg, R. Richter, Physics Procedia 9, **199**, (2010).

[5] R. Richter and J. Bläsing, Rev. Sci. Instrum. **72**, 1729 (2001).

Observation of transient networks in vibrated magnetic granular layers

Robin Maretzki[1] and Reinhard Richter[1]

[1] *Experimentalphysik 5, Universität Bayreuth, 95440 Bayreuth Germany*

Introduction

Permanent magnetic dipoles may self-assemble to linear chains and rings, even without an externally applied magnetic field. This has been investigated for nano-sized particles in ferrofluids; see e.g. [1,2]. However, in this system the emerging structures and their dynamics are difficult to observe. Similar aggregates have also been observed in a mixture of glass beads and magnetized steel spheres, which are shaken in a vessel [3]. In our contribution we focus on the formation of transient networks in this system, when quenching the amplitude of the vibrations.

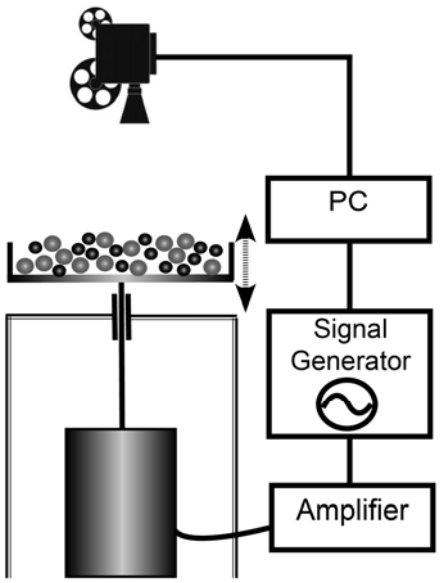

Figure1: Sketch of the experimental setup.

Experimental setup

Steel spheres with a diameter of 3mm are permanently magnetized in a homogeneous field of 1.15T. Consecutively they are filled together with glass spheres (diameter of 4mm) in a rectangular vessel which is vibrated by an electromagnetic shaker. As sketched in Fig.1, a long rod takes care that the alternating magnetic field generated in the shaker has no significant influence on the steel spheres. A personal computer controls the sinusoidal output of a signal generator, connected via an amplifier to the shaker. The beads are illuminated from below utilizing an electroluminescent display. The dynamics of the beads is recorded from above using a charge coupled device camera connected to the computer.

Experimental observations

For large shaker amplitudes we observe a gas-like state of single steel and glass spheres. After a quench of the shaker amplitude to a lower value we record the assembly of steel spheres to chains, networks, and eventually compact clusters, as shown in Fig. 2. A movie of this transition can be accessed at [4].

We estimate the evolution of order parameters like chain length, or Euler characteristics during the transitions. Moreover we discuss our observations in the context of a recently proposed model of *viscoelastic phase separation* [5]. In this model the dy-

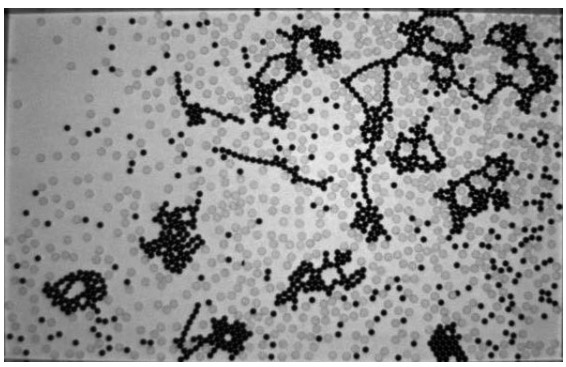

Figure2: The steel spheres (black) form transient networks which eventually are coarse grained to more compact aggregates. The glass spheres appear grey.

namic asymmetry between the glass spheres and the magnetized steel spheres, with their enhanced shear viscosity, leads to phase separation and the formation of transient networks.

Acknowledgments

The authors would like to thank K. Oetter for construction work with the setup, and I. Rehberg for discussion.

References

[1] P.G. De Gennes and A. Pincus, *Pair Correlations in a Ferromagnetic Colloid*, Phys. Kondens. Mater. **1**, 189 (1970).

[2] T. A. Prokopieva, V. A. Danilov, S. S. Kantorovich, Ch. Holm, *Ground state structures in ferrofluid monolayers*, Phys. Rev. E **80**, 031404 (2009).

[3] D. L. Blair, A. Kudrolli, *Clustering transitions in vibrofluidized magnetized granular materials*, Phys. Rev. E **67**, 021302 (2003).

[4] A movie can be accessed at http://www.youtube.com/watch?v=Tt82K6osdzM

[5] H. Tanaka, *Viscoelastic phase separation*, J. Phys.: Condens. Matter. **12**, R207 (2000). H. Tanaka, Y. Nishikawa and T. Koyama, *Network-forming phase separation of colloidal suspensions*, J. Phys.: Condens. Matter. **17**, L143 (2005).

Synthesis of different kind of Au coated magnetic nanoparticles

N. Matoussevitch[1], T. Schwartz[2], T. Ebbesen[2]

[1]*Karlsruher Institut fuer Technologie (KIT), matoussevitch@web.de*
[2] *ISIS, University of Strasbourg, CNRS*

The gold coated magnetic nanoparticles are very interesting for scientific investigation and also can be used for optical and bio-medical applications. Au@Co nanoparticles have also a great interest as catalysts.

We have synthesized Au @ magnetic particles by different ways, with magnetite and Co magnetic particles, using the pre-prepared stable magnetic fluids in water or in toluene.

Gold coated cobalt nanoparticles (Au@Co) are synthesized via redox reaction by reducing Au precursor solution in toluene in the presence of Co-Magnetic fluid which was prepared via thermal decomposition of Co carbonyl in presence of $Al(octyl)_3$ under ambient conditions and stabilized by Korantin SH.

Using the permanent magnet the gold coated cobalt particles were separated from pure gold nanoparticles. After washing a few times with toluene and ethanol the Au@Co particles were easily re-dispersed in toluene by just adding some amount of toluene and disperse 1-2 min in US- bath.

In result, the long time (longer then 1 year now) stable (chemically and colloidal) Au@Co particles and Au@Co – Magnetic fluid were obtained.

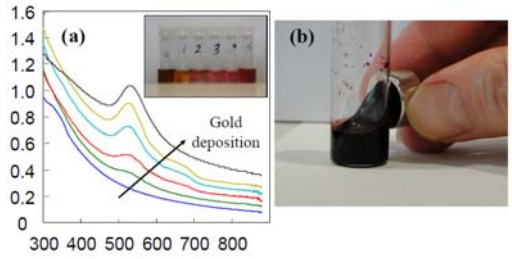

(a) –UV-Vis-Spectra; (b) – Au@Co-magnetic fluid

By using the different synthesis procedures and surfactants for preparing and stabilization of magnetic particles (Co and magnetite) and varying the conditions of gold coating reactions the different kind of anisotropic gold/magnetic particles, or structures, like wires, belts or rods, were also obtained.

These particles and structures are presently under further investigation.

Influence of electric and magnetic fields on colloidal suspensions of anisometric pigment particles

K. May[1], A. Eremin[1], R. Stannarius[1], Yu. Reznikov[2], S. Klein[3]

[1] *Otto-von-Guericke Universität, FNW/IEP/ANP, 39106 Magdeburg, Germany*
[2] *Institute of Physics, National Academy of Sciences of Ukraine, Kyiv, Ukraine*
[3] *HP Laboratories, Long Down Avenue, Stoke Gifford, Bristol BS34 8QZ, UK*

Suspensions of anisometric nanoparticles show a wide range of interesting characteristics, like their concentration dependent phase behavior and response to electric and magnetic fields. Specifically the electro-optical switching by aligning the colloidal particles in electric or magnetic fields makes them good candidates for the development of new devices.

The investigated colloidal particles are rod-shaped commercial pigment particles stabilized with a polymer and suspended in dodecane [1]. The aspect ratio of the pigment particles is about 5. This anisometry leads to the formation of ordered phases at concentrations above 15 wt%, see Fig. 1. At very high concentrations (> 27 wt%), a nematic like phase can be observed. In electric AC fields, the suspension can be electrically switched already at lower concentrations, which has been studied using depolarizing microscopy and X-ray scattering experiments [1].

In addition to the alignment of the pigment rods, a phase separation in the isotropic phase into particle-rich and particle-poor regions can be achieved at some combinations of frequency and field strength of an electric AC field.

The next step is the work on the alignment of the colloidal particles in a magnetic field. For that, very high magnetic fields in the range of 25 T are necessary. To increase the response to magnetic fields the suspensions will be doped with magnetic nanoparticles. This has already been performed by S. Kredentser et al. [2] in a different system, where suspensions of vanadium-pentoxide rods were doped with iron-oxide rods. They showed, that the magnetic field strength, which is necessary to orient the vanadium-pentoxide rods, can be lowered by two orders of magnitude by this method. This is due to the coupling of the non-magnetic nanorods to the magnetic particles, which orient in the magnetic field.

The aim of our work is to dope the colloi-

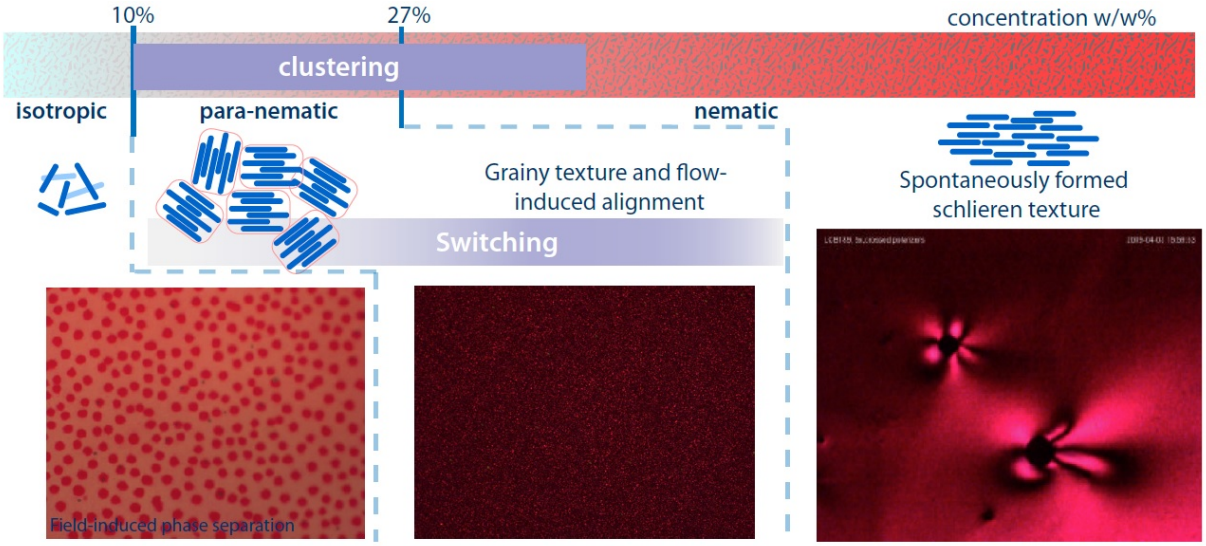

Figure 1: Mesophase-behaviour of the suspensions of rod-shaped particles at various concentrations

dal suspension of pigment particles with rod-shaped magnetic nanoparticles and carbon nanotubes filled with ferromagnetic nanoparticles. This is expected to reduce the critical magnetic field strength needed to align the pigment particles, which is interesting for magneto-optical devices.

Acknowledgments

The project will be funded by the DFG (SPP1681).

References

[1] A. Eremin, R. Stannarius S. Klein, J. Heuer, R. M. Richardson, Adv. Func. Materials, **21**, 566 (2011).

[1] S. Kredentser, O. Buluy, P. Davidson, I. Dozov, S. Malynych, V. Reshetnyak, K. Slyusarenkoab, Yu. Reznikov, Soft Matter, **9**, 5061 (2013).

Investigations on the transfer of magnetic nanoparticles at the blood-placenta barrier

R. Müller[1], C. Göhner[2], M. Gläser[1,3], E. Schleussner[2], A. Hofmann[4], W. Fritzsche[1]

[1] *Institute of Photonic Technology (IPHT), Jena, Germany*
[2] *Department of Obstretrics and Gynecology, Jena University Hospital, Germany*
[3] *University of Applied Sciences, Jena, Germany*
[4] *HTS Systeme GmbH, Wallenfels, Germany*

Nanoparticles (NP) are potential tools for medical applications. Nevertheless, the current lack of knowledge about their potential toxicity connected with a possible spatial distribution in the human body requires new methods to determine the latter one. Placentae can play a central role as human tissue models as they do not constitute an ethical problem. Furthermore, magnetic NPs are used as MRI contrast agent but their behaviour at the placenta barrier is not known. To date, no standardised methods are available for quantification of NP in human tissue.

Aim of our work are long term measurements of NP in a floating suspension in tube shaped sample volume in order to conclude their (time dependent) whereabouts after perfusion of a placenta in the range of hours, i.e. to answer the question: Can NP overcome the blood-placenta barrier? We used a modified MagnetReader [1, 2] what detects magnetic moments of a few μAm^2 (VSM in the order of 100 μAm^2) via analysis of the higher harmonics caused by a frequency mix of ac-magnetic fields with a field amplitude of 4.5 mT. Since the signal depends as well on the magnetisation curve of NPs the method is only semiquantitative. The characteristics of our measuring system were determined in experiments only on the maternal side of the placenta. The results are compared with absolute values of higher concentrated suspensions in steady state measured by VSM. The influence of the material of the measuring cuvette (NP adsorption at the cuvette leads to a misinterpretation of the results.), the flow rate of the suspension (i.e. integration time) and changes in the particle concentration were investigated. Successful measurements were done with an initial particle concentration of about 8 µg/ml. The setup of the experiment is shown in Fig. 1. Only after excluding the mentioned above effects a statement about a binding of particles in the placenta tissue is possible.

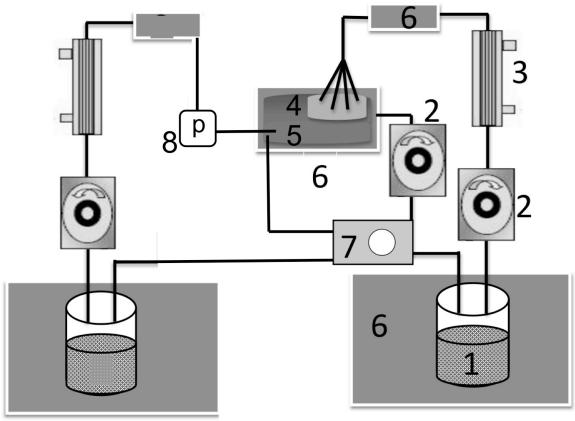

Fig. 1: Setup of the double sided perfusion experiment - left part: fetal side, right part: maternal side
1 magnetic particles suspended in perfusion media (stirrer is not shown)
2 pump
3 oxygenator
4 placenta, maternal side with connected cotyledon
5 placenta - fetal side
6 heating bath 37°C
7 MagnetReader (computer not shown)
8 perfusion pressure measurement
The fetal circuit is a closed circuit and needs only one pump (in contradiction to the maternal circuit).

Because of the smaller blood vessels the fluid pressure in the („closed“) fetal circuit is higher than in the („open“) maternal circuit. There shouldn't be a transfer of fluid from the maternal to the fetal side even if there is a leakage of the tissue.

Fig. 2 shows the magnetic signal (particle concentration) vs perfusion time measured on starch coated particles by Magnetreader. Because of different cuvettes in the maternal and in the fetal circuit the signal can't compared directly, but may differ up to 10%. The measurement suggests an average value > 0 (about 0.003V) at the fetal side.

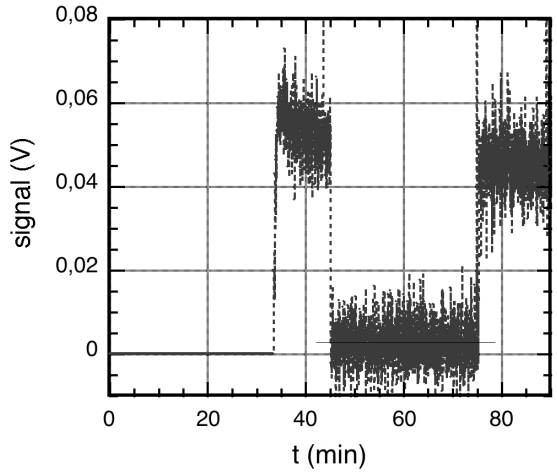

Fig. 2: Offset corrected measurement of particle suspension (Fluid-Mag-D) in the perfusion system.
Injection of particles into the system at 33mins; signal of the maternal side at 33-45mins and after 75 mins; signal of fetal side at 45-75mins

Histological investigations showed particles in the maternal (intervillous space) as well as in the fetal tissue (villous stroma) of the placenta, what could be an indication for a particle transfer at the placental barrier. Beside the usual parameters like pH-value and glucose/lactate ratio the formation of cytokines was observed, what is influenced by the presence and type of particles [3].

However a possible small damage of the tissue what can't be excluded and the low number of measurements do not allow a final statement on the transfer of particles at the blood-placenta barrier yet. Further experiments are in progress.

Acknowledgments

The particles were provided by chemicell GmbH in Berlin.
The work was supported by the BMBF grant 03X0104E, project "NanoMed".

References

[1] H.-J. Krause "Biomagnetsensor für die point-of-care-Diagnostik", Final report Project 16IN0244, Forschungszentrum Jülich, 2007
[2] P. Miethe et al, Patent WO 2004/077044 A1
[3] BMBF-Project „Toxikologische Charakterisierung von Nanomaterialien für die diagnostische Bildgebung in der Medizin – NanoMed“ 03X0104D, Report June 2013, part 4: University Jena

Thermodynamic and structural properties of magnetic fluids: the influence of granulometric composition and interparticle interactions.

E. Novak[1], E. Pyanzina[1], E. Minina[1,2],
M. Avdeev[3], A. Ivanov[1], S. Kantorovich[1,4]

[1] *Ural Federal University, Lenin av. 51, 620000, Ekaterinburg, Russia.*
[2] *now working at: Institute for Computational Physics, Universi¨at Stuttgart, Allmandring 3, 70569, Stuttgart, Germany*
[3] *Frank Laboratory of Neutron Physics, Joint Institute for Nuclear Research, Joliot-Curie 6, 14198, Dubna, Russia*
[4]*University of Vienna, Sensengasse 8, 1090, Wien, Austria*

Introduction

Nowadays, soft magnetic materials with controllable macro-properties are gaining more-and-more applications in technology and medicine [1]. One of the examples of such a magnetic soft matter system is magnetic fluid. One of the mostly used and widely spread techniques to study the microstructure is by interpreting scattering patterns obtained via small angle neutron scattering (SANS) [2-4]. These experiments result in the dependence of the so-called structure factor (SF) on the wave vector. It turned out that the properties of magnetic fluids were strongly influenced by two factors: the magnetic dipole-dipole interaction between particles and particle polydispersity. In the present contribution we investigate thermodynamic and structural properties of bi and polydisperse magnetic fluids.

Bidisperse case

Theory&MD computer simulations. If the dipole-dipole interaction is on the order of thermal energy, no clusters are formed, but the role of magnetic interparticle correlations turns out to be still prominent. To take these correlations into account one could use diagram technique. We get the first-order density expansion and take into account all terms up to λ^4 (the intensity of the dipole-dipole interaction) of the RDF. All diagrams are presented in Fig. 1. We used two types of steric potential: soft and

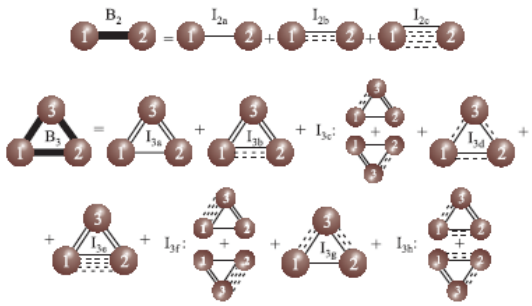

Fig. 1. Two particle and three particle diagrams which are taken into account for calculation of the pair correlation function for arbitrary sized particles

hard spheres and obtained formulas for partial RDF and SF (see [6]). To make the analysis broader we decided to consider two different bidisperse models with various granulometric compositions.

Results. We found that the steric potential does not play a crucial part in the qualitative behaviour of structure factors, however, when interpreting experimental results it is absolutely essential to know the short range part of the interactions, as the pair correlation functions are extremely sensitive to the latter (see Fig.2). We developed a method of extracting the dominant fraction of particles from the SF first peak position, width and height. Initial susceptibilityand internal pressure strongly depends on the granulometric composition.

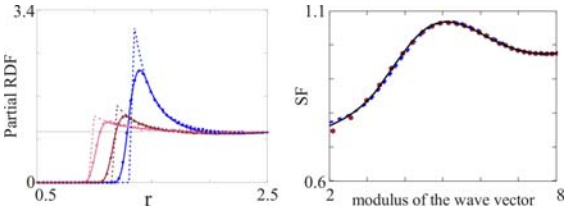

Fig. 2. Partial RDFs and SF. Symbols correspond to the simulation data, solid lines obtained theoretically using the soft-sphere potential; dashed lines are theoretical predictions, in which hard-sphere potential is considered.

As we have just shown, the validity range of the theory depends not only on the density of particles, but also on the granulometric composition and interaction strength in the system.

Outlook

Granulometric composition plays important part in the system behaviour as well as intensity of the dipole-dipole interaction. Bidisperse model can qualitatively describe the thermodynamic and structural properties of ferrofluids. We would like to underline, that all diagrams for dipolar hard spheres were calculated in a general form, meaning that if more fractions are considered, the formulas obtained here can be used to analyse pair correlations of really "polydisperse" systems. To this end, we are currently investigating how strong is the contribution from polydispersity in comparison to a bidisperse approximation.

Acknowledgments

This work is supported by the RFBR Grant 12-02-12063-ofi-m. S.K. is grateful to RFBR grant mol-a-ved 12-02-33106, has been supported by Ministry of Science and Education of RF 2.609.2011 and by Austrian Science Fund (FWF): START-Projekt Y 627-N27. E.N. and E.P. were supported by RFBR grant mol-a 12-02-31330.

References

[1] D. Ortega, N. Perez, J. L. Vilas, J. S. Garitaonandia, K. Suzuki, J. R. Marin, and M. Rodriguez, "Nonylphenol polyethoxylate coated body-center-cubic iron nanocrystals for ferrofluids with technical applications" J. Appl. Phys. 113, 17B505 (2013)

[2] L. Pop and S. Odenbach, "Investigation of the microscopic reason for the magnetoviscous effect in ferrofluids studied by small angle neutron scatting" J. Phys.: Cond. Mat. 18, 2758 (2006)

[3] M. V. Avdeev, E. Dubois, G. Meriguet, E. Wandersman, V. M. Garamus, A. V. Feoktystov, and R. Perzynski, "Small-angle neutron scattering analysis of a water-based magnetic fluid with charge stabilization: contrast variation and scattering of polarized neutrons," J. Appl. Crystallog. 42, 1009-1019 (2009)

[4] M. Barrett, A. Deschner, J. P. Embs, and M. C. Rheinstadter, "Chain formation in a magnetic fluid under the influence of strong external magnetic fields studied by small angle neutron scattering" Soft Matter 7, 6678-6683 (2011)

[5] A.O. Ivanov et al., "Magnetic properties of polydisperse ferrofluids: A critical comparison between experiment, theory, and computer simulation", Physical Review E 75, 061405 (12 pp) (2007)

[6] E. Novak et al., "Structure factor of model bidisperse ferrofluids with relatively weak interparticle interactions", J. of Chem. Phys, in progressing (2013)

The Magnetoviscous Effect in a Biocompatible Ferrofluid and Sheep's Blood

J.Nowak[1] and S. Odenbach[1]

[1] *Chair of Magnetofluiddynamics, Measuring and Automation Technology, Technische Universität Dresden, Dresden 01062, Germany*

Suspensions of magnetic nanoparticles in suitable carrier liquids receive a growing importance in regards of technical applications and in the biomedical context. The latter approach uses biocompatible ferrofluids being composed of a magnetite or maghemite core as well as a biocompatible carrier liquid like e.g. water. To ensure a stable suspension the particles are surrounded by a surfactant preventing an agglomeration due to v. d. Waals interactions [1]. While technical ferrofluids are composed of singlecore particles, in the biomedical context multicore particles with a hydrodynamic diameter of 20 nm up to several hundred nm [2] become more important as they enable a higher particle diameter without remanence magnetization. A known effect of ferrofluids is the magnetoviscous effect (MVE), i.e. an increase of viscosity in the presence of a magnetic field due to the formation of certain structures. Although it has been investigated for ferrofluids used in the engineering context, this effect received only small efforts [4] for biocompatible multicore ferrofluids up to now. In this respect the interaction of the structures of magnetic particles as well as the red blood cells is of major interest to enable a safe and effective application in the biomedical context for e.g. magnetic drug targeting or magnetic hyperthermia, which are both potential treatment methods of cancer.

Fluid	d_h [nm]	Φ [%]	M_S [kA/m]
fluidMAG_D	200	0,29	1,32

Table 1: Characteristic parameters of the ferrofluid under investigation: d_h refers to the mean hydrodynamic diameter given by the manufacturer, Φ to the volume fraction of magnetic materials and M_S denotes the saturation magnetization.

In this experimental study the MVE is investigated for the ferrofluid fluidMAG_D distributed by ChemiCell GmbH (Berlin, Germany) which features a starch surfactant as well as iron oxide multicore particles suspended in water. Characteristic magnetic parameters are shown in table 1.
The sheep blood was provided by the University Hospital Carl Gustav Carus, Dresden. It was prevented from coagulation with ethylenediaminetetraacetic acid (EDTA) with a concentration of 1,5 mg/ml. The haematocrit was measured to be 47%.
The rheological characterization for vanishing field was carried out using an Anton-Paar Physica MCR 301 with a cone-plate geometry featuring a cone opening angle of 1° and a diameter of 49,964 mm. Rheological experiments under the influence of a magnetic field were performed using a specially designed shear rate controlled rheometer [3] with a cone-plate geometry as well, featuring a cone opening angle of 1° and a diameter 76 mm. Regarding the measurement of important magnetic parameters a Lake Shore 7407 vibrating sample magnetometer was used to determine e.g. the actual dilution factor with the use of the saturation magnetization of the respective samples.

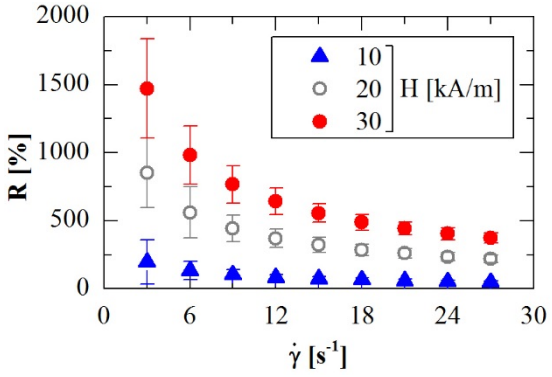

Figure 1: MVE of the ferrofluid used in this study for several magnetic field strengths.

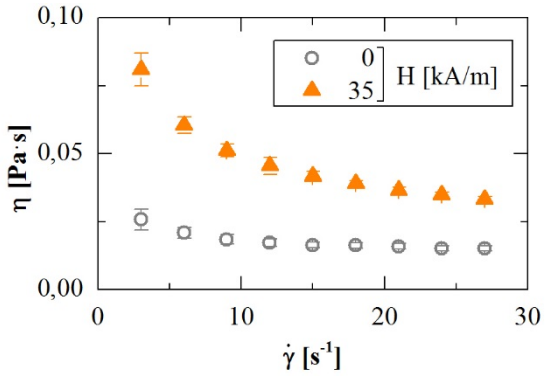

Figure 2: Viscosity for vanishing field and 35 kA/m and a dilution factor of K=10 for the ferrofluid and sheep blood.

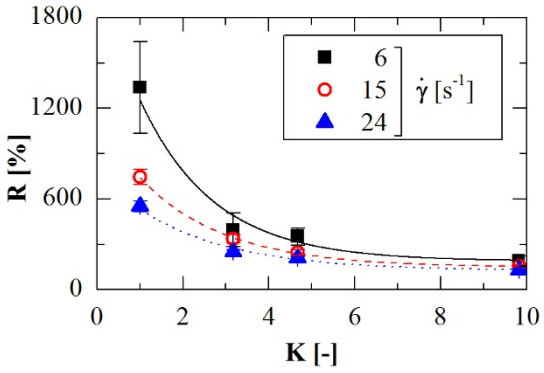

Figure 3: The MVE for several dilutions of the investigated ferrofluid and sheep blood. The magnetic field strength is 35 kA/m

All measurements were carried out using a constant temperature of 20 °C.

While the pure ferrofluid showed a Newtonian behaviour without the influence of a magnetic field, the flow curve could be fitted with the Herschel-Bulkley model for magnetic fields of certain strength as shown in [4] for a comparable fluid. A strong MVE was detectable for the ferrofluid depending on the particular magnetic field strength as presented in figure 1. The MVE is denoted as R and calculated with the use of the viscosity for vanishing magnetic field $\eta_{(H=0)}$ and the viscosity under the influence of a magnetic field $\eta_{(H)}$ [1]:

$$R = \frac{\eta_{(H)} - \eta_{(H=0)}}{\eta_{(H=0)}}. \qquad (1)$$

When mixing the ferrofluid with sheep blood a dilution factor K has to be introduced:

$$K = \frac{V_{mix}}{V_{FF}}, \qquad (2)$$

with the volume of ferrofluid V_{FF} and the volume of the resulting dilution V_{mix}.

Rheological measurements of the dilutions revealed a strong MVE of the ferrofluid, even if diluted with the sheep blood. A strong change of the viscosity as well as of the flow behaviour, showing a stronger shear thinning, can be observed (figure 2).

The measured MVE decreases with increasing dilution factor K, still being detectable for K = 10 (figure 3). A theoretical description is enabled with the MVE for pure ferrofluid R_0, the MVE for an infinite dilution R_∞ and the decrease rate p:

$$R_{(K)} = R_0 \cdot exp\left(-\frac{K-1}{p}\right) + R_\infty . \qquad (3)$$

The existence of R_∞ might be caused by the particle interaction of the blood cells and the nanoparticles, requiring further research.

The strong effect observed even for a dilution in sheep blood might influence the application of such fluids and should be taken into account for further investigations.

Acknowledgments

We thank the University Hospital Carl Gustav Carus Dresden for providing the sheep blood. Financial support by the Deutsche Forschungsgemeinschaft under grant no. OD18/13-3 is gratefully acknowledged.

References

[1] S. Odenbach; (2002) The Magneto-viscous Effect in Ferrofluids; Berlin: Springer

[2] S. Dutz, D. Eberbeck, R. Müller, M. Zeisberger, (2012) Fractionated Magnetic Multicore Nanoparticles for Magnetic Particle Imaging; Springer Proc. in Phy. 140: 81-85

[3] S. Odenbach, T. Rylewicz and M. Heyen; (1999) A rheometer dedicated for the investigation of viscoelastic effects in commercial magnetic fluids; J.Magn.Mater 201:155-158

[4] J. Nowak, S. Odenbach; (2013) The Magnetoviscous Effect in a Biocompatible Ferrofluid; IEEE Trans. Mag. 49 (1):208-212

Influence of *shape* and *internal* particles anisotropy on the macro-properties and structure of magnetic fluids.

E. Pyanzina[1], J. Donaldson[2], S. Kantorovich[1,2]

[1] *Ural Federal University, Lenin av. 51, 620000, Ekaterinburg, Russia.*
[2]*University of Vienna, Sensengasse 8, 1090, Wien, Austria*

Introduction

Magnetic anisotropic particles in the last several years have become an independent fast-emerging branch of dipolar soft matter research. In the long run, these systems will completely fulfill the idea of fine tuning and designing new materials with controllable properties. It is convenient to distinguish between two possible types of anisotropy. In the first case, the particle is characterised by shape anisotropy, which leads to the orientation-dependent steric interparticle interaction (see, for example, magnetic rods [1], ellipsoids [2], cubes [3]). In the second case the particle retains spherically symmetric shape but possesses an internal anisotropy, which leads to the change in the interparticle magnetic interaction (see, for example, magnetic Janus particles [4]). In the present contribution we develop various analytical methods and employ molecular dynamics (MD) simulations to investigate both types of anisotropy and describe their influence on the macroscopic properties and microstructure of fluids with anisotropic particles.

Shape Anisotropy

We propose a method of calculating analytically the pair correlation function for the combination of Gay-Berne [5] and magnetic dipole-dipole potential based on the group integral technique [6]. Using this approach we can explicitly separate contributions coming from various types of interactions: magnetic and steric. We analyse the influence of particle anisotropy on the structure factor of these systems, and investigate pressure. We also study magnetization of anisotropic particles. To verify our theoretical predictions we perform MD computer simulations for dipolar Gay-Berne particles in ESPResSo [7] and extensively compare obtained results. We also make a comparative analysis of the properties of anisotropic dipolar particle systems with those of ordinary dipolar hard and soft spheres. In this manner, we are trying to find the control parameters related to the shape anisotropy for obtaining dipolar systems with desired properties.

In addition, we present a preliminary MD study on systems composed of cubic particles. The proposed cubic model is constructed from spherical components arranged in a crystalline fashion to form a cube-like structure. For example, such a particle could consist of three layers each containing nine spheres arranged directly on top of one another. The dipole is then positioned within the central sphere and is orientated along the 100 direction of the cube. The microstructure present in the system is evaluated through the radial distribution function and an analysis of the interparticle steric interaction. The results are then related to that of spherical dipolar particles whereby illustrative comparisons are made.

Internal anisotropy

Initial studies on the second class of anisotropy are also included in this contribution. We perform MD simulations on systems of magnetic Janus particles with the aim of once again elucidating the nature of the specfic microstructure. In contrast to recent experiment work on these particles, in the presence of an external magnetic field [8], we conduct simulations under zero field

conditions. As such, the intrinsic magnetic interaction can be studied in detail, and the cluster formation assessed.

Outlook

If the dipole-dipole interaction is strong, various aggregates might form both in the systems of shape-anisotropy and internally anisotropic particles. We are currently actively working on the DFT approach to elucidate the clusters' distributions, their topology and their influence on the diffusion, magnetization and scattering.

Acknowledgments

This work is supported by the RFBR gr. 12-02-31374 and Ural Federal University development program with the financial support for young scientists. S.K. is grateful to RFBR grant mol-a-ved 12-02-33106 and Austrian Science Fund (FWF): START-Projekt Y 627-N27.

References

[1] Günter A. et al, "Rotational diffusion of magnetic nickel nanorods in colloidal dispersions", Journal of Physics: Condensed Matter 23, 325103 (14pp) (2011)

[2] Sacanna S. et al, "Fluorescent monodisperse silica ellipsoids for optical rotational diffusion studies", Langmuir 22, 1822-1827 (2006)

[3] Rossi L., Sacanna S., Irvine W. T. M., Chaikin P. M., Pine D. J., Philipse A.P., "Cubic crystals from cubic colloids", Soft Matter 7, 4139-4142 (2011)

[4] J. Yan, M. Bloom, S. C. Bae, E. Luijten and S. Granick "Linking synchronization to self-assembly using magnetic Janus colloids", Nature, 491, 578-581 (2012)

[5] Gay J. G. and Berne B. J., "Modification of the overlap potential to mimic a linear site-site potential", Journal of Chemical Physics 74, 3316-3319 (1981)

[6] Elfimova E. and Ivanov A., "Pair correlations in magnetic nanodispersed fluids", Journal of Experimental and Theoretical Physics 111, 146-156 (2010)

[7] http://espressomd.org/

[8] Ruditskiy A. et al, "Behaviour of iron oxide (Fe_3O_4) Janus particles in overlapping external AC electric and static magnetic fields." Soft Matter, *Advanced Article* (2013)

A flow phantom setup to study magnetic drug targeting efficiency of different magnetic nanoparticles

P. Radon[1], M. Liebl[1], N. Pömpner[2], M. Stapf[2], F. Wiekhorst[1], K. Gitter[3], I. Hilger[2], S. Odenbach[3], L. Trahms[1]

[1] *Physikalisch-Technische Bundesanstalt, Berlin*
[2] *Universitätsklinikum Jena*
[3] *Technische Universität Dresden*

Introduction

Biomedical applications of magnetic nanoparticles (MNP) as contrast agents, drug carriers or heat production in the blood flow of organisms or humans are presently intensively investigated [1]. To assist the choice of suitable MNP for a preclinical combined magnetic drug targeting/hyperthermia study in a tumor mice model we built up a simple flow phantom. Magnetic Particle Spectroscopy served as a sensitive quantitative detection technique of MNP. In pilot experiments we demonstrated the capability of our setup to quantify the retention of MNP by magnetic targeting (MT) under adjustable physiological blood flow and MNP concentration conditions.

Materials and Methods

Phantom setup and MT procedure
The MT flow phantom consisted of a peristaltic pump with fixed inlet and outlet tubes, a small cubic neodymium magnet (7 mm edge length) on a slider, a reservoir for MNP suspension input and a removable tube of 1 mm inner diameter (120 µl total volume) - the so called retention tube - clamped at the targeting area. For our experiments we used a flow rate of 350 µl/min (average flow velocity of 8 mm/s in the retention tube) and a fixed distance of the targeting magnet to the retention tube (1.2 mm to outside wall of tube). From hall probe measurements we estimated a mean magnetic field gradient of about 80 T/m at the center of the retention tube in good agreement with simulations.

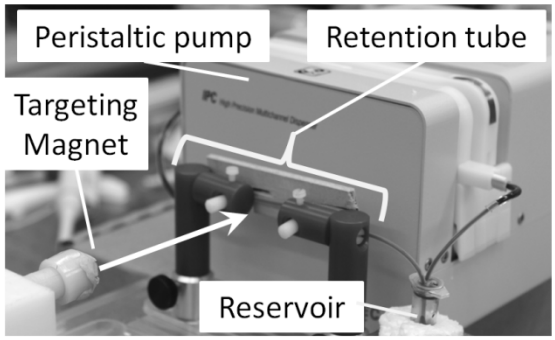

Fig. 1: Setup of the MT flow system.

First the MNP suspension (1.8 ml total input volume) was inserted into the reservoir and pumped through the flow system without magnetic field for several minutes. Then, 10 µl reference samples to determine the exact input MNP concentration were taken from the reservoir. After that the magnet was quickly moved to the retention tube defining the starting time point t_0 of MT. After defined time intervals t_{MT} (t_{TM}=1, 5, 10, 30, 100, 1000 min) the flow was stopped, the magnet withdrawn and the MNP suspension inside the retention tube was carefully harvested and vortexed. Out of retention and reservoir MNP suspension 10 µl aliquots were taken to determine the iron concentration by means of magnetic particle spectroscopy. This procedure was repeated for all MT time intervals.

Magnetic Particle Spectroscopy (MPS)
MPS employs the nonlinear magnetic response of MNP exposed to a strong oscillating magnetic field (up to 25 mT at 25 kHz), while biological tissue and para-

magnetic blood iron do not contribute. The MNP quantification follows from the third harmonic moments ratio $A_{3,samp}/A_{3,ref}$ between the sample and a corresponding reference of known iron amount. By this the iron concentrations in the retention tube and reservoir were determined for each t_{TM}. By reference to the input iron concentration the changes in the MNP concentration due to the magnet were calculated.

Magnetic nanoparticles

We used hydroxyethyl starch coated MNP of 50 nm, 200 nm, and 300 nm mean hydrodynamic diameter (chemicell, Berlin). The MNP suspension was diluted in 0.1% bovine serum albumin to an iron concentration of 7.5 mol/l (corresponding to a 300 µmol iron per kg body weight dosage, typically used in preclinical experiments). In addition, we performed MT also for t_{MT}=30 min and 100 min in EDTA stabilized human blood using the 200 nm MNP.

Results

Fig 2 shows the retention of MNP having three different hydrodynamic diameters as a function of t_{TM} determined for the samples taken from the retention tube. As expected the MT yield is crucially determined by the hydrodynamic diameter d_{hydr}. For d_{hydr}=50 nm MNP we found nearly no retention (<1% even after 1000 min), while for d_{hydr}=330 nm MNP after 30 min about 70% of the MNP were accumulated and the retention process showed already a saturation behavior for longer times t_{MT}. For d_{hydr}=200 nm the retention is only about 25% at 30 min and reaches about 65% at 1000 min. For d_{hydr}=200 nm in blood, the retention is further reduced to about 10%, probably due to the higher viscosity.

Changes in the shape of the MPS spectrum (not shown here) indicate a moderate increase of larger MNP in the retention tube during MT. These alterations in the size distribution were confirmed by magneto-relaxometry measurements of the same samples.

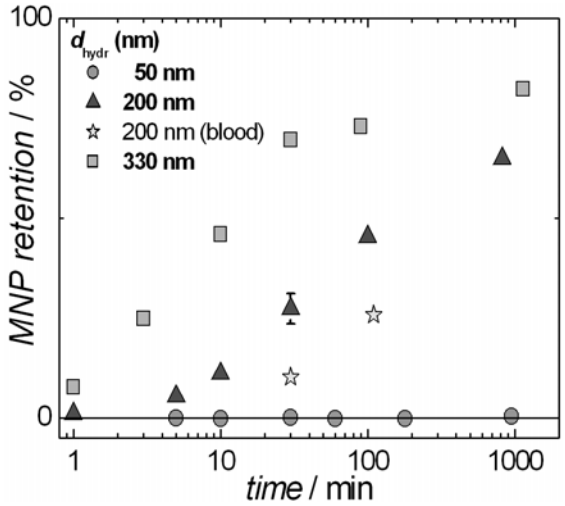

Fig 2: MNP retention as a function of MT-time for MNP of three different hydrodynamic diameters. The input concentration (7.5 mol/l) was the same for all MNP.

Accordingly, the quantification of the reservoir samples confirm the retention profiles. The MPS spectra here reveal a decrease of larger particles with increasing t_{MT}.

Conclusions

We demonstrated with our setup the quantitative assessment of magnetic targeting efficiency of MNP at biologically tolerable (clinical) concentrations. Using different tube diameters or flow rates and tube materials together with variations of the flow rate and magnetic field gradients this allows for controlled investigations of physical and physiological properties during MT. In a next step we will incorporate a dedicated targeting magnet with defined gradients developed for mice tumor studies.

Acknowledgments

This work was financially supported by the DFG research program “Magnetische Nanopartikel für die Krebstherapie” TR408/4-3, OD18/13-3 and HI698/7-4

References

[1] Lascialfari A et al. *In vivo biomedical applications of magnetic resonance and magnetic materials* (2013) Riv N. CIM. 36:211-271.

Nanoscale rheology of polymer solutions using magnetically blocked $CoFe_2O_4$ nanoparticles

E. Roeben, S. Teusch, M. Dörfer, M. Effertz, A. M. Schmidt*

*Department Chemie, Institut für Physikalische Chemie, Universität zu Köln, Luxemburger Straße 116, D-50939 Köln, *E-Mail: annette.schmidt@uni-koeln.de*

Rheology is an important tool for the investigation of viscoelastic complex materials like polymers. In the context of nanostructured materials and composites, it is of growing interest to determine the material properties on the micro- and nanoscale, and experience the interaction between the particles and the surrounding matrix. In this respect different tracer particle-based microrheological methods are applied, which in addition have the advantage that only a small sample volume is required. Therefore it is possible to examine the viscoelastic properties of materials which cannot be produced in bulk quantities like biological polymers or living cells.[1] It is distinguished between passive and active microrheology. In passive microrheology the particle motion is induced by thermal fluctuations, whereas in active microrheology the probe is actively driven within the material, either in oscillatory or steady mode.[2,3] A tracer-free method is based on dielectric spectroscopy, and the relation of the complex dielectric function to the complex dynamic viscosity on the base of the DiMarzio-Bishop model.[4]

In the present work, we introduce a novel approach for providing nanorheological properties of different materials by investigating the dynamic response of magnetic tracer nanoparticles to oscillating magnetic fields. For this purpose we employ $CoFe_2O_4$-nanoparticles with well defined hydrodynamic properties as magnetic tracers in Newtonian fluids and complex fluids like polymer matrices, and explore the validity of this nanorheological technique to extract the zero shear viscosity and/or the complex shear modules on the particle scale.

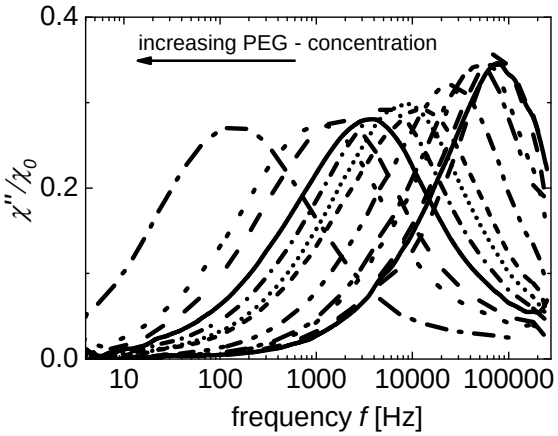

Figure 1: AC susceptometry of aqueous poly(ethylene glycol) solutions (M_n = 1000 g·mol^{-1}) with different polymer concentration.

The particle-matrix interactions are investigated by AC susceptometry (Figure 1). The experimental data are fitted by means of the Debye equation, taking into account the volume size distribution of the magnetic particles. Dynamic rheological properties like the loss or storage modulus are calculated based on a modified version of the DiMarzio-Bishop model, adapted to the magnetic case. By comparing the results with findings for the bulk properties obtained by conventional rheology, we observe a good correspondence for Newtonian fluids, while significant deviations are obtained for polymer solutions that increase with molecular weight and concentration of the polymer. We demonstrate the method development and validation, as

well as discuss the first outcomes for complex fluid characterization.

Acknowledgments

We acknowledge the Deutsche Forschungsgesellschaft (DFG) for financial support within in the framework of SPP 1259 “Intelligent Hydogels” and 1681 “Field Controlled Particle Matrix Interaction”

References

[1] C. Wilhelm, J. Browaeys, A. Ponton, J.-C. Bacri, *Physical Review E* 67, 011504, **2001**
[2] T. M. Squires, T. G. Mason, *Annu. Rev. Fluid Mech.* 42, 413-438, **2010**
[3] A. Mukhopadhyay, S. Granick, *Curr. Opin. Colloid In.* 6, 423-429, **2001**
[4] E. A. DiMarzio, M. Bishop, *J. Chem. Phys.* 60, 3802-3811, **1974**

Anisotropic Magnetic Hydrogels with Hematite Ellipsoids

L. Roeder, H. Jiang, A. M. Schmidt*

*Department Chemie, Institut für Physikalische Chemie, Universität zu Köln, Luxemburger Str. 116, D-50939 Köln, *E-Mail: annette.schmidt@uni-koeln.de*

In anisotropic magnetic particles, the micromagnetic structure is mainly affected by the magnetocrystalline and the shape anisotropy energies. While in most elongated particles, the shape anisotropy greatly exceeds crystal lattice effects, in ellipsoidal hematite particles the magnetocrystalline anisotropy dominates because the saturation magnetization is low (2048 A m^{-1}).[1, 2]

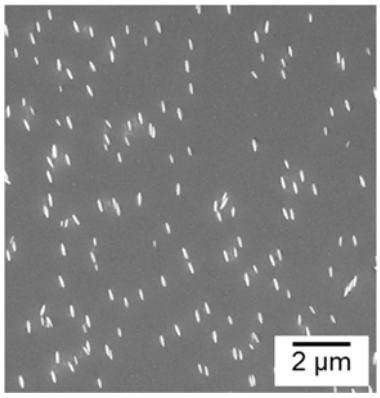

Figure 1. SEM-image of oriented α-Fe_2O_3 ellipsoids by applying a magnetic field of 590 mT.

These ellipsoids with unusual magnetic axis are readily accessible in different lengths and aspect ratios by thermolysis of iron(III) chloride in the presence of sodium dihydrogenphosphate.[3]
Here, we present the analysis of the magnetic properties of ellipsoidal hematite particles, and their performance in orientational fields is investigated. (Fig. 1)
The field-dependent behavior is supposed to be transferred to particle-linked poly(acrylamide) (PAAm) ferrohydrogels. For this reason the ellipsoids are surface functionalized with polymerizable methacrylic groups, and ferrohydrogels are prepared based on different acrylamide content in an applied magnetic field in order to obtain anisotropic ferrohydrogels. (Fig. 2) Due to the functionalization, the particles are covalently linked to the network.

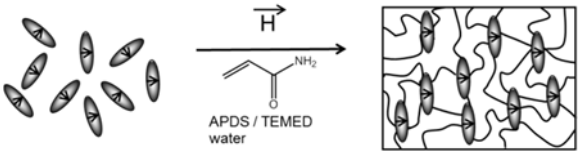

Figure 2. Synthesis of an anisotropic ferrogel crosslinked with α-Fe_2O_3 ellipsoids.

The magnetic characteristics of the gels are investigated by angular-dependent quasi static magnetometry in different planes. The angular-dependent hysteretic effects are analyzed based on a modified Stoner-Wohlfarth model, giving insight into the magnetic particle characteristics and the interaction between particles and polymer chains.[4]

Acknowledgments

We acknowledge the DFG for financial support in the framework of SPP1259, “Intelligent Hydrogels” and SPP 1681, “Feldgesteuerte Partikel-Matrix-Wechselwirkungen”, and Ruth Bruker, Universität zu Köln, for SEM investigations.

References

[1] M. Reufer, H. Dietsch, U. Gasser, B. Grobety, A. M. Hirt, V. K. Malik, P. Schurtenberger, *J. Phys.: Condens. Matter* (23), 065102 (11pp), **2011**.
[2] The Landolt-Börnstein Database – *Group III Condensed Matter, Numerical Data and Functional Relationships in Science and*

Technology, (12b) SpringerMaterials (http://www.springermaterials.com).
[3] M. Ozaki, S. Krathovil, E. Matijevic, *J. Colloid Interface Sci.* (102), 146-151 **1984**.
[4] L. Roeder, P. Bender, A. Tschöpe, R. Birringer, A. M. Schmidt, *J Polym. Sci. Part B: Polym. Phys.* (50), 1772-1781, **2012**.

Local melting of colloidal crystals and local defects

Marcel Roth, Jinyu Zhao, and Günter K. Auernhammer

Max Planck Institute for Polymer Research, Ackermannweg 10, 55128 Mainz, Germany

In this contribution I will discuss the possibilities and limitations of confocal microscopy for the analysis of colloidal systems under mechanical and magnetic fields [1]. Almost all magnetic materials are absorbing light. This makes the usage of confocal microscopy challenging for structural analysis of magnetic or magnetorheological gels. First experiments with magnetic particles dispersed in a carrier liquid show however that the usage of high numerical aperture objective opens a way to (partially) circumvent this problem.
Whereas electric fields exert weak forces on both magnetic and non-magnetic colloids, magnetic fields act strongly and exclusively on magnetic colloids. The magnetophoretic force acting on magnetic colloids is given by:

$$\vec{F}_{mag} = \mu_{mag} m_{ef} \cdot \nabla \vec{B}, \qquad (1)$$

where μ_{mag} is the magnetic permeability of the medium, m_{ef} is the magnetization of the particle, and $\vec{B}$ is the external magnetic field.
We used the magnetophoretic force to selectively address the superparamagnetic polystyrene particles in a mixture of polystyrene (diameter: 4.4μm) and PMMA (diameter: 1.6μm) colloids.
At sufficiently high concentrations the PMMA colloids form a crystalline lattice. The coordinates and structural properties of the fluorescently labeled PMMA particles were determined from confocal microscopy images. Superparamagnetic particles were added to disturb the crystalline order. Non-moving magnetic tracer particles disturbed the crystal structure only close to their nearest neighbours. To investigate melt-

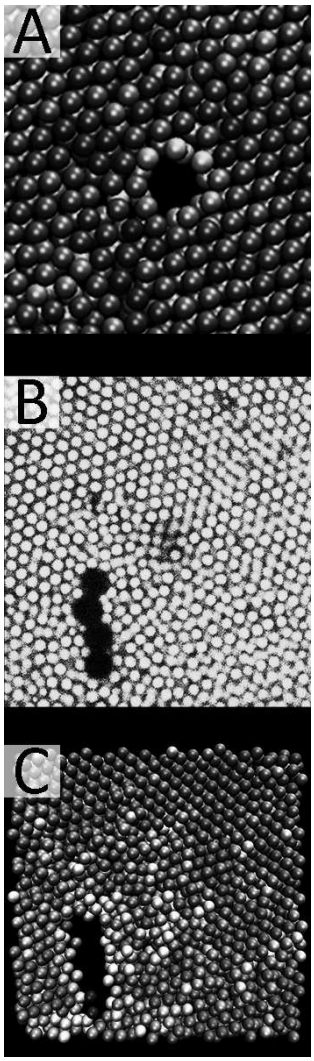

Figure 1: (A) In a static situation, only the very first layer of the colloidal crystal is distorted due the presence of the defect (green: low order; blue: high order). (B) and (C) A moving chain shows a stronger and longer ranged reduction of the local order parameter. B) shows a 2D slice out of the 3D data set. In C) the degree of crystalline oder is color coded (red: high order, white: low order).

ing and recrystallization magnetic tracer particles were pulled through the matrix. A minimum force (pinning force) is necessary to induce motion of the tracer particles. The pinning force strongly depended on the concentration of the matrix colloids. In the fluid phase the pinning force was below our experimental resolution. In the crystalline phase, the moving moving tracer particles melted the crystalline structure a few lattice constants ahead of the magnetic particles, Fig. 1. The matrix only slowly recrystallized after the magnetic particles passed [2]. Also in the direction perpendicular to the motion of tracer particles the melting of the colloidal crystal was limited to a few lattice constants. Most of the disturbance went into elastic deformation of the colloidal crystal.

Acknowledgments

Financial support by the DFG through the SPP 1273, SPP 1486 and the SFB TR6 is gratefully acknowledged by GKA, RS, and JW, respectively. MR is a recipient of a fellowship through funding of the Excellence Initiative (DFG/GSC 266).

References

[1] M. Roth, C. Schilde, P. Lellig, A. Kwade, and G. K. Auernhammer, *Colloidal aggregates tested via nanoindentation and simultaneous 3D imaging*, Eur. Phys. J. E **35**, 9801 (2012).

[2] J. Zhao, P. Papadopoulos, M. Roth, C. Dobbrow, E. Roeben, A. Schmidt, H.-J. Butt, G. K. Auernhammer, and D. Vollmer, *Colloids in external electric and magnetic fields: colloidal crystals, pinning, chain formation, and electrokinetics*, EPJ-ST, accepted (2013).

Homogeneous breast cancer biomarker assay based on optical detection of the rotational dynamics of magnetic nanorods

J. Schotter[1], S. Schrittwieser[1], F. Ludwig[2], J. Dieckhoff[2], Katerina Soulantika[3], Sergio Lentijo Mozo[3], Beatriz Pelaz[4], Wolfgang Parak[4]

[1] *Molecular Diagnostics, AIT Austrian Institute of Technology, Vienna, Austria*
[2] *Institute of Electrical Measurement and Fundamental Electrical Engineering, TU Braunschweig, Braunschweig, Germany*
[3] *Université de Toulouse, INSA, UPS, LPCNO, and CNRS, LPCNO, Toulouse, France*
[4] *Philipps-Universität Marburg, Germany*

We recently introduced a novel homogeneous biosensor concept that is based on optically observing the rotational dynamics of noble metal coated magnetic nanorods [1, 2]. These nanorods are functionalized by antibodies that specifically bind biomarker molecules present in the sample solution. Due to the small size of the nanorods, such binding events significantly alter their hydrodynamic volumes. Consequently, when the orientation of the nanorods in the solution is continuously altered by applying a rotating magnetic field (RMF), nanorods with bound biomarkers experience a higher hydrodynamic drag and follow the applied rotating magnetic field at a larger phase lag angle. This angle α is measured optically by picking up the nanorod-orientation-dependent transmission of a polarized laser beam shining through the sample dispersion (Fig. 1). Here, we report on the detection of the soluble domain of the breast cancer biomarker (sHER2) by our method.

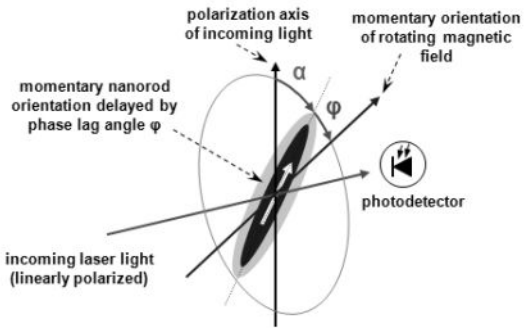

Fig. 1: Concept sketch of nanorod rotation and detection

Nanoprobe synthesis

As base particles, we employ magnetic nanorods synthesized by an organometallic approach which produces single crystalline (hcp) Co-nanorods with a uniform diameter of 6 nm and adjustable length between 40 and 200 nm with narrow size distribution [3]. Next, a noble metal shell is synthesized around the Co-core in order to protect the core from oxidation and to provide amplification of the optical signal. This is accomplished via a thin interlayer and sequential deposition of platinum (Pt) and gold (Au), which provides the best protection of the core against oxidation, resulting in stability periods of aqueous nanorod dispersions of more than ten weeks.
Following synthesis, the nanorods are stabilized with hydrophobic surfactants in organic solvents such as toluene. For transfer into and stabilization in aqueous solutions, we coat the nanorods by an amphiphilic polymer, i.e. a polymer comprising hydrophobic side chains for the linkage to the nanorod surface and a hydrophilic backbone that provides water solubility through charged groups [4]. After water stabilization, the nanorods are functionalized by monoclonal Herceptin® antibodies as recognition agents for HER2 assays by EDC / Sulfo-NHS carboxyl activation.

System characterization

Characterization of nanoprobe dispersions before and after functionalization with

Herceptin antibodies as well as following addition of large amounts of bovine serum albumin (BSA, 15 µM) as unspecific binding control and an amount of sHER2 protein sufficient for saturation of the antibody binding sites (positive control using recombinant sHER2 protein, 200 nM) are shown in Fig. 2 (symbols) along with corresponding fits according to an empirical model developed previously (lines) [5]. Clearly, the phase lag of the nanorods with respect to the applied rotating magnetic field increases with the binding of both Herceptin antibodies and sHER2 antigen, and data fits according to our empirical model result in reasonable added shell thicknesses of about 15 nm for the antibodies and another 10 nm for the antigens.

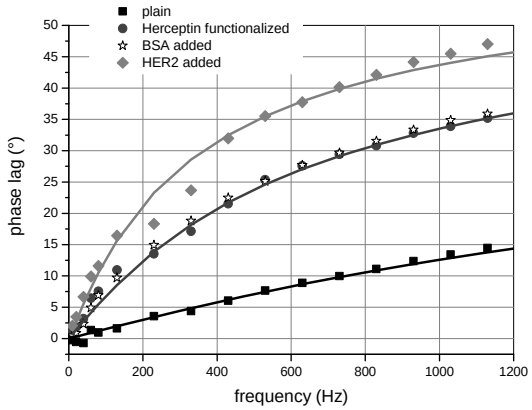

Fig. 2: Phase lag spectra of bare, functionalized and analyte-covered nanorod dispersions (~175 pM).

HER2 assay results

While phase lag spectra are well-suited for characterizing the nanorod dispersions and extracting average molecular shell thicknesses by fitting the spectra, for actual measurements it is sufficient to only look at the relative phase lag difference of the nanoprobes exposed to the sample with respect to nanoprobes immersed in a reference solution at a single magnitude and frequency of the applied rotating magnetic field. Fig. 3 shows the resulting phase lag differences for different concentrations of spiked sHER2 along with a logistic fit. Clearly, the measured phase lag difference increases systematically with the concentration of added sHER2 antigen, indicating a rising hydrodynamic volume of the nanorods due to binding of sHER2 protein to the immobilized Herceptin antibodies. All measurements are done under physiological salt conditions (25 mM Tris, 150 mM NaCl, pH 7.4) with 15 µM of BSA present as unspecific control and at a nanorod concentration of ~175 pM.

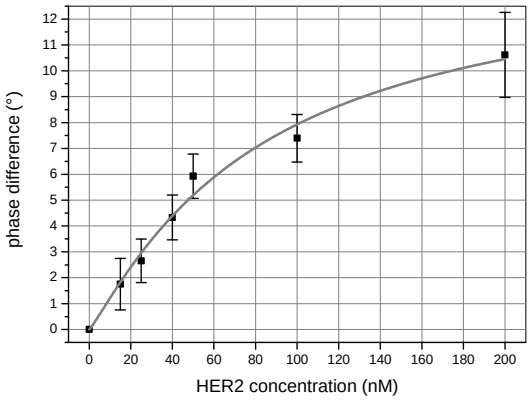

Fig. 3: HER2 assay results (RMF: 5 mT, 1030 Hz).

The logistic fit indicates a maximum saturation phase lag change of about 14° and a limit of detection (LoD) of about 20 nM. Regarding the LoD, there is still a lot of room for improvement by optimizing the antibody functionalization and assay conditions and by decreasing the lower limit of detectable nanorod concentrations.

Acknowledgments

The research leading to these results has received funding from the European Community's 7th Framework Programme under grant agreement n° NMP4-LA-2010-246479.

References

[1] Schrittwieser et al., ACS Nano 6 (2012), 791-801.
[2] Schrittwieser et al., SMALL, (2013) DOI: 10.1002/smll.201300023.
[3] Soulantica et al., Appl. Phys. Lett. 95 (2009), 152504.
[4] Pellegrino et al., Nano Letters 4 (2004), 703-707.
[5] Yoshida et al., J. Appl. Phys. 111 (2012), 053901.

The effect of magnetic particles on the pore size distribution in soft polyurethane foams

M. Schümann, S. Günther and S. Odenbach

Chair of Magnetofluiddynamics, Technische Universität Dresden, Dresden 01062, Germany

Introduction

Magnetoelastic foams are a new kind of magnetic field-responsive smart materials developed in the last years. Due to their high elasticity, soft foams loaded with magnetic particles show a great potential for an usage as magnetorheological material [1].
X-ray computed micro tomography proved to be an excellent tool to analyse foam structures [2] and micro particle arrangements [3]. Nevertheless the overall pore size distribution of polyurethane foams loaded witch magnetic particles was not reported up to the present. Detailed knowledge of the distribution and its dependency on given process parameters will enable a more precise prediction of the properties of the foam. In this work computed microtomography and digital image processing were utilized to determine the pore size distribution in soft polyurethane foams and to investigate, how this distribution is effected by the introduction of magnetic micro particles.

Materials and Methods

All investigated foam samples were produced using components provided by the company Elantas Beck GmbH. BASF Carbonyl iron powder CIP CC (d_{50} = 3.8-5.3 µm) was used as magnetic particles in concentrations up to 50 wt%.
The tomography site TomoTU utilizing a nanofocus X-ray tube with cone beam was utilized for the investigations.
After performing the separation algorithm the pore volume was determined for 20.000 to 40.000 evaluable pores in each sample.
To guarantee the reproducibility, the results from foams within the sample series were compared. All samples within a series indicate very similar values for their pore size distribution parameters. A homogeneous distribution of the particles in the foams was ensured.

Results

The high resolution tomography showed mostly closed pore foam with the particles homogeneously arranged in the vertices and the plateau borders (Figure 1).

Figure 1: Highly resolved 3D reconstruction, single particles and polyurethane matrix visible.

The analysis of the quantity based pore volume distribution proves the applicability of the Weibull distribution.

$$F(x) = 1 - e^{-\frac{x^n}{x'}}; \quad x', n > 0 \qquad (1)$$

For the cumulative distribution function equation (1) was applied. x' represents the scale parameter and n represents the shape parameter. All results show a small but significant deviation of the shape parameter n from the value n = 1. If n takes the value 1 the Weibull distribution coincides with the exponential distribution. It was observed that with increasing particle concentration, the shape parameter is decreasing. This is recognizable as a decrease of the slope of the lines in Figure 2.

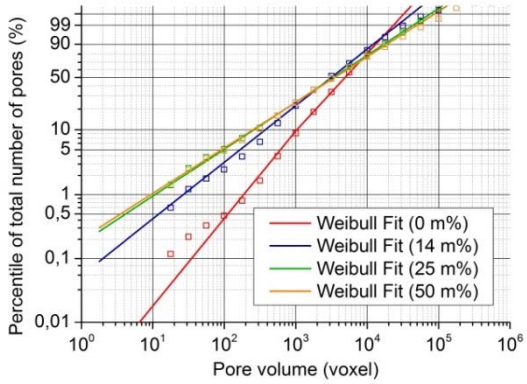

Figure 2: The fit of the cumulative pore size distribution with the Weibull function for several concentrations of carbonyl iron particles.

Because of occurring artefacts as a result of beam hardening the threshold for the binarization had to be manually adjusted to the specific particle concentration. This proceeding was necessary to ensure proper separation of the pores but caused an error in the estimation of the distribution parameters. For this reason an error estimation was performed computing the results for several thresholds which indicates merely a small influence on the shape parameter. Thus, the detected decrease of the shape parameter can be clearly assigned to the increase of the particle concentration (Figure 3).

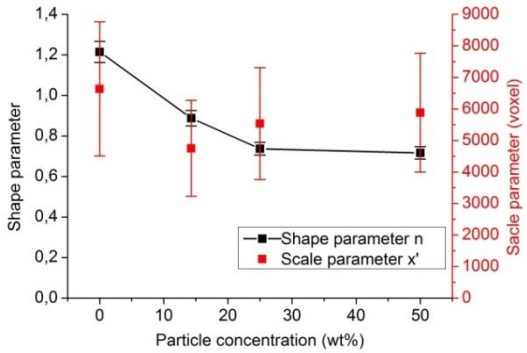

Figure 3: Plot of the distribution parameters against the particle concentration. The error bars are based on the threshold variation.

It has also been found, that a threshold variation results in significant variations of the scale parameter. Within this investigation an evaluation of the gradient of the scale parameter was not executed.

Interpretation

The most well-known application of the Weibull distribution occurs in survival analysis, where the shape parameter modifies the probability of a specific event (e.g. component failure) over time. This model which describes a probability distribution was successfully applied on the present frequency distribution of the pore sizes [4]. The merging of two pores that results in one large pore could be identified as the specific event whose probability is modified by the shape parameter. A shape parameter smaller than 1 leads to a decrease of the probability for two pores to merge, depending on the size of the involved pores. This effect gets more prominent for an increasing particle concentration.
It can be stated that the particles stabilise the foam. Especially one well-known effect could be observed: introduced particles decelerate the drainage of the fluid material. Finally this delays the merging of the pores [5].

Conclusion

In the context of this work the pore sizes in soft polyurethane foams were evaluated in a statistically relevant scale for the first time. Based on the recorded data it was possible to prove that the Weibull distribution can be applied to the pore size distribution. The variation of the shape parameter could be linked to the foam stabilizing effect of the particles.

Acknowledgements

We gratefully thank the company Elantas Beck GmbH for providing the components.

References

[1] Gong Q., Wu J., Gong X., Fan Y., Xia H. RSC Advances **3** 3241 (2013)
[2] Kastner J, Kickinger R, Salaberger D 2010 CNDT 2010
[3] Günther D., Borin D., Günther S., Odenbach S. Smart Mater. Struct. **21** 015005 (2011)
[4] Møller S. K. Scand. J. Statist. **3** 107-115 (1976)
[5] Hunter T., Pugh R., Franks G., Jameson G. Advances in Colloid and Interface Science **137** 57–8 (2008)

Multi-component Raspberry-like Magnetic Structures

X. Song, S. Sprott, A. M. Schmidt[1,*]

[1] *Institut für Physikalische Chemie, Universität zu Köln, Luxemburger Str. 116, D-50939 Köln*
**E-Mail: annette.schmidt@uni-koeln.de*

Raspberry architectures based on nonmagnetic and magnetic nanoparticles (NPs) are considered as a novel approach to prepare multi-component nanomaterials. They are of substantial scientific and technological interest with application potential in magnetic storage,[1] as separable catalysts, and for biomedical applications.[2]
In this work, cobalt NPs and palladium NPs are deposited on functionalized silica cores (~ 100 – 300 nm) by chemical methods.[3]

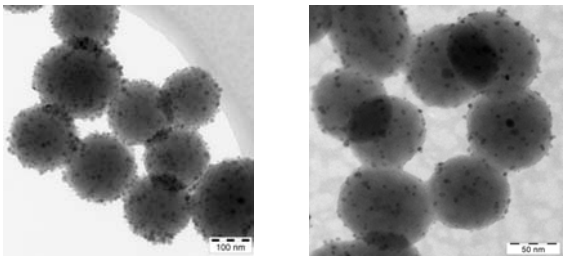

Fig 1: TEM images of $Co@SiO_2$ NPs (left) and $Pd@SiO_2@Fe_3O_4$ NPs (right).

TEM analysis (Fig 1) indicates the raspberry-like morphology of $Co@SiO_2$ NPs and $Pd@SiO_2@Fe_3O_4$ NPs. The smaller Co NPs and Pd NPs are well distributed all over the surface of the silica cores.
We utilize $Co@SiO_2$ and $Pd@SiO_2@Fe_3O_4$ raspberry-like nanoparticles as novel type of solid stabilizer for water-in-oil (w/o) and oil-in-water (o/w) emulsions. Microscopic methods were applied to investigate how the concentration of nanoparticles affects the properties of the Pickering emulsions.

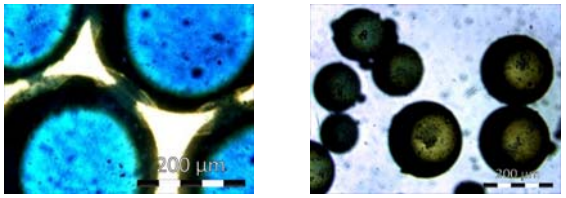

Fig 2: Light microscopy images of stained w/o emulsion stabilized by $Co@SiO_2$ NPs (left) and o/w emulsions stabilized by $Pd@SiO_2@Fe_3O_4$ NPs (right).

In order to get information on the type of emulsion obtained, the samples are stained with a water-soluble dye. As is shown in Fig 2, the emulsions stabilized by $Co@SiO_2$ are w/o, while stabilized by $Pd@SiO_2@Fe_3O_4$ are o/w. A direct correlation between the particles composition, the solid content of the emulsion and the resulting droplet size and surface coverage, is observed.

Acknowledgments

We thank Dr. L. Belkoura for TEM images. Financial support from the China Scholarship Council is gratefully acknowledged. The project "Sustainable Chemical Synthesis (SusChemSys)" is co-financed by the European Regional Development Fund (ERDF) and the state of North Rhine-Westphalia, Germany, under the Operational Programme "Regional Competitiveness and Employment" 2007 - 2013.

References

[1] F. Caruso, *Adv. Mater*. **2001**, 13, 11-22.
[2] G. Reiss, A. Huetten, *Nat. Mater*. **2005**, 4, 725-726.
[3] D. Yi, S. Lee, J. Ying, *Chem. Mater.* 2006, 18, 2459-2461.

Microscopic modeling of magnetorheological elastomers and their macroscopic behavior by applying the extended Finite-Element-Method

C. Spieler, P. Metsch, M. Kästner, J. Brummund and V. Ulbricht

Institute of Solid Mechanics, Technische Universität Dresden, 01062 Dresden, Germany

Motivation

This study is motivated by the need to develop a multiscale modeling approach for magnetorheological elastomers (MRE). On the microscale the proposed composite material consists of a polymeric matrix with embedded magnetizable particles. The rheological properties of the MRE can be altered by the application of an external magnetic stimulus. This so called magnetorheological effect is caused by magnetic and mechanical interactions between the micron sized particles. A coupled magneto-mechanical field problem involving large deformations and material nonlinearities has to be solved.

Field equations

The problem is formulated in the framework of large deformations. For the stationary magnetic field the Maxwell equations are presented in the current configuration of deformable media together with appropriate pull back operations of the magnetic field variables linking them to a reference configuration. The particles of the MRE exhibit a nonlinear magnetization behavior with saturation at higher values of the magnetic field but negligible hysteresis effects. Beside a linear approach, a phenomenological model is used to describe this magnetic nonlinearity.

Based on a microscopically motivated model for the electrodynamics of continua [1,2] the balance of momentum is expressed in terms of the total stress tensor. It consists of a mechanical and a magnetic part. A crucial task is the formulation of thermodynamically consistent constitutive equations for large deformations [3] which should coincide in the limit case with a small deformation model used in [4, 5]. The nonmagnetic polymeric matrix of the MRE is modeled by a compressible neo-Hookean material.

The magneto-mechanical coupling is considered to be weak. Therefore, the stationary magnetic and mechanical problems are solved consecutively and are coupled by the deformation dependence, magnetic loads and the material behavior.

Numerical solution and validation

Generating numerical models is a problem in particular if complex local material structures are considered. In this case, the application of the standard Finite-Element-Method (FEM) tends to result in an extensive modeling and meshing effort including problems related to distorted elements. The extended Finite-Element-Method (XFEM) [4, 6] offers the possibility to use nonconforming meshes which do not have to be adapted to internal details, e.g. material interfaces, of the structure under consideration. Hence, it is applied to model the local heterogeneous material structure of the composite mentioned above.

Studies concerning the h- and p-convergence of the numerical XFEM solution for a magnetic, a purely mechanical and a coupled magneto-mechanical boundary value problem demonstrate the applicability of the implemented two-dimensional ele-

ments. Therefor an analytical solution for a two-dimensional linear bimaterial problem is provided, without considering effects of the deformation on the magnetic field problem. This solution is new and cannot be found in literature. A circular inclusion is loaded by a homogeneous magnetic field and mechanical stresses at a boundary far away from the material interface. We are able to calculate the magnetic and the mechanical field variables. They are used to prescribe boundary conditions for the numerical solution and for the error computation in the context of the mentioned convergence study.

Effective behavior of MRE with small deformations

The XFEM is used to model a representative volume element (RVE) of the MRE under the consideration of small deformation. Based on the energy equivalence theorem and volume averages over the RVE domain, microscopic and macroscopic variables are linked. An assumed periodicity of the local composite structure allows for the application of periodic boundary conditions to prescribe macroscopic magnetic and mechanical loads. By computing the reactions in terms of nodal currents and forces the effective composite behavior is determined.
We obtain effective magnetization curves. In the magnetic linear case macroscopic anisotropic permeabilities are derivable. The coupled magneto-mechanical response is analyzed in terms of macroscopic actuation stresses. These are mechanical stresses caused by a magnetic stimulus with suppressed macroscopic deformation. Furthermore, the macroscopic magnetostrictive strain of the magnetoactive composite material can be studied.

Acknowledgments

This project (ECEMP-B4; SAB: 13854/ 2379) is funded by the European Union and the Free State of Saxony.

References

[1] S. R. de Groot and L. G. Suttorp: Foundations of Electrodynamics. North-Holland, Amsterdam, 1972

[2] A. C. Eringen and G. A. Maugin: Electrodynamics of Continua I. Springer, New York, 1990

[3] C. Spieler, P. Metsch, M. Kästner and V. Ulbricht in Technische Mechanik, submitted manuscript

[4] M. Kästner, S. Müller, J. Goldmann, C. Spieler, J. Brummund and V. Ulbricht in International Journal for Numerical Methods in Engineering, 2013, doi: 10.1002/nme.4435

[5] C. Spieler, M. Kästner, J. Goldmann, J. Brummund and V. Ulbricht in Acta Mechanica, 2013, doi: 10.1007/s00707-013-0948-5

[6] T. P. Fries and T. Belytschko in International Journal for Numerical Methods in Engineering, 2010, doi: 10.1002/nme.2914

Diffusivity and Thermal Diffusion in Magnetic Fluids

L. Sprenger, A. Lange and S. Odenbach

TU Dresden, Institute of Fluid Mechanics, Chair of Magnetofluiddynamics, Measuring and Automation Technology, 01062 Dresden, Germany

Introduction

Diffusivity and thermal diffusion, also called thermodiffusion, in magnetic fluids highly depend on the fluid's properties. The diffusivity is characterised by the molecular diffusion coefficient D. It can be described via an expression of Einstein [1] $D_E = \frac{k_B T}{6\pi\eta_s(r+s)}$ with k_B the Boltzmann constant, T the temperature, η_s the dynamic viscosity of the carrier liquid, and $(r+s)$ being the radius and the surfactant thickness of one nanoparticle. Else it can be written as $D_B = D_E(1 + 1.45\varphi)$ by Batchelor [2], with φ denoting the particles' volume concentration. Thermal diffusion is characterised by the Soret coefficient S_T which can be expressed by the quotient of the thermal and the molecular diffusion coefficient $\frac{D_T}{D}$. Since thermal diffusion indicates the ability of the fluid's nanoparticles to move along a temperature gradient as diffusion itself along a concentration gradient, both transport processes primarily depend on the fluid's volume concentration [1–4]. Therefore this dependency is investigated in the following.

Fluid Characterisation

For the experimental determination of $S_T = S_T(\varphi)$ and $D = D(\varphi)$ a fluid set of a kerosene-based magnetite ferrofluid is used. The concentration varies from 0 vol.% to 10 vol.% including a carrier liquid's sample (Ferrotec). The particles' magnetic diameter and the volume concentration are determined via the magnetisation curves of the fluids, detected by a vibrating sample magnetometer. Fig. 1 shows the resulting curves and fluids' properties. The averaged diameters of the particles in descending order are determined to

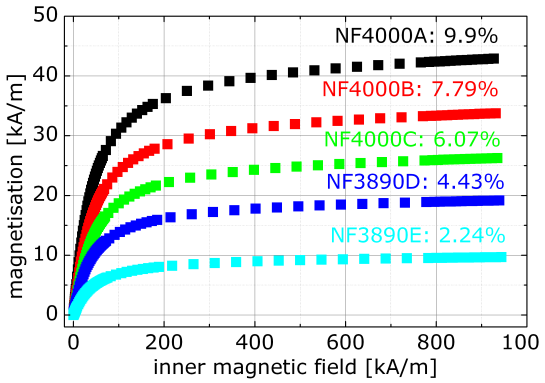

Figure 1: Magnetisation curves for five differently concentrated magnetite ferrofluids.

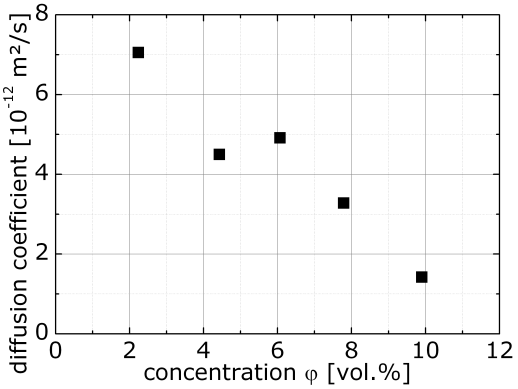

Figure 2: Diffusion coefficient dependent on the concentration of nanoparticles of the ferrofluid [2].

9.05 nm, 8.87 nm, 8.76 nm, 9.19 nm, and 9.02 nm. The fluids' viscosities η at 298.15 K - also in descending order - are determined to $\{35.2; 14.2; 8.9; 8.8; 5.2; 3.3\}$ mPa·s. The diffusion coefficient based on the mentioned data and considering the particles' diameter

obtained by the magnetisation curves is calculated and shown in Fig. 2, with rising concentration diffusivity decreases.

Experiments on diffusion

Based on a design of Völker [5] a horizontal thermodiffusion cell is used to carry out as well the separation measurements leading to S_T as preliminary homogenisation experiments that could lead to D. The measured signal thereby is the difference in concentration between the lower and the upper part of the fluid container. The measurements are carried out by first applying a temperature gradient of approx. 900 K/m to the cylindrical fluid container with a height of 14 mm. The fluid concentration becomes inhomogeneous over the cell's height. After 50 to 70 hours of separation time a constant temperature of 298.15 K is applied to the fluid, rehomogenising the fluid concentration. The Soret coefficient obtained by the experiments is calculated regarding the diffusion coefficient [5] and presented in Fig. 3. Thermal diffusion becomes weaker with the decrease of the fluids' volume concentration. Fig. 4 presents the prove of principle that the rehomogenisation process, driven by diffusion can be detected by the horizontal thermodiffusion cell as well.

Conclusion and Outlook

A set of five differently concentrated magnetite ferrofluids has been investigated regarding its diffusive behaviour. While molecular diffusivity in the fluids becomes stronger with the decrease in particle concentration, thermal diffusivity becomes weaker for the same dependency.

Acknowledgments

Financial support by the DFG Grant No. LA 1182/3 is gratefully acknowledged.

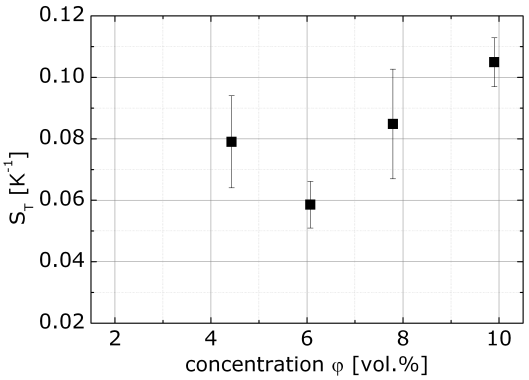

Figure 3: Dependency of the Soret coefficient on the fluid's volume concentration, the higher the concentration, the higher the thermal diffusion effect.

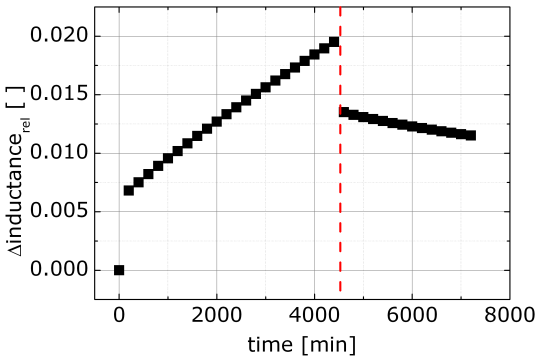

Figure 4: Separation experiment followed by a rehomogenisation experiment for a prove of principle.

References

[1] A. Einstein, Ann. Phys. **322**, 549-560 (1905)

[2] J. Lenglet, et al., J. Fluid Mech. **74**, 1-29 (1976)

[3] J. Lenglet, et al., Phys. Rev. E **65**, 031408 (2002)

[4] T. Völker, et al., Int. J. Heat Mass Transfer **47**, 4315-4325 (2004)

[5] T. Völker, et al., Phys. Fluids **17**, 037104 (2005)

[6] R. W. Chantrell, et al., IEEE MAG-**14**, 975-977 (1978)

Multiphase catalysis based on magnetic carriers

S. Sprott[1], M. Barton[2], P. Wand[2], M. H. G. Prechtl[2*], A. M. Schmidt[1*]

[1] *Institute for physical chemistry, Department for chemistry, University of Cologne*
[2] *Institute for inorganic chemistry, Department for chemistry, University of Cologne*

Chemical production processes based on multiphase catalytic systems benefit from the advantages of both homogeneous and heterogeneous catalysis, the reduction of organic solvents, and catalyst recovery.
In this respect, we employ raspberry-like particles with a magnetic core as easily recoverable catalysts with high efficiency (Fig. 1).

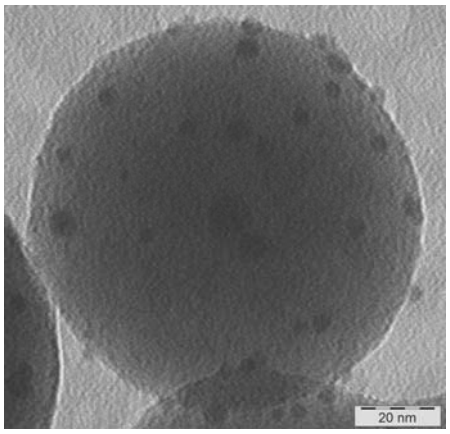

Figure 1: Magnetic carrier with immobilized catalysts.

The role of the particles is three-fold. Palladium nanoparticles (Pd-NP) serve as catalytic active species on the surface of the hybrid carrier particles, providing a high catalytic activity for Heck, Suzuki, and Sonogashira type couplings, as well as for hydrogenation and oxidation reactions.[1-6] The particles are suitable stabilizers for multiphase *Pickering* emulsions (Fig. 2), and the magnetic core serves for easy separation of catalyst and emulsion phase.

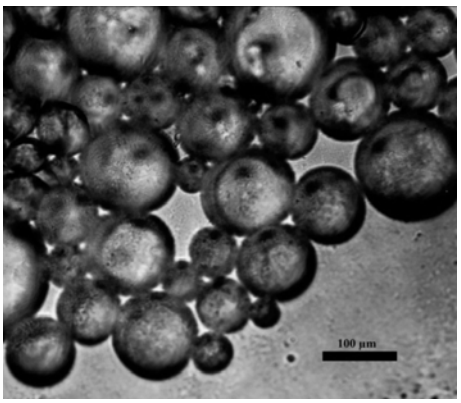

Figure 2: Microscopy image of an oil-in-water *Pickering* emulsion.

By adjusting the amount of precursor used to encapsulate the magnetic core, magnetic properties as well as thickness of the shell can be adjusted (Fig. 3).

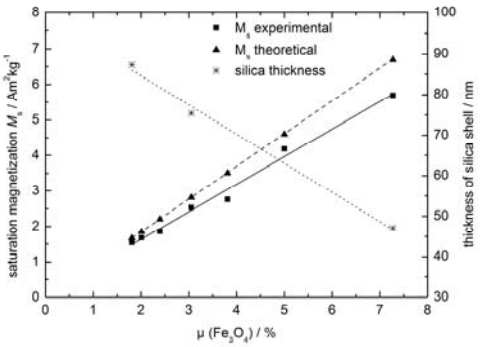

Figure 3: Theoretical (triangles, dashed line) and experimental (squares, line) saturation magnetization of different sized magnetic carriers. The dotted line represents the thickness of the silica shell.

The catalytic activity of the hybrid nanoparticles was successfully tested in various Suzuki coupling experiments in aqueous phase (Fig. 4).

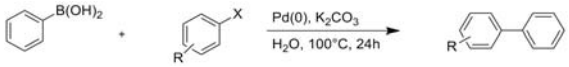

Figure 4: Tested Suzuki coupling in aqueous system.

The positioning of the catalysts on the water-oil-interface provides the advantage to bring reaction partners of both phases into contact. If the system is properly designed, it is further possible to separate product and byproduct in aqueous and organic phase, respectively. Because of the magnetic properties, the solid stabilized, product containing emulsion droplets can be magnetically separated from the aqueous reaction medium, residual educt and byproducts, after reaction. The latter feature highly facilitates product purification and catalyst recovery.

Acknowledgments

The project "Sustainable Chemical Synthesis (SusChemSys)" is co-financed by the European Regional Development Fund (ERDF) and the state of North Rhine-Westphalia, Germany, under the Operational Programme "Regional Competitiveness and Employment" 2007 - 2013.
For TEM measurements we are grateful to Dr. L. Belkoura.

References

[1] D. Astruc, *Inorg. Chem.* **2007**, *46*, 1884-1894.
[2] D. A. Alonso, C. Najera, *Chem. Soc. Rev.* **2010**, *39*, 2891-2902.
[3] M. Perez-Lorenzo, *J. Phys. Chem. Lett.* **2012**, *3*, 167-174.
[4] C.-J. Jia, F. Schüth, *Phys. Chem. Chem. Phys.* **2011**, *13*, 2457-2487.
[5] M. H. G. Prechtl, J. D. Scholten, J. Dupont, *Molecules* **2010**, *15*, 3441-3461.
[6] R. Venkatesan, M. H. G. Prechtl, J. D. Scholten, R. P. Pezzi, G. Machado, J. Dupont, *J. Mater. Chem.* **2011**, *9*, 3030-3036.
[7] A. Kaiser, A. M. Schmidt, *J. Phys. Chem. B* **2008**, *112(7)*, 1894-1989.
[8] A. Kaiser, T. Liu, W. Richtering, A. M. Schmidt, *Langmuir* **2009**, *25(13)*, 7335-7341.
[9] N. Frickel, R. Messing, T. Gelbrich, A. M. Schmidt, *Langmuir* **2010**, *26(4)*, 2839-2846.

Slow dynamics of structure-forming ferrofluids in zero field

Aparna Sreekumari[1] and Patrick Ilg[1]

[1] *Polymer Physics, ETH Zürich, Wolfgang-Pauli Str. 10, CH-8093 Zürich*

Computer simulations of model ferrofluids are performed that mimic Cobalt-based ferrofluids used in experiments. We have investigated both, internal structures and dynamical properties of these systems for varying dipolar interaction strengths. We find indications for a qualitative different structure and behavior above a critical interaction strength which is close to the estimated value for the experimental system.

Introduction

From the classical work of de Gennes and Pincus [1], it is known that dipolar colloids having strong interactions tend to form chain-like structures. In experimental as well as numerical studies under zero field conditions [2, 3], microstructure formation has indeed been found in ferrofluids, which strongly influences their rheological properties. In addition, some numerical studies [4, 5] have also shown evidence for network formation in ferrofluids having strong dipolar coupling, as predicted theoretically by Tlusty and Safran [6].

Model System

We have used a model system which has been studied previously [4, 7], where magnetically hard particles experience steric repulsion and dipole-dipole interactions. We have performed Langevin dynamics simulations in a system of 1000 particles using translational and rotational Langevin equations of motion. We choose a small volume fraction of magnetic nanoparticles, $\phi = 0.007$, that corresponds to the fluid used in Ref. [8]. The range of dipolar interaction strengths we study covers the weakly ($\lambda \lesssim 2$) up to the strongly interacting ($\lambda \gtrsim 5$) regime.

Results

For weak dipolar interactions, most particles are isolated, whereas we observe significant structure formation for strong dipolar interaction, see Fig. 1. These observations are in agreement with earlier simulations [2, 3, 4] and theoretical predictions of the chain model [9]. However, we also observe that not only chains but more complicated, connected structures are formed at higher interaction strengths.

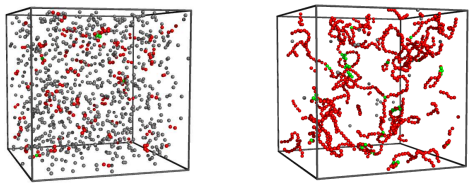

Figure 1: Snapshots of particle configurations for weakly (left) and strongly (right) interacting ferrofluids. Gray, red and green colors correspond to isolated particles, particles with one or two neighbors, and particles having more than three neighbors, respectively.

The formation of multiply-connected, network-type structures is responsible for slow relaxation in these fluids. From the incoherent scattering function for wave-vector $\mathbf{q}$, $F_s(q,t) = \langle e^{-i\mathbf{q}\cdot\Delta\mathbf{r}(t)}\rangle$, we determine a length-scale dependent relaxation time $\tau(q)$ known from colloidal gels [10]. For small length scales, the relaxation is roughly independent of λ, whereas relaxation on larger length scales increases significantly

with λ, see Fig. 2.

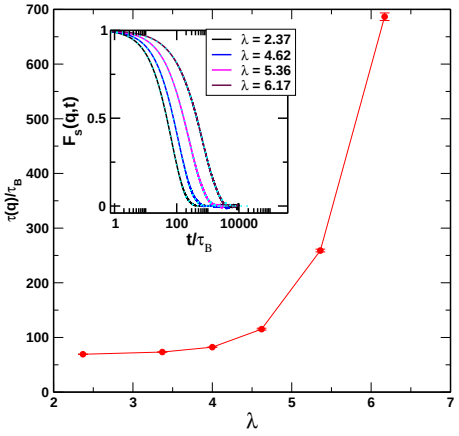

Figure 2: Relaxation time τ for large length scales as a function of dipolar interaction strengths. The inset shows the corresponding decay of the relaxation function.

The structure formation and the resulting relaxation time increase is also responsible for the slowing down of translational and rotational diffusion, as well as the increase in the zero-shear viscosity, see Fig. 3.

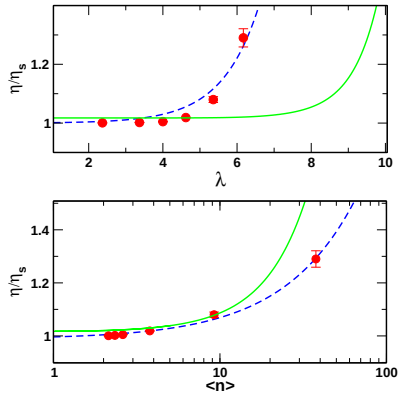

Figure 3: Zero-shear viscosity as a function of λ (top) and the mean cluster size $\langle n \rangle$ (bottom). Green line is the prediction of the chain model, blue a fit to $\eta = \eta_s[1 + ae^{\lambda}]$ and $\eta = \eta_s[1 + a\langle n \rangle]$.

References

[1] P. G. de Gennes and P. A. Pincus, Phys. Kondens. Mater 11, 189-198 (1970).

[2] P. J. Camp and G. N. Patey, Phys. Rev. E 62, 4 (2000).

[3] L. Rovigatti, J. Russo and F. Sciortino, Phys. Rev. Lett 107, 237801 (2011).

[4] Z. Wang, C. Holm and H. W. Müller, Phys. Rev. E 66, 021405 (2002).

[5] P. Ilg and E. Del Gado, Soft Matter, 7, 163 (2011).

[6] T. Tlusty and S. A. Safran, Science, 209, 1328-1331 (2000).

[7] P. Ilg, M. Kröger and S. Hess, Phys. Rev. E 71, 051201 (2005).

[8] M. Gerth-Noritzsch, D. Yu Borin and S. Odenbach, J. Phys. Condens. Matter, 23, 346002 (2011).

[9] A. Yu. Zubarev, Phys. Rev. E 61, 5415 (2000).

[10] E. Del Gado and W. Kob, Phys. Rev, Lett., 98, 028303 (2007).

Polydehydroalanines as Coatings for Fe_3O_4@Polymer Hybrid Particles

M. von der Lühe[1], U. Günther[1], S. Dutz[2,3], and F. H. Schacher[1]

[1] *Institut für Organische und Makromolekulare Chemie (IOMC) and Jena Center for Soft Matter (JCSM), Friedrich Schiller Universität Jena, Germany; felix.schacher@uni-jena.de*
[2] *Department of Nano Biophotonics, Institute of Photonic Technology, Jena, Germany*
[3] *Institute of Biomedical Engineering and Informatics, Ilmenau University of Technology, Ilmenau, Germany*

Introduction

Typically, the application of nanoparticles into biological systems leads to the formation of a protein corona around these particles[1]. This protein corona is supposed to have drastic influence on the biocompatibility and the interactions of such nanoparticular systems with the surrounding environment.

Overall our work focuses on the investigation of the influence of a polymer shell with tunable charge and/or charged distribution around superparamagnetic iron oxide nanoparticles (SPION) on the formation and composition of such a protein corona. For this, at the first stage of our study suitable polymer coatings for the magnetic cores have to be developed.

Results

Starting from 2-*tert*-butoxy-carbonylaminomethylacrylate (*t*BAMA) different polymers with molar masses ranging from 10.000 to 225.000 g/mol have been synthesized and characterized[2]. By deprotection of either one or both of the protected functionalities, these materials were transformed into polycationic (poly(amino methylacrylate), PAAMe), polyanionic (poly(*tert*-butoxycarbony-lamino-acrylic acid), P*t*BAA) or even polyzwitterionic materials (polydehydro-alanine, PDhA) as shown in [2].

These polymers were then used for coating Fe_3O_4 nanoparticles at different pH-values. The influence of the molar mass of the used polymer on the formation, size and stability of hybrid core-shell nanoparticles were investigated by dynamic light scattering

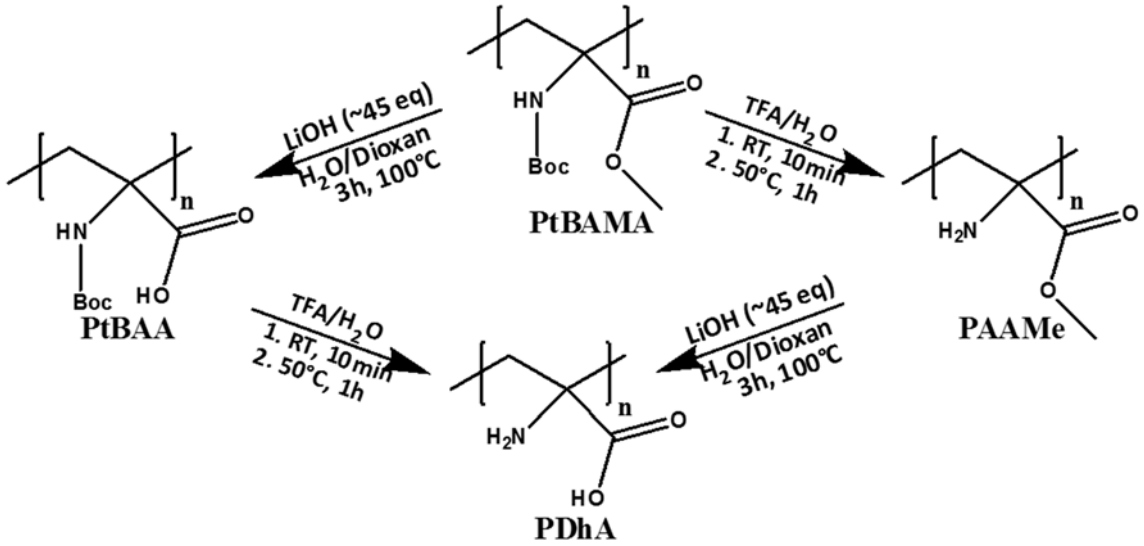

Figure 1: deprotection of PtBAMA to polycationic PAAMe, polyanionic PtBAA, or potentially zwitterionic PDha.

(DLS), transmission electron microscopy (TEM), and zeta potential measurements. We found significant differences concerning size, size distribution, and solution stability at different pH-values after coating of the particles and subsequent washing to remove any free polymer.

As found in magnetic measurements (VSM) there is no alteration of the magnetic properties of the particles resulting from this coating process, e.g. agglomeration of the primary cores.

After successful coating of small magnetic cores in the superparamagnetic size range with polymers showing a tuneable surface charge and charge distributions the influence of this parameter field on the formation of the protein corona will be investigated in the following step of our study. For this the hybrid core-shell nanoparticles have to be incubated within a protein source (fetal calf serum) and the formed protein corona has to be investigated as a function of surface charge behavior of hybrid core-shell nanoparticles

References

[1] S. Tenzer, D. Docter, S. Rosfa, A. Wlodarski, J. Kuharev, A. Rekik, S. K. Knauer, C. Bantz, T. Nawroth, C. Bier, J. Sirirattanapan, W. Mann, L. Treuel, R. Zellner, M. Maskos, H. Schild, R. H. Stauber, *Acs Nano* **2011**, *5*, 7155-7167.

[2] U. Günther, L. V. Sigolaeva, D. V. Pergushov, F. H. Schacher, *Macromolecular Chemistry and Physics* **2013**, *in press (DOI: 10.1002/macp.201300324)*.

Direction dependend diffusion of aligned spindle-shaped hematite particles

Joachim Wagner[1], Christian Märkert[1], Birgit Fischer[2], Leonard Müller[2]

[1]*Institut für Chemie, Universität Rostock, Albert-Einstein-Straße 3a, 18051 Rostock*
[2]*Deutsches Elektronensynchrotron, Notkestraße 85, 22607 Hamburg*

Well defined, ansisotropic hematite particles can be prepared with tunable aspect ratio as spindle-shaped single domain particles. Due to their negative anisotropy of the magnetic susceptibility $\chi_\parallel < \chi_\perp$, spindle-shaped he-ma-tite particles align with their principal axis perpendicular to an external field already at moderate flux densities of several millitesla [1]. Due to the axial symmetry of the particles two different friction coefficients $\xi_\parallel$ and $\xi_\perp$ for motions parallel and perpendicular to the principal particle axis exist.

Since dynamic scattering methods probe the projection of the diffusive motion to the direction of the scattering vector $\mathbf{Q}$, direction dependent diffusion coefficients $D_\parallel$ and $D_\perp$ are accessible by choosing the direction of the scattering vector $\mathbf{Q}$ parallel and perpendicular to the direction of an external magnetic field $\mathbf{H}$.

In absence of an external field, in highly diluted suspensions the orientation of the particles is random with the orientational distribution function (odf) $f(\vartheta) = 1/(2\pi)$. In this situation the averaged diffusion coefficient $\langle \underline{\underline{\mathbf{D}}}(\vartheta,\varphi)\rangle_{\vartheta,\varphi} = (2D_\perp + D_\parallel)/3$ is observed. In presence of a sufficiently large magnetic flux density, however, the particles align perpendicular to the field direction leading to a delta shaped odf $f(\vartheta) = \delta(\vartheta - \pi/2)$. Since all particles are aligned perpendicular to the field, the diffusive motion in the field direction is also perpendicular to the particle axis. Hence choosing $\mathbf{Q} \parallel \mathbf{B}$ the diffusion coefficient $D_\perp$ is directly accessible.

Since the particles can still freely rotate around the short axis, for the diffusive motion perpendicular to the field direction the averaged diffusion coefficient $\langle \underline{\underline{\mathbf{D}}}(\pi/2,\varphi)\rangle_\varphi = (D_\parallel + D_\perp)/2$ can be observed.

The diffusion coefficients of highly diluted suspensions with different aspect ratios are determined by means of X-ray Photon Correlation Spectroscopy (XPCS) in dependence on the modulus and direction of the scattering vector $\mathbf{Q}$ with respect to the direction of an external field. Unlike light scattering employing visible light as a probe, X-ray scattering is not affected by the opacity of magnetic materials. The XPCS experiments are carried out at the coherence beamline ID10A at the European Synchrotron Radiation Facility ESRF in Grenoble, France.

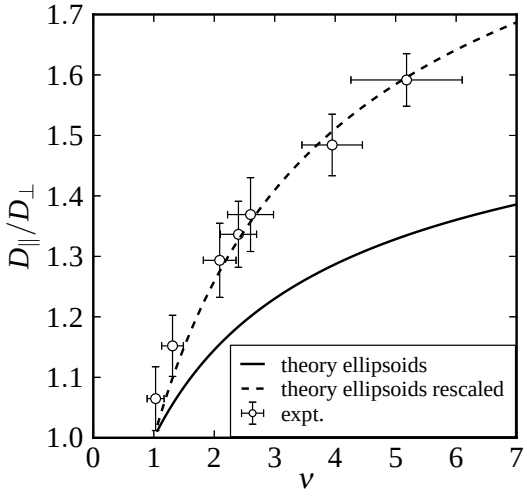

The ratio of the diffusion coefficients $D_\parallel/D_\perp$ for particles with increasing aspect ratio ν is compared to the theoretical prediction for ellipsoids of revolution derived by Perrin [2]. The ratio of $D_\parallel/D_\perp$ is for spindles larger than the one predicted for ellip-

soids of revolution and can be heuristically described via a rescaled Perrin approach [3].

Acknowledgments

The authors gratefully acknowledge support from the staff of the beamline ID10@ESRF during the experiments.

References

[1] C. Märkert, B. Fischer, J. Wagner, *Small-angle scattering from spindle-shaped colloidal hematite particles in external magnetic fields*. *Journal of Applied Crystallography*, **44**, 441–447 (2011)

[2] F. Perrin. *Mouvement brownien d'un ellipsoide - i. dispersion diélectrique pour des molécules ellipsoidales*, *J. Phys. Radium*, **5**, 497–511 (1934)

[3] J. Wagner, C. Märkert, B. Fischer, L. Müller. *Direction dependent diffusion of aligned magnetic rods by means of x-ray photon correlation spectroscopy*, *Phys. Rev. Lett.*, **110**,048301 (2013)

Microstructure and magnetic response of particles with shifted dipoles

Rudolf Weeber[1], Marco Klinkigt[1], Sofia Kantorovich[2], Christian Holm[1]

[1]*Institute for Computational Physics, University of Stuttggart, Allmandring 3, 70569 Stuttgart, Germany*
[2]*University of Vienna, Sensengasse 8, 1090 Vienna, Austria*

In an effort to tailor the properties of magnetic soft matter, many systems have been developed that deviate in one way or another from spherical magnetic nanoparticles in a simple fluid. Two approaches are possible: either the carrier fluid is replaced by something else, for instance, a polymer gel, in order to introduce a coupling of magnetic and elastic forces, or the magnetic particles themselves are modified in order to change their interaction. This contribution deals with an example of the latter case. We present results from simulation studies of particles with a non-central dipole moment, so-called shifted dipole particles (SD-particles). The dipole moment always points outwards radially, in oder to mimmic the experimental system studied in Ref. [3] . The amount by which it is shifted outwards is controlled by the parameter s, where $s = 0$ denotes a central dipole, whereas $s = 1$ denotes a dipole on the particle's surface.

Due to the additional anisotropy introduced by the shift of the dipole moment, we observe strong deviations in both, the ground state configurations and the cluster structure of a bulk system. While, for particles with central dipoles ($s = 0$), the ground states are chains and rings, we observe close-packed structures with a triangular dipole arrangement for intermediate shift, and pairs with anti-parallel dipole alignments for very high shifts. The same trends can also be observed in systems at a temperature larger than zero. While chains, rings and branched structures dominate suspensions for particles with central dipoles, the clusters become more close-packed at intermediate shifts. This is accompanied by a slight increase in cluster size. At high shifts, the cluster size drops sharply, and the suspension is mainly composed of single particles, pairs with anti-parallel dipole configuration, and triplets with triangular dipole configurations.

The change in the local dipole configuration in systems of SD-particles also changes the magnetic response drastically. For particles with central dipoles, the application of an external magnetic field enhances the formation of chains. This is, because chains allow for both, maximizing the attraction between dipole moments within the chain, and aligning all the dipoles to the external field by an alignment of the chain as a whole. This is different for SD-particles with high shift. As neighboring particles assume anti-parallel or ring-like dipole configurations, either the external field breaks up the local order and thereby destroys the clusters, or the clusters are maintained but some of the dipoles have an unfavorable alignment with respect to the field. This conflict leads to the surprising result that an applied magnetic field can lead to a reduction of cluster size in a system of SD-particles, while it enhances the clustering for particles with central dipoles.

In this contribution, we briefly summarize the results for suspensions of SD-particles without an external field [1]. Then, we show detailed result for the magnetic response and the change of the microstructure when an external field is applied [2]. We also make connections to experimental systems like capped colloids [3] and particles with embedded magnetic cubes [4].

Acknowledgments

RW and CH are grateful for financial support from the SRC SimTech, and for acces to the computer facilities of the HLRS. SK was supported by Austrian Science Fund (FWF): START-Project Y 627-N27, RFBR grants mol-a 1202-31-374 and mol-a-ved 12-02-33106, and the Grant of Ministry of Science and Education of RF 2.609.2011.

References

[1] Marco Klinkigt, Rudolf Weeber, Sofia Kantorovich, and Christian Holm. Cluster formation in systems of shifted-dipole particles. *Soft Matter*, 9:3535–3546, 2013.

[2] Rudolf Weeber, Marco Klinkigt, Sofia Kantorovich, and Christian Holm. Microstructure and magnetic properties of magnetic fluids consisting of shifted dipole particles under the influence of an external magnetic field *Submitted to J. Chem. Phys*.

[3] Larysa Baraban, Denys Makarov, Manfred Albrecht, Nicolas Rivier, Paul Leiderer, and Artur Erbe. Frustration-induced magic number clusters of colloidal magnetic particles. *Phys. Rev. E*, 77:031407, 2008.

[4] Stefano Sacanna, Laura Rossi, and David J. Pine. Magnetic click colloidal assembly. *Journal of the American Chemical Society*, 134(14):6112–6115, 2012.

A guideline for atomistic design and understanding of ultrahard nanomagnets

H. Wende[1], C. Schmitz-Antoniak[1], M.E. Gruner[1], M. Spasova[1], A.V. Trunova[1], F.M. Römer[1], A. Warland[1], B. Krumme[1], K. Fauth[2], S. Sun[3], Peter Entel[1], Michael Farle[1]

[1]*Faculty of Physics and Center for Nanointegration Duisburg-Essen (CENIDE), University of Duisburg-Essen, Lotharstr. 1, D-47048 Duisburg, Germany.*
[2]*Experimentelle Physik IV, Universität Würzburg, Am Hubland, Würzburg D-97074, Germany.*
[3]*Department of Chemistry, Brown University, 324 Brook Street, Providence, Rhode Island 02912, USA.*

Magnetic nanoparticles are of immense current interest because of their use in biomedical and technological applications. Here we demonstrate that the large magnetic anisotropy of FePt nanoparticles can be significantly modified by surface design [1]. We employ X-ray absorption spectroscopy offering an element-specific approach to the magnetocrystalline anisotropy and the orbital magnetism [1,2]. Experimental results on oxide-free FePt nanoparticles embedded in Al are compared with large-scale density functional theory calculations of the geometric- and spin-resolved electronic structure, which only recently have become possible on world-leading supercomputer architectures. The combination of both approaches yields a more detailed understanding that may open new ways for a microscopic design of magnetic nanoparticles and allows us to present three rules to achieve desired magnetic properties. In addition, concrete suggestions of capping materials for FePt nanoparticles are given for tailoring both magnetocrystalline anisotropy and magnetic moments.

These observations imply that it is possible to design nanoparticular systems with the desired magnetic properties by choosing the right capping material from a technological perspective or for basic research. The origin of these different magnetic properties for different capping materials is due to both electronic hybridization effects and structural distortions of the nanoparticle itself, which can be separated by means of state-of-the art first-principles calculations.

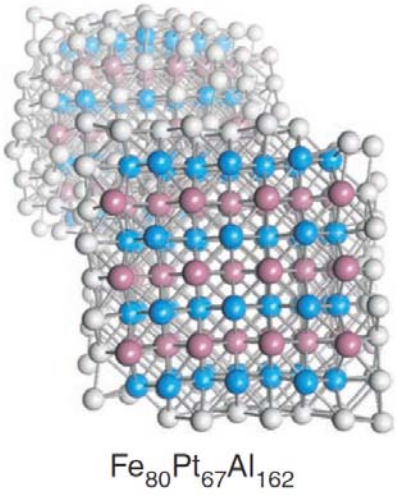

Figure 1: Morphology of FePt nanoparticles. $L1_0$ $Fe_{80}Pt_{67}$ nanoparticles embedded in an Al-matrix after structural relaxation. Grey spheres refer to Fe, dark spheres to Pt atoms and the light grey colours to Al. The foreground shows the nanoparticles in cross-section.

References

[1] C. Antoniak *et al*., Nature Communications **2**, Article number: 528 (2011).

[2] C. Antoniak *et al*., J. Phys. D: Appl. Phys. **43**, 474007 (2010).

Magnetic Particle Spectroscopy to quantify blood half-life and organ uptake of superparamagnetic iron oxide nanoparticles in a mouse stroke model

F. Wiekhorst[1], T.D. Farr[2], M. Füchtemeier[2], U. Harms[2], M. Endres[2], Ch. Harms[2], L. Trahms[1]

[1] *Physikalisch-Technische Bundesanstalt, Berlin, Germany*
[2] *Charite, Berlin, Germany*

Introduction

The application of magnetic resonance imaging (MRI) in combination with superparamagnetic iron oxide nanoparticles (SPIOs) as a contrast agent is presently investigated in preclinical studies as a modality to monitor signal intensity changes by SPIOs in the ischemic region during the acute stage of (experimental) stroke [1]. Present preclinical studies focus on two questions: The properties of nanoparticles that render them most suitable for phagocytosis and the appropriate time for administration of the SPIO to gain best MRI contrast. The SPIO coating determines the hydrodynamic diameter and surface charge, which in turn influences the pharmacokinetic properties of the particles such as blood half-life, organ uptake, and elimination.
In a preclinical stroke study of middle cerebral artery occlusion (MCAO) in mice we employed Magnetic Particle Spectroscopy (MPS) to determine the blood half-life of three different types of SPIOs and their uptake in organs [2]. We demonstrated the ability of this quantitative magnetic technique for sensitive and specific (unaffected by body iron) SPIO detection in blood and tissue samples.

Blood and tissue sample preparation

EDTA stabilized blood samples (between 50 and 100 µL) of twelve mice were collected before and at approximately 2, 5, 15, 30, and 45 minutes after *i.v.* injection of the SPIOs. We used VSOP (citrate coated, Charité Berlin) and Feraheme® (carbohydrate coated, Amag Pharmaceuticals) at two different dosages (300 µmol/kg and 1000 µmol/kg), both types having about 6 nm mean diameter as determined by magnetometry. After final blood sampling at 45 minutes, the animals were euthanized and perfused transcardially with physiological saline. The heart, lungs, kidneys, livers, and spleens were extracted and weighed. Livers and spleens were divided for quantification and histology.

Quantification by Magnetic Particle Spectroscopy (MPS)

For the quantification of nanoparticle iron content in blood and tissue samples we used a MPS device (Bruker Biospin). MPS detects specifically the nonlinear magnetic response of magnetic nanoparticles exposed to an oscillating magnetic field. The amplitude of the MPS signal is proportional to the amount of SPIOs in the sample. Biological tissue and paramagnetic blood iron do not contribute to the MPS signal.
Blood and organ samples (up to 180 µL volume) were collected in sample tubes and placed into the pick-up coil of the MPS system for the measurement. The magnetic response of the samples to an AC magnetic field of a frequency f_0 of 25 kHz and an amplitude B_{excit} of 25 mT was recorded for 10 s. The amplitude of the third harmonic A_3 in the MPS signal was taken as a meas-

ure of the absolute nanoparticle iron content. By referring to a reference sample (5 µL of the stock SPIO suspension) of known iron content measured under the same conditions, the total amount of iron in each sample was determined. From the magnetic moment sensitivity of the device ($\sim 5 \cdot 10^{-12}$ A/m^2) and the measured A_3 amplitude of the reference, we estimated individual detection limits for the two SPIOs, mainly determined by the dynamic magnetic properties: 5 ng of iron for Feraheme, and 30 ng of iron for VSOPs.

SPIO half-life in blood

Before injection, no SPIO, could be detected in blood, while the SPIO concentration increased dramatically within the first two minutes after the infusion reaching concentrations larger than 100 (400) ng Fe/mg blood for the 300 (1000) µmol/kg dosage. With increasing time after infusion the SPIO concentration monotonically decreased as shown in Fig. 1 (left) for the two SPIOs at 300 µmol/kg dosage. By fitting a single exponential $c(t)=c_0 \exp(-t/\tau)$ the blood half-life τ was extracted. As depicted in Fig. 1 (right) Feraheme circulate longer than VSOPs. Furthermore the half-lives are dosage dependent.

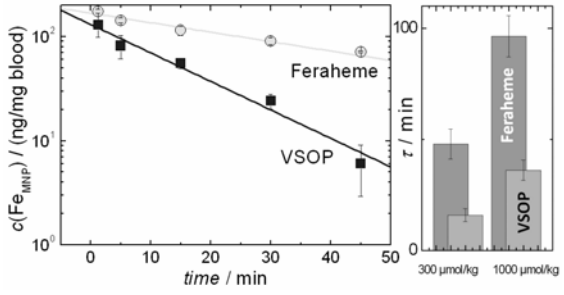

Fig.1 Blood half life τ for Feraheme and VSOP.

Organ uptake of SPIO

In the organs we found that after 45 min of circulation the SPIO mainly accumulated in the liver and spleen, while the other organs only contained small iron concentrations.

Interestingly, a marked iron concentration was quantified in lungs for VSOPs in the high 1000 µmol/kg dosage (for all three mice).

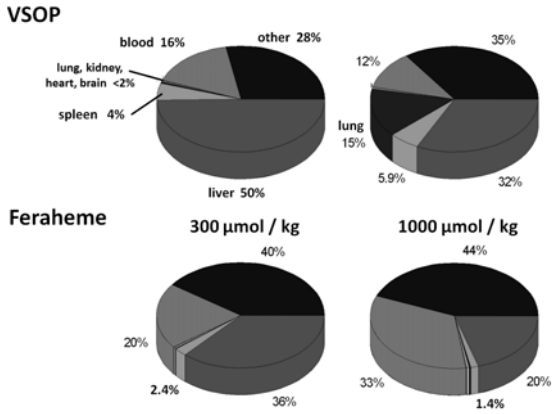

Fig.2 Organ uptake of VSOP and Feraheme at 300 µl/kg and 1000 µmol/kg dosage.

Conclusion

MPS allows the fast and reliable detection of SPIOs in tissue samples. Due to its high sensitivity only small sample volumes of 10 to 100 nanograms of SPIO iron per sample are required for a safe SPIO quantification not hampered by natural body iron.

Acknowledgments

This work was financially supported by the DFG research programs “Magnetische Nanopartikel für die Krebstherapie” TR408/4-3 and “Magnetische Nanopartikel für die Zelluläre und Molekulare MR-Bildgebung” TR408/5-2 and HA5741/1-2.

References

[1] Deddens LH, et.al. (2012) Imaging neuroinflammation after stroke: current status of cellular and molecular MRI strategies. Cerebrovasc Dis 33: 392–402.

[2] Ch. Harms, et.al. (2013) Certain types of iron oxide nanoparticles are not suited to passively target inflammatory cells that infiltrate the brain in response to stroke. Journal of Cerebral Blood Flow & Metabolism 33:e1–e9.

Dipolar Soft Spheres in Rotational Fields

A. Yener[1], S. Jäger[1], S.H.L. Klapp[1]

[1]*Institut für Theoretische Physik, Sekr. EW 7-1, Technische Universität Berlin, Hardenbergstrasse 36, 10623 Berlin*

We model ferromagnetic particles by quasi-twodimensional [1] and threedimensional [2] spherical particles with centred magnetic dipole moments $\vec{\mu}_i$ interacting via the short ranged soft core potential
$u(r_{ij}) = 4\epsilon\,(1/r^{12})$ and the dipolar potential $u(\vec{r}_{ij}, \vec{\mu}_i, \vec{\mu}_j) = \vec{\mu}_i\vec{\mu}_j/r_{ij}^3 - 3(\vec{\mu}_i\vec{r}_{ij})(\vec{\mu}_j\vec{r}_{ij})/r_{ij}^5$.
We simulate the system in rotational magnetic fields $\vec{B} = B_0(\cos(\omega_0 t)\vec{e}_x + \sin(\omega_0 t)\vec{e}_y)$ with variying field strengths B_0 and frequencies ω_0. While the particles arrange in chain-like head to tail configuartions in zero field, they form layered structures in the rotational field. Using computer simulations as well as convenient order parameters, Single Particle and Density Functional Theories (DFT), we investigate the dynamical and structural properties of the layered states. We present a diagram for the nonequilibrium, layered states for different B_0 and ω_0. Besides, we show results of single particle theory and DFT for the high and low frequency borders to the unlayered state, respectively.
In a next step, we pass to a system with the same interactions but with laterally shifted dipole moments from the centre. Herewith, we model experimentally created particles such as partciles with magnetic caps [3] or Janus partciles [4]. The shift affects the dynamics by leading to an additional torque on the particles. This is caused by the distance dependent dipolar forces which now does not act on the centres any more. We present simulation results of the shifted system.

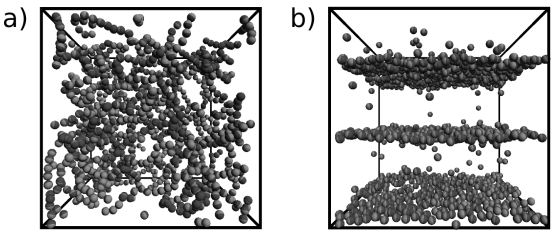

Figure 1: (a) Dipolar soft spheres in zero field at $\rho^* = 0.1$, $T^* = 1.35$ and $\mu^* = 3$. (b) The same system exposed to a rotational field with $B_0^* = 12$ and $\omega_0^* = 15$.

We thank the DFG for funding via the GRK 1558.

References

[1] S. Jäger, and H. Schmidle, and S. H. L. Klapp, Phys. Rev. E **86**, 011402 (2012)

[2] S. Jäger, and S. H. L. Klapp, Soft Matter **7**, 6606 (2011)

[3] D. Zerrouki, J. Baudry, D. Pine, P. Chaikin, and J. Bibette, Nature **455**, 380 (2008)

[4] J. Yan, M. Bloom, S. C. Bae, E. Luijten, and S. Granick, Nature **491**, 578 (2012)

Acknowledgments